Processing and Interpretation of Multichannel Seismic Data from Isfjorden, Svalbard

Abrar Asghar

Dissertation for the Master Degree (M.Sc)

Petroleum Geosciences

Department of Earth Sciences
University of Bergen
Norway

November, 2011

ABSTRACT

This research project is based on the processing and interpretation of nine 2D multichannel seismic profiles from Isfjorden, which is the largest fjord in Western Spitsbergen. These profiles were acquired in eastern part of Isfjorden with NNE-SSE orientation during the geophysical surveys in 2008, 2009 and 2010 by the University of Bergen. The first part of the thesis describes the processing of the seismic data, while in the second part a broad seismic interpretation was done in order to define the sedimentary packages and type of geological structures present in the subsurface based on the pre-defined framework of seismo-stratigraphy of Spitsbergen.

During the seismic data processing, removal of strong water bottom multiples was one major challenge. These strong water bottom multiples were generated because of the high velocities in the sea bed, which are around 4000 m/s in the study area. The shallow water depth (100-300 m) leads to short distances between the multiples, which causes the actual arrivals to be masked by multiples. These multiples were removed by different processes applied during the processing flow. A spiking deconvolution filter was used to remove the bubble pulses. The data were then subjected to the multi-channel marine predictive deconvolution, a process that estimates a filter for removal of the water bottom multiples. Shot and receiver assemblies with CDP position were calculated and the rest of the noise present in the data was attenuated by applying various types of filtering such as F-K filtering and time variant BP filtering. In order to improve the signal to noise ratio, some other processes e.g. velocity analysis, pre-stack migration and final frequency filtering were carried out on the seismic data. The processing of the seismic data removed most of the multiple energy and depicts the geological structures in the subsurface down to approximately 2.5 or 3 sec (TWT).

In the second part, the processed seismic data were interpreted with the main focus on identification and investigation of the sedimentary successions, which also helps in obtaining a better understanding of the tectonics of the study area. The identification of different sedimentary successions present in the subsurface was mostly done on the basis of previous studies carried out in the study area. The interpreted sedimentary successions include Carboniferous–Tertiary units (2 sec TWT) lying on the Devonian and deformed metamorphic basement. Poor resolution of the data prevents certain interpretation of the deeper successions and the basement. The deepest reflector interpreted is assumed to represent the top of Hecla Hoek which has been observed in some of the profiles. The presence of sills (dolerite intrusions) was interpreted as a result of reflections with strong amplitudes. These occur from Triassic up to Tertiary, but are more prominent in the Cretaceous succession. The Tertiary deformation observed in the successions is compressional and includes thrusts, backthrusts, imbricates, duplex structures, pop-up structures and fault-bend folds, which suggest complex kinematics. Several decollements are assumed to be present at different levels. The Tertiary succession seems to be more deformed and shortened compared to the Cretaceous and Jurassic successions. This intensity of deformation seems to decrease towards the north, which may indicate the location of the transition to the foreland. The different structures interpreted, such as thrusts, backthrusts, duplex system and thrusts sequences represent very complex geometries which are oblique to the real tectonical transport direction. Therefore, the

actual transport direction is difficult to identify from the interpreted structures. Several possible structure and decollements present in Triassic and Permian remain uninterpreted as a result of poor resolution of the seismic data.

ACKNOWLEDGEMENTS

It would have been next to impossible to write this thesis without my supervisors, professor Rolf Mjelde and senior engineer Bent Ole Rudd, whose help, guidance, encouragement, and supervision from preliminary to concluding levels, enabled me acquire and develop new analytical techniques. I express my deepest gratitude to my supervisors.

I am grateful to all my lecturers in the section of Petroleum Geosciences in UiB, UiO and QAU, for their support, constructive feedback and recommendations. I would always be indebted to you all.

Many thanks go to my friends and course mates in the Petroleum Geology and Geophysics who make up a significant diversity from different continents, and enabled me develop alternative models of thinking and an open minded culture.

My deepest and very special thanks go to my friends, especially Muhammad Farooq, Aamir Ali (Assist. Prof. QAU) and Khalid Abbas. Your moral, emotional, and spiritual support throughout my studies will forever be cherished.

And the last but not least, I am very thankful to my family, my parents for their endless and rewardless efforts and support throughout my life.

Abrar Asghar

November, 2011

Table of Contents

1. INTRODUCTION

1.1 Research objectives

The aim of this research work is to set an initial framework for general understanding of the subsurface structures and tectonics of the area. This involves processing and interpretation of nine 2D multichannel seismic profiles, acquired during the Svalex course of 2008, 2009 and 2010 by University of Bergen. Emphasis was laid on removal of sea bottom multiples which were dominant in the seismic raw data obscuring the seismic reflections. The main objectives can be outlined as follows:

- To perform the seismic processing of the raw seismic data in the field in a way to enhance the signal to noise ratio. This also includes imaging the subsurface to get the useful geological information.
- Interpretation of seismic data in order to identify and define the sedimentary packages present in the subsurface along with geological structures present in the area.

1.2 Study area

The study area is located in western Svalbard (figure. 1.1). The acquisition of the seismic data was done in Isfjorden in central Spitsbergen. Svalbard is an archipelago in the Arctic Ocean, located about midway between Norway and the North Pole at latitude 74° to 81° North and between longitudes 10° to 35° East. The main islands including the study area "Isfjorden" are Spitsbergen, Nordaustlandet, Barentsøya, Edgeøya, Kong Karl's Land, Prins Karl's Foreland, and Bjørnøya. The total area of Svalbard is 62,160 km^2.

Spitsbergen has a complex tectonic history with the latest major tectonic event related to the Tertiary opening of the Norwegian-Greenland Sea. Greenland slid passed Svalbard creating transpressional stresses related to transform movement along the Spitsbergen fracture zone. This resulted in the formation of Spitsbergen fold and thrust belt and a foreland basin in Spitsbergen. Figure (1.2) shows the geological overview and stratigraphic groups in Svalbard.

1.3 Seismic data

The seismic data used for this thesis project comprises a set of nine NNW - SSE trending 2D mutlichannel seismic profiles from Isfjorden, Svalbard (figure 1.3a & b). The seismic data acquisition was done by the Department of Earth Science (UiB) as part of Svalex course 2008, 2009 and 2010 (Mjelde, 2008 & 2009; Svalex cruise reports). Few of the profiles shot in 2009 were just repeated in 2010. An additional set of E-W trending multi-channel profiles from Isfjorden has been used for correlation and support for the seismic data interpretation part (Mjelde, 2008; cruise report).

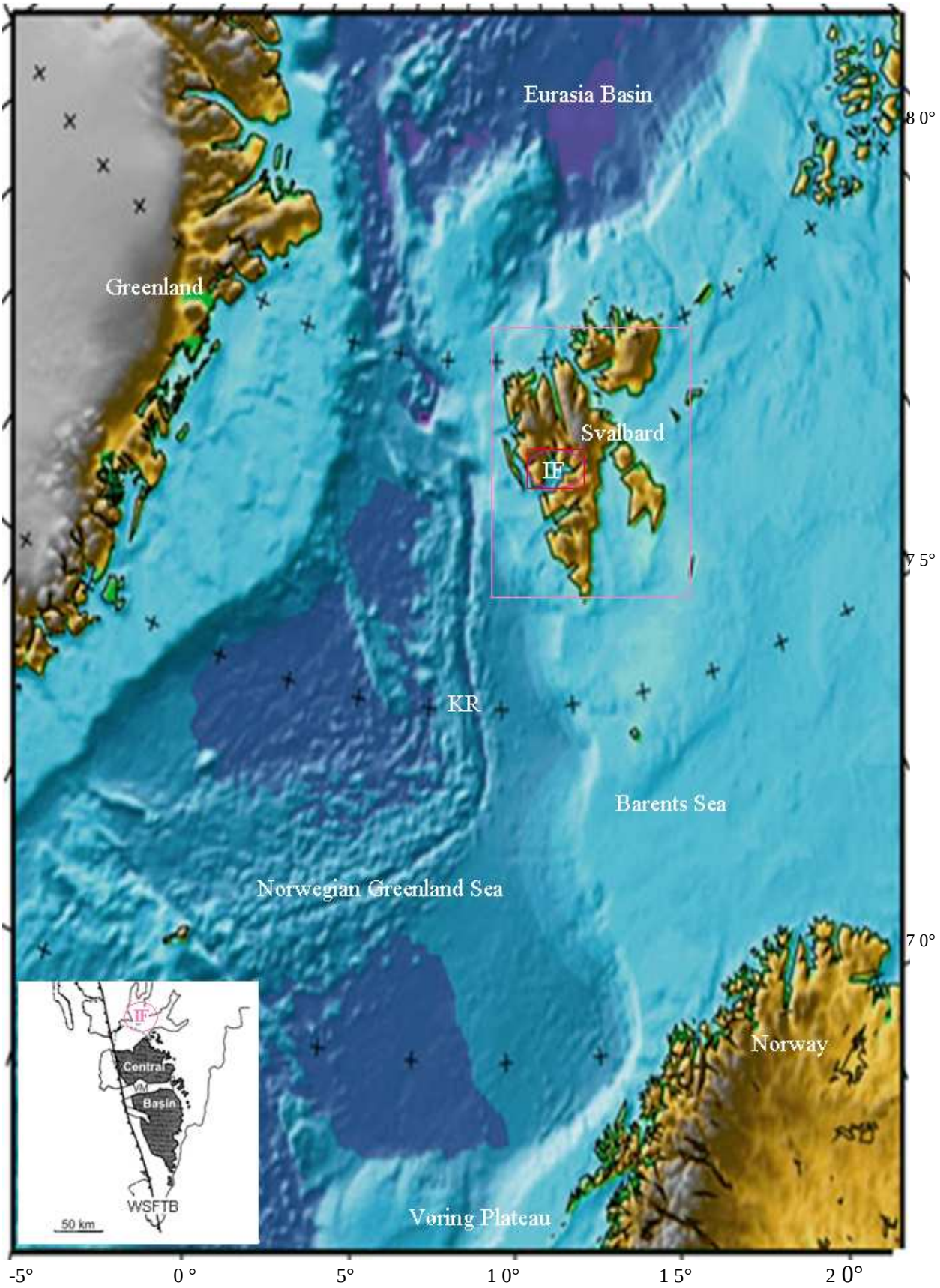

Figure 1.1: Map showing the location of study area and the surrounding areas (regional settings, (bathymetry/topography)). The study area is located within the red circle. In the inset view, the image defines the Western Spitsbergen fold and thrust belt (WSFTB, (bold line)) and the dark area shows the Spitsbergen Central Basin. KR = Knipovich Ridge, IF = Isfjorden, modified from Faleide et al. (2010).

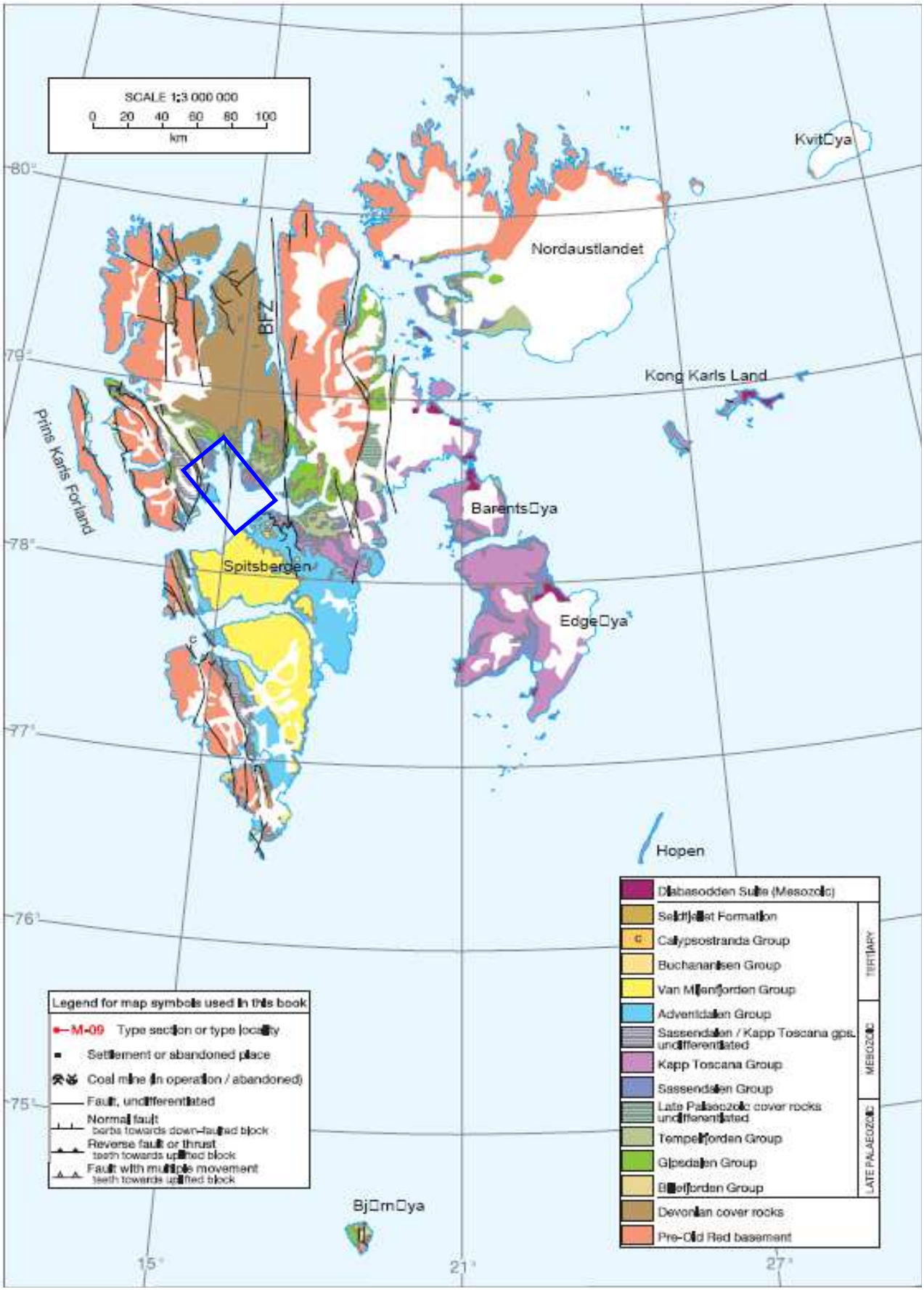

Figure 1.2: Map showing the geological overview with litho-stratigraphic groups and major lineaments. The blue rectangle marks the location of the study area. BFZ = Billefjorden Fault Zone (modified from Dallmann, 1999).

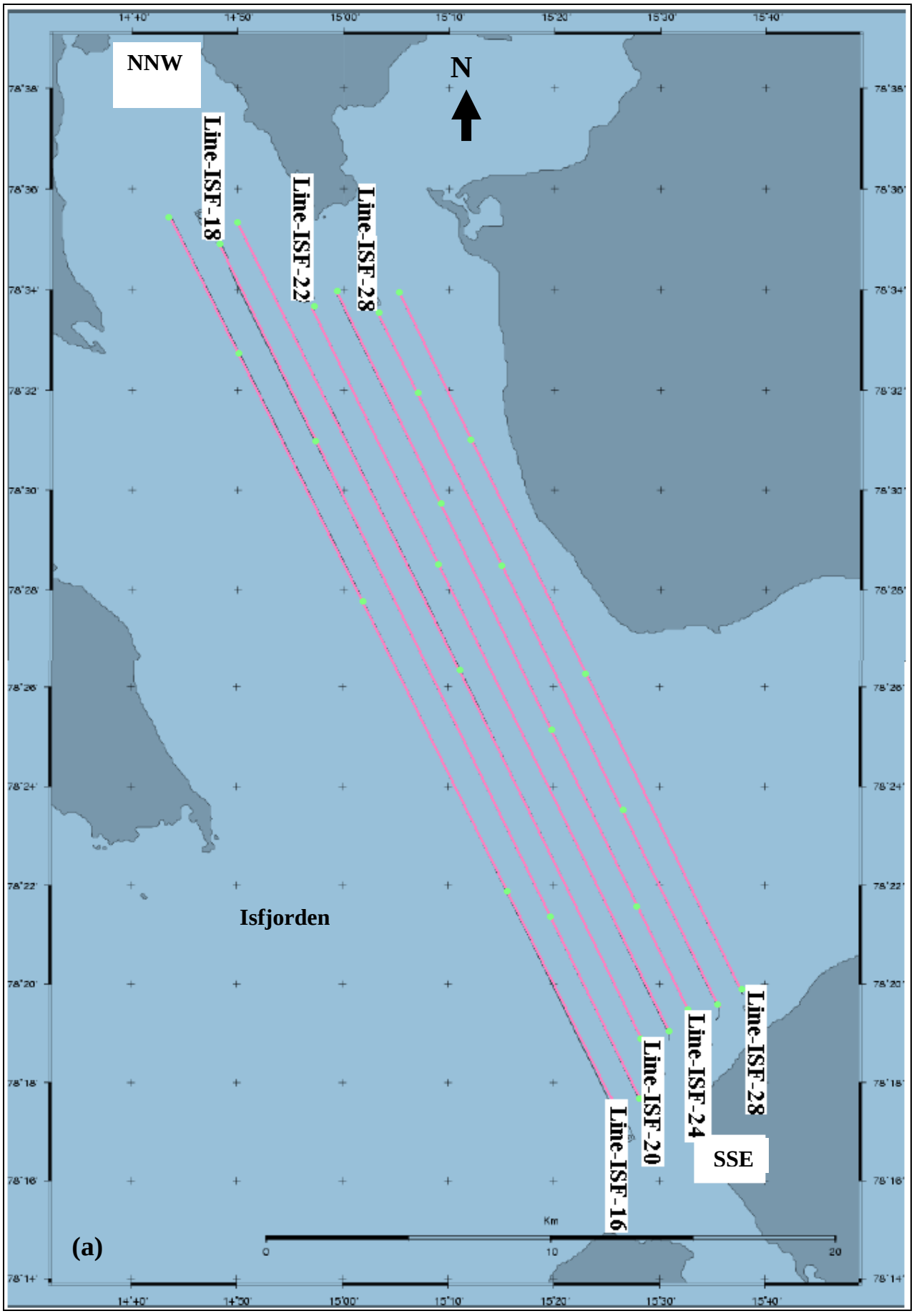
NNW
N
Line-ISF-18
Line-ISF-22
Line-ISF-28
Isfjorden
Line-ISF-28
Line-ISF-24
Line-ISF-20
Line-ISF-16
SSE
(a)
Km
0
10
20

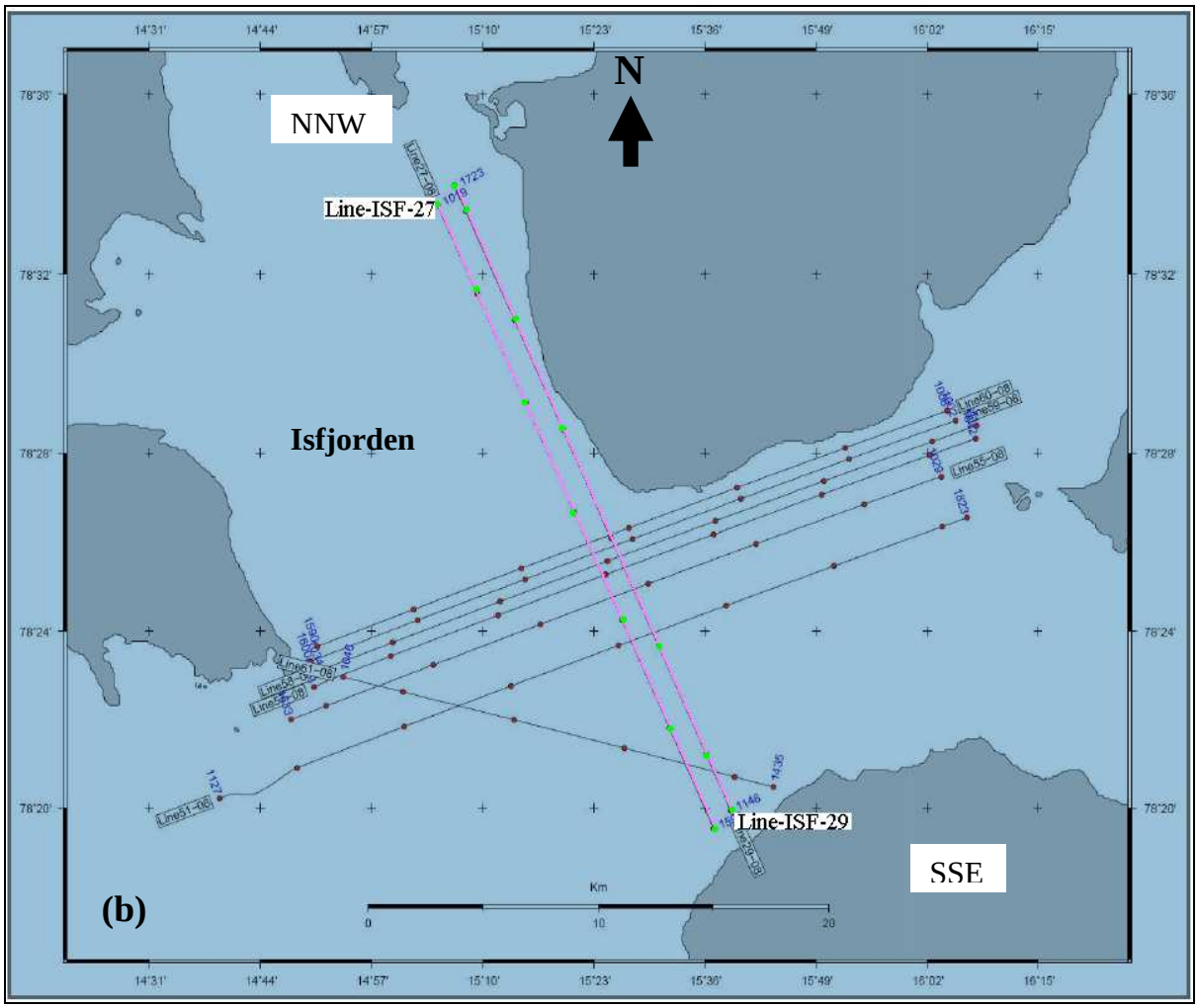

Figure 1.3: The location of multi-channel seismic profiles collected in Isfjorden under the Svalex, 2009 & 2010 (figure 1.3 a) and 2008 (figure 1.3b). The red marked lines were used in this study project for the processing and interpretation, and that the other lines were used as support in the interpretation (modified from Mjelde, (2008 & 2009); cruise reports).

2. GEOLOGICAL BACKGROUND OF SVALBARD

2.1 Introduction

Svalbard has a very rich, diverse and long geologic history that makes it appealing for geologists. It is a place where a great variety of geology can be studied and much can be learned about the development of tectonic features and sedimentary environments through time as well as the drift of continents across the Earth's surface. Svalbard is situated at the uplifted north-western corner of the Barents shelf. A more or less complete stratigraphical succession ranging from Late Precambrian to Early Tertiary is present in Svalbard. The oldest till deposits on Svalbard were probably deposited when Spitsbergen was situated close to the South Pole, some 600 million years (MY) ago, and the red Devonian sandstone of northern Spitsbergen was deposited when Svalbard was close to the Equator, some 350-400 MY ago. Figure (2.1) shows the simplified geology, structural lineaments of Svalbard and the distribution of strata in geological time scale. Since the vegetation cover is so sparse and the glacially eroded landscape so fresh, there are continuous bedrock sections that span more than 11 km (Hjelle, 1993; Ingólfsson, 2004).

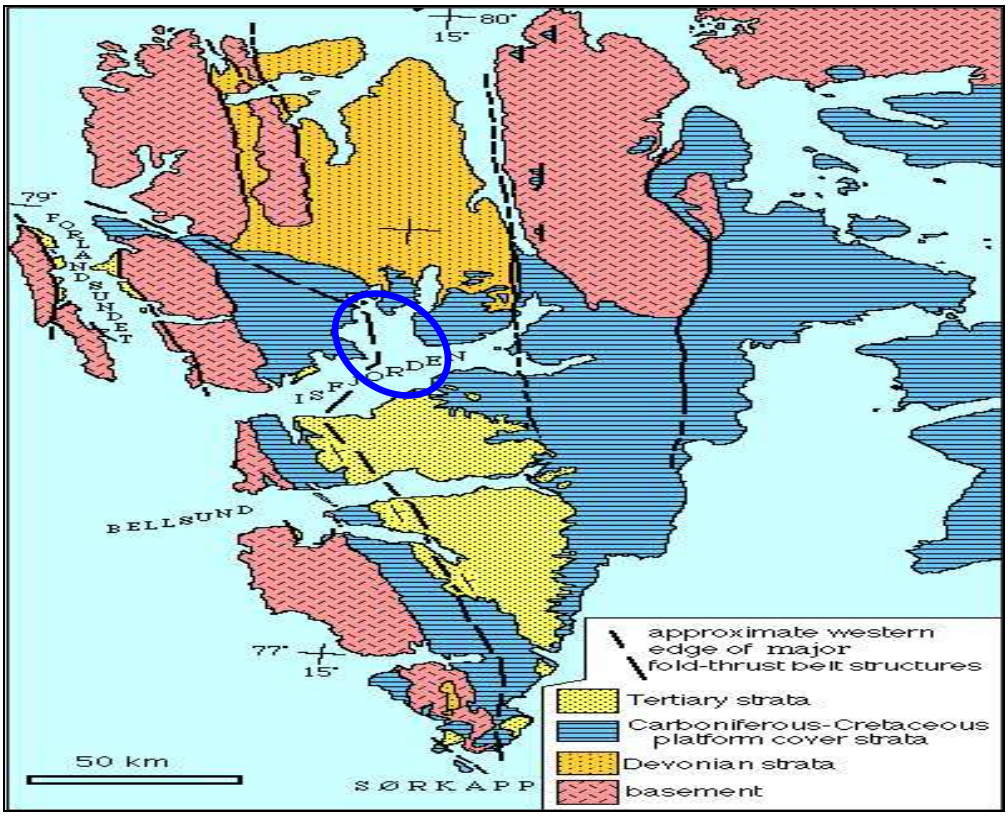

Figure 2.1: Map of Svalbard showing structural lineaments and strata distribution of Svalbard, blue circle represents the study area (Source: Hjelle, 1993).

2.2 Evolution of Norwegian–Greenland Sea

The western continental margin of Svalbard began to develop when major plate reorganizations took place in the North Atlantic and Arctic at the Palaeocene - Eocene transition, and Greenland commenced relatively northward movements as a separate plate.

(Talwani & Eldholm, 1977; Srivastava, 1978, 1985; Tessonsohn & Piepjohn, 2000). Initially the western Spitsbergen margin developed as a sheared margin and as an obliquely rifted passive margin associated with the Hornsund Fault Zone (HFZ) (figure 2.2), which is parallel to it (Faleide et al., 1996).

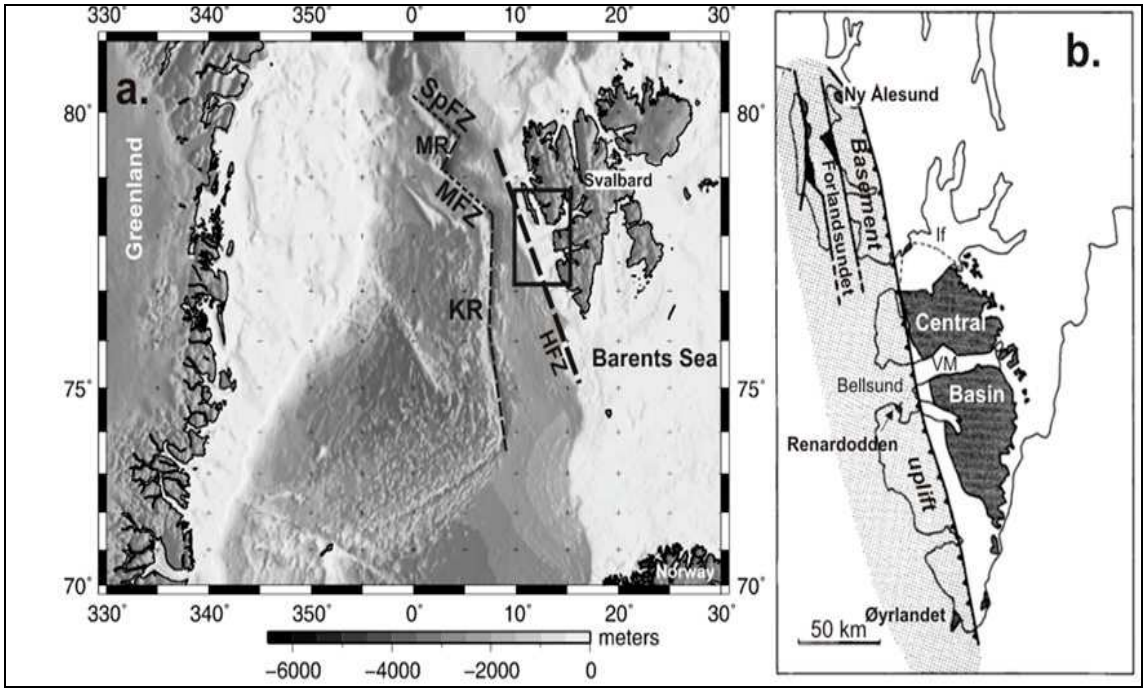

Figure 2.2: (a) Different features like, KR-Knipovich Ridge, MFZ-Molloy Fracture Zone, MR-Molloy Ridge, SFZ-Spitsbergen Fracture Zone, and HFZ-Hornsund Fault Zone. b) Tertiary sediments and location of uplifted basement along the western Spitsbergen. IF-Isfjorden, VM-Van Mijenfjorden, Dark grey colour-Tertiary sediments, Light grey colour-Tertiary fold belt (Faleide at al., 1996; Ritzmann et al., 2002; Manum & Throndsen, 1986).

Since the late Cretaceous, the Spitsbergen continental margin has been affected by the evolution of the North Atlantic region. To understand these phenomena we can divide the evolution of North Atlantic into three stages:

i. Palaeocene stage
ii. Eocene Stage
iii. Oligocene-present

A brief review of theses stages is discussed below:

2.2.1 Palaeocene stage

Before the opening of the Norwegian-Greenland Sea, Greenland belonged to the Eurasian plate and there existed a land bridge between North Greenland and Svalbard (Talwani & Eldholm, 1977); Tessensohn & Piepjohn, 2000). Sea-floor spreading on the western side of Greenland took place in the Early Palaeocene according to the evolution model of the Labrador Sea. Since that time Greenland moved to the northeast, oblique to Ellesmere Island with minor sinistral strike-slip motion along the Nares Strait that is defined as the boundary between the North American plate and Greenland (Srivastava, 1985; Tessensohn & Piepjohn, 2000; Oakey & Stephenson, 2008). The Norwegian-Greenland Sea underwent rifting and

dextral wrench movements along and old zone of weakness during that time, the De Geer Zone, shown in the figure (2.3), (Srivastava, 1978; Faleide et al., 1993).

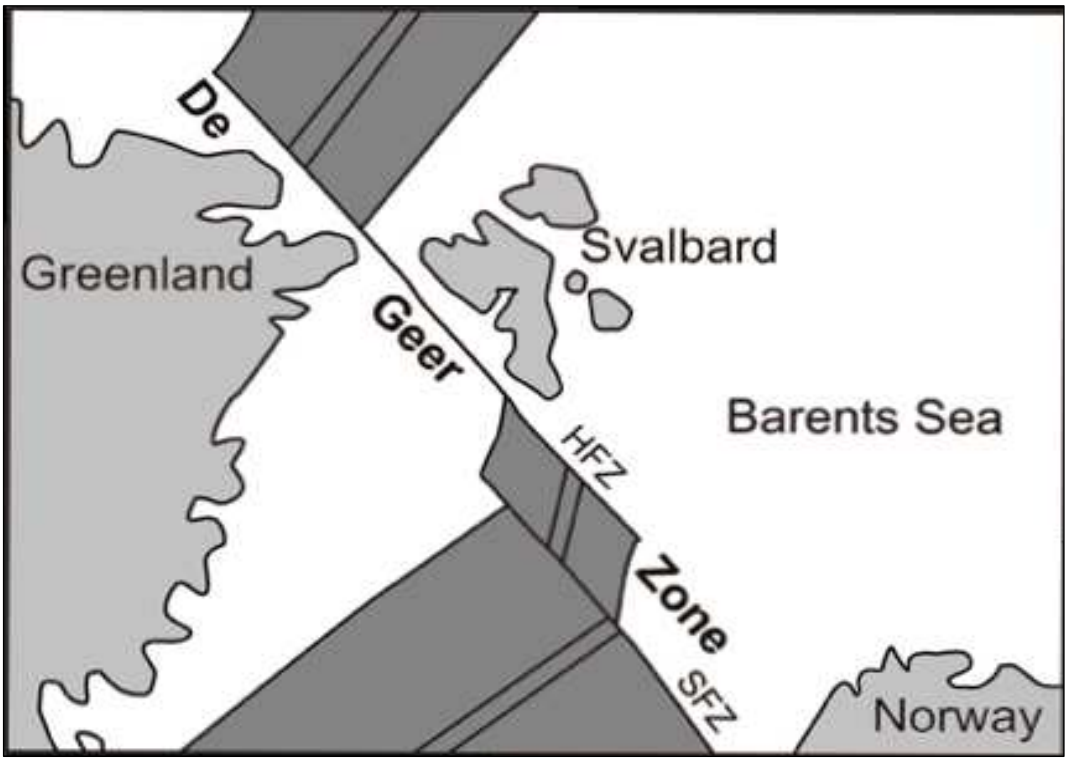

Figure 2.3: The sketch of De Geer Zone during Mid-Tertiary SFZ-Senja Fracture Zone, HFZ-Hornsund Fault Zone (Faleide et al., 1993).

2.2.2 Eocene stage

Reorganization of the plates took place in the North Atlantic and Arctic regions, when the sea-floor spreading began in Baffin Bay, Norwegian-Greenland Sea and in the Eurasian Basin (Talwani & Eldholm, 1977; Srivastava & Tapscott, 1986; Tessensohn & Piepjohn, 2000; Oakey & Stephenson, 2008). The spreading systems of the Labrador Sea/Baffin Bay and Norwegian-Greenland Sea were connected in a triple junction south of Greenland, that started to move northward (Tessensohn & Piepjohn, 2000) as a separate plate oblique to Ellesmere Island and Western Spitsbergen. This caused the main compressive deformation within the Eurekan and West Spitsbergen fold belt systems north of Greenland (Tessensohn & Piepjohn, 2000; Oakey & Stephenson, 2008). During the later stages of West Spitsbergen fold belt (WSFTB) development, formation of synsedimentary graben structures was followed or accompanied by compressive deformation which took place along the western coast of Spitsbergen (Steel et al., 1985).

2.2.3 Oligocene to present

The West Spitsbergen Fold belts and Eurekan became inactive when spreading in the Labrador Sea Baffin Bay system finished in the earliest Oligocene and a transtensional regime took place along the De Geer Zone. Generation of oceanic crust then started between Svalbard and Greenland. Greenland became part of the North American plate and began to move to the

WNW relative to Eurasia (Talwani & Eldholm, 1977; Srivastava, 1985; Srivastava & Tapscott, 1986; Tessensohn & Piepjohn, 2000). Normal faulting, collapse of the earlier compressional structures, down-faulting of blocks on the western side of Hornsund Fault Zone and formation of the final graben geometry happened due to oblique extension along western Spitsbergen since earliest Oligocene (Harland & Dowdeswell, 1988; Myhre et al., 1992). Thinning of the continental crust of the western Svalbard margin occurred due to the extension of the area, causing subsidence and accumulation of a thick pile of Cenozoic sediments on the outer part of the continental shelf.

2.3 Tectonic setting

The tectonic of Svalbard consists of several lineaments, provinces and fault zones as shown in the figure (2.4) e.g. western basement provinces, the central Tertiary basin, the northwest basement province, the Devonian basin, the eastern basement province and eastern Paleozoic and Mesozoic platform area. The provinces are bounded and intersected by several north-south oriented fault zones (Siggerud, 2008).

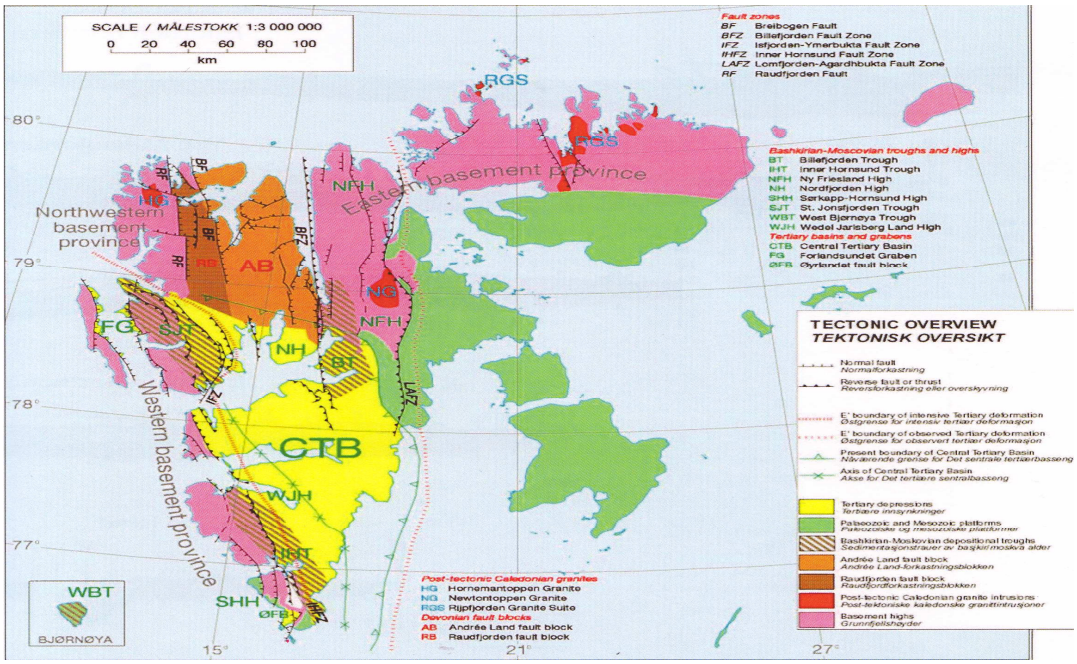

Figure 2.4: The main tectonic lineaments, fault zones and provinces on Svalbard (source Siggerud, 2008).

These fault zones are presented below:

- Lomfjorden-Agardbbukta fault zone.
- Billefjorden fault zone.
- Breibogen fault zone.
- Raudfjorden fault zone.
- Isfjorden- Ymerbukta fault zones.

A small series of horst and graben structures of Carboniferous age are found to be associated with Isfjorden-Ymerbukta fault zone (Siggerud, 2008). Western Svalbard continental margin

is primarily a sheared margin with components of transpression and transtention. Shear movement in the late Devonian and folding in early Tertiary are the two major tectonic episodes that may be considered as the most important episodes in the development of Svalbard (Steel & Worsley, 1984). There has been volcanic activity on the north western part of Spitsbergen in the Tertiary and Quaternary time (Eiken, 1985). The tectonic framework of Spitsbergen is dominated by a series of NNW to SSE oriented lineaments, formed by several tectonic episodes.

The tectonic activity has taken place during most of the geological period but mostly it happened in the earliest and latest phase of sediment deposit period, in Devonian, Carboniferous and early Tertiary (Steel & Worsley, 1984; Eiken, 1985). Based on tectonic and depositional history, the geology of Spitsbergen may be divided into following units:

2.3.1 Pre-old red Basement

The oldest formations, the so-called Basement, including Precambrian, Cambrian and Ordovician rocks occur as a belt along the west-coast of Spitsbergen, in a large area between Wijde-fjorden and Hinlopenstretet in the north, as well as in the northern part of Nordaustlandet and in the southern part of Bjørnøya. The Precambrian bedrock of Svalbard is more than 570 MY old, and there is evidence of repeated mountain-building and metamorphic episodes (Orogenies) dating from ca. 1700, 1000 and 600 MY ago. The mountain chains have disappeared long time ago due to erosion, and what left is the inner and deeper parts of the rocks. The Precambrian rocks on north-western Spitsbergen are generally very strongly metamorphosed. This means that they have once been buried deep in the crust where they melted and re-crystallized due to high pressure and temperature in the subsurface (Hjelle, 1993; Ingólfsson, 2004).

These basement rocks have normally suffered strong movements and alterations. They were folded (figure 2.5), displaced along faults, and partly metamorphosed, (chemically altered under high pressure and temperature) at depth. Those which lie at the surface today may have lain as deep as 20 km below the surface at that time. During the Silurian and Devonian, when the Caledonian mountain chain was uplifted, large portions of the basement came to the surface, while overlying rocks were removed by erosion(Dallmann, 2009).

Figure 2.5: Folded granitic gneisses and amphibolites of Palaeoproterozoic age in the basement rocks of Ny-Friesland (Dallmann, 2009).

2.3.2 Silurian (mountain building)

Folding and faulting on large-scale occurred when two continental plates collided during the Silurian age in the region which subsequently formed the North Atlantic (the Caledonian Orogeny). All rocks on Svalbard that are older than late-Silurian are therefore folded and metamorphosed. Granites intruded in the older rocks during late Silurian. The highest peak on Svalbard is Newtontoppen (1714 m), consists of late Silurian granite. Palaeomagnetic research has shown that at this time Svalbard was located at the Equator. The metamorphic and igneous rocks system, which was the result of the Caledonian Orogeny, is traditionally called the Hecla Hoek series. The name Spitsbergen, meaning the Pointed Peaks, comes from the wild and rugged Hecla Hoek terrain on north-western Spitsbergen (Hjelle, 1993; Ingólfsson, 2004).

2.3.3 Devonian (erosion and sedimentation)

Northern Svalbard began to subside during the Devonian Period and the Caledonian mountains were eroded away by rivers. A total of more than 8000 m thick sandstones, conglomerates and shales were deposited in near-shore environments, deltas and lakes. The Devonian beds often consist of characteristic red sandstone (Hjelle, 1993; Ingólfsson, 2004). The red color implies dry period, desert-like climate. At this time, 360-400 MY ago Svalbard was located just north of the Equator. The Devonian is called “the Age of Fishes”, and fossils of primitive fish, the first known vertebrates have been found on Svalbard.

2.3.4 Carboniferous

Svalbard was a relatively flat and undulating terrain during the early Carboniferous time period, with lakes, lagoons and alluvial plains. The Svalbard plate drifted from desert climate to wetter, more tropical climate during the Carboniferous. Coal seams with plant fossils found in the carboniferous sandstone in the central part of Spitsbergen document swamp vegetation

during that period. Alternating deposition in shallow marine sea and on land occurred on Svalbard during Middle and Upper Carboniferous. Gypsum, dolomite and anhydrate were deposited due to strong evaporation in dry and temperate climate. Gypsum beds, dolomite, limestone and breccia are the typical rocks from that time in Svalbard (Hjelle, 1993; Ingólfsson, 2004).

2.3.5 Permian

Permian beds on Svalbard resemble the Carboniferous upper most beds, with marine shallow water deposits in areas that became dry periodically. Dolomite, anhydrate and gypsum formation got renewed due to intensive evaporation during the dry period. Along the north coast of Isfjorden and Linnedalen these Permian beds are found to have numerous fossils of shells and sponges (Hjelle, 1993; Ingólfsson, 2004). Figure (2.6) shows the regional palaeogeography of the Svalbard and Barents Sea in Late Permian.

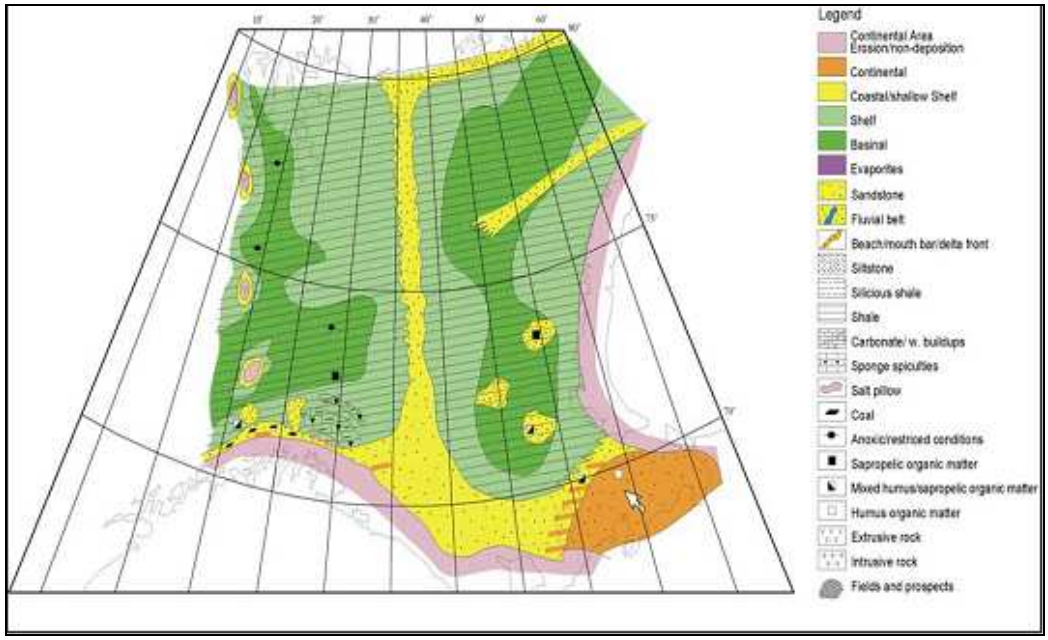

Figure 2.6: The Late Permian regional palaeogeography of Svalbard and Barents Sea (source Worsley, 2006).

2.3.6 Mesozoic

Svalbard drifted from 45^{o}N to about 65^{o}N during the Triassic, Jurassic and Cretaceous Periods. The Mesozoic was considerably globally warmer than at present, and with higher sea levels. The climate of Svalbard was temperate and humid throughout this time. The Svalbard Mesozoic deposits are mostly marine alternating with terrestrial deposits, and volcanic intrusions towards the latter part of the Era. Most of the Svalbard area was covered by a shallow sea during the Jurassic and lowermost Cretaceous. The sedimentary rocks consist mostly of marine shales, often very rich in fossil ammonites, belemnites (squids) and bivalves. Svalbard had extensive sand alluvial plains during the period of early Cretaceous. During that time plants remains preserved abundantly in the sandstone. The remains of

Dinosaurs suggest a mild climate at Cretaceous with abundant vegetation (Hjelle, 1993; Ingólfsson, 2004).

2.3.7 Tertiary (folding and sedimentation)

Svalbard and Greenland collided in the Cretaceous and Tertiary transition periods, some 65-60 MY ago, causing intense folding of the Svalbard west-coast strata, as well as the formation of a depression basin to the east where sedimentation occurred. The geology of the central-southern part of Spitsbergen, from the Isfjorden area to Storfjorden is dominated by the Central Tertiary Basin (CTB). Lower Tertiary deposits in the basin mainly consist of sandstones, with numerous coal seams. The Longyearbyen glacier today erodes a Tertiary coal seam, and plant fossils can be sampled from its frontal moraine. When the plate pressure started to diminish, Svalbard was subject to intense faulting and volcanism. Basaltic lava flows occur on northern Spitsbergen. The climate of Svalbard got successively cooler as a consequence of the slow northward drift, and because of a late Tertiary global cooling (Hjelle, 1993; Ingólfsson, 2004).

2.4 Central Spitsbergen Basin (CSB)

The Central Spitsbergen Basin is a foreland basin that was formed when Greenland slipped past the opening of the Svalbard North Atlantic resulting in trans-pressional and trans-tensional movements in the Eocene period (Steel & Worsley, 1984). The Central Spitsbergen Basin is approximately 200 km long and 60 km wide and is bounded by Lomfjorden fracture zone to the east and West Spitsbergen Fold and Thrust belt in the west. The Central Spitsbergen Basin (CSB) is characterized by various Tertiary settings (Steel et al., 1985). There was greatest sediments infill (schematic example shown in figure 2.7). These sediments were transported dominantly from west when the Central Spitsbergen Basin (CSB) was marked by transtensional stresses in the early to middle Palaeocene (Steel et al., 1985).

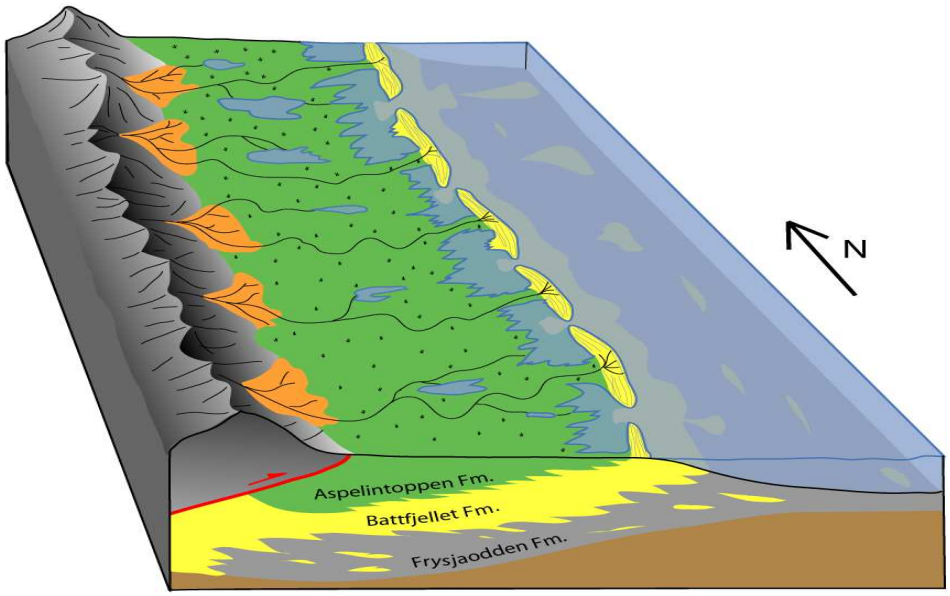

Figure 2.7: A schematic illustration of the infill of Tertiary foreland Basin (modified from Helland-Hansen, 1990).

Due to the uplift of the western margin of Central Spitsbergen Basin (CSB) there was a significant change in the tectonic setting from Palaeocene to early Eocene. The Central Spitsbergen Basin (CSB) can be considered as a foreland basin from Palaeozoic time, with a mixed cyclic infill of continental and marine clastic deposits (Steel et al., 1985; Nøttvedt, 1993a).

2.5 West Spitsbergen fold and thrust belt (WSFTB)

The West Spitsbergen folds and thrust belt (WSFTB) is one of the main geological features located along the western coast of Spitsbergen. The formation of the West Spitsbergen Fold and Thrust belt is related to Cretaceous-Tertiary compressional-transpressional deformation, which was induced by relative movements of the American and Eurasian plats during the opening of North Atlantic (Talwani & Eldholm, 1977; Srivastava, 1985; Johansen et al., 2007 & Faleide et al., 2008). As a result, the Central Spitsbergen basin (CSB) formed, it also caused the 50 km wide and 300 km long fold and thrust belt (figure 2.8) along the western coast of Spitsbergen (Eiken, 1985; Steel et al., 1985).

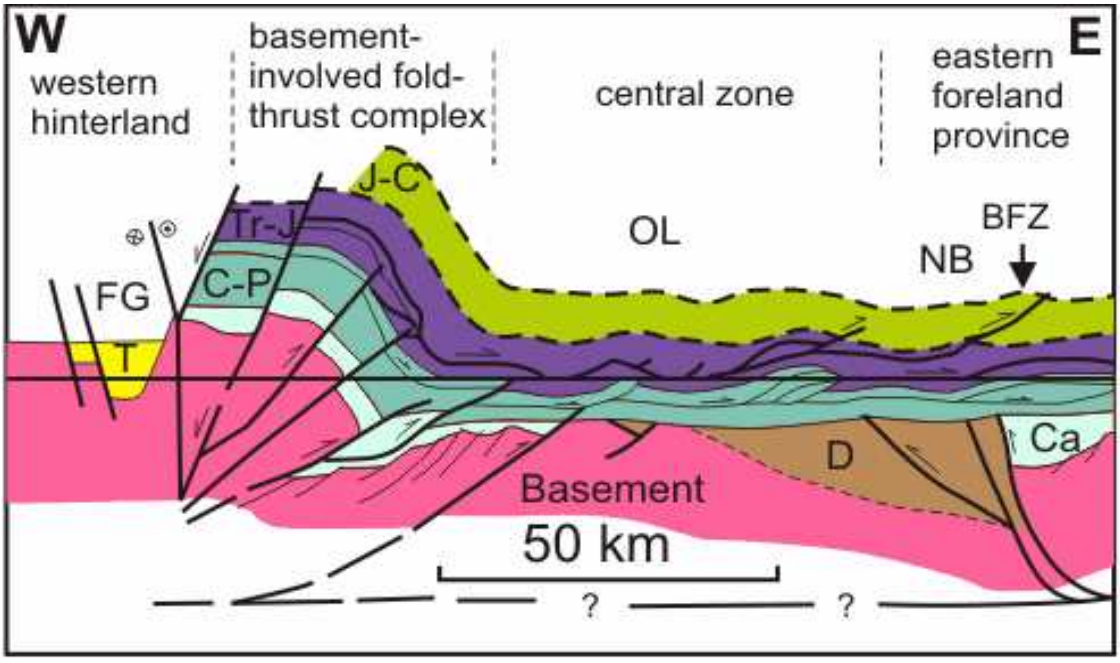

Figure 2.8: The generalized cross section of the WSFTB. FG-Forlandsundet Graben, OL-Oscar II Land, IF-Isfjorden, NB-Nordfjorden block. T-Tertiary, J-C Jurassic and Cretaceous, Tr-J – Triassic and lowermost Jurassic, C-P-Carboniferous and Permian, Ca-Lower-Middle Carboniferous), D-Devonian (from Braathen et al., 1999).

The opening of the Norwegian-Greenland Sea occurred, when the reorganization of major plates took place in the North Atlantic and Arctic caused the Tertiary tectonic activity along the western Spitsbergen (Talwani & Eldholm, 1977; Srivastava & Tapscott, 1986; Tessonsohn & Piepjohn, 2000). The West Spitsbergen Fold and Thrust belt formation was associated with uplift and erosion in the area along the western coast of Spitsbergen and clastic sediments accumulation in the Central Tertiary Basin (Steel et al., 1985; Dallmann, 1999). Sediments, deposited in the Tertiary Central Basin are deltaic deposits of the Van Mijenfjorden Group (Steel &Worsley, 1984; Ohta, 1992).

The Tertiary deformation was dominated by compression in ENE-WSW direction and this deformation was transferred in Paleozoic and Mesozoic strata (Dallmann, 1999). The slope of the southern post Caledonian strata leads to the deeper decollement of southeast Spitsbergen (Bergh & Anderson, 1990). The West Spitsbergen Fold and Thrust belt can be divided into different zones having different tectonic nature. The Eocene to Oligocene development of the fold belt also includes the formation of small sedimentary basins with a more complex structure in the westernmost part of the area (Dallmann, 1999). In the west of Svalbard a passive continental margin was formed when the Greenland continental plate was separated from Svalbard in the post Eocene (Steel & Worsley, 1984). Figure (2.9) shows some of the structural features related to the fold and thrust belt.

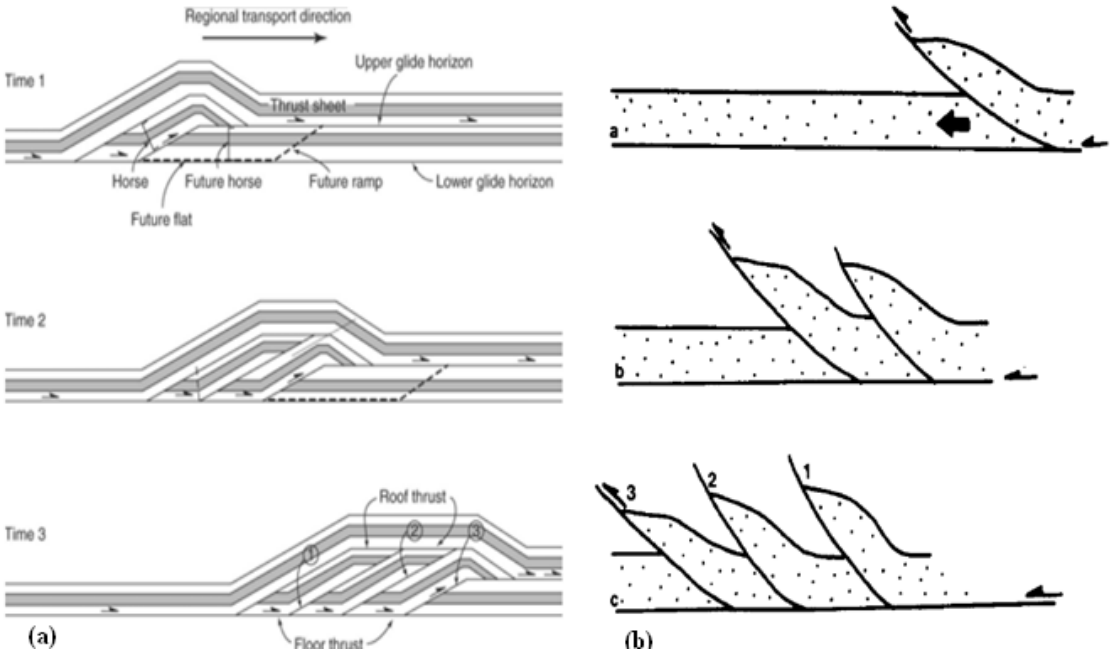

Figure 2.9: (a) Schematic model for duplex structures developed by break – forward faulting (Pluijm & Marshak, 2004; (b) sequential development (a – c in time) of a piggy – back thrust sequence (Butler, 1982).

2.6 Stratigraphic setting

During the late Devonian, also called the "Svalbardian deformation" and Tertiary Orogeny huge amount of sediments were deposited on Svalbard. This sedimentary package was affected by different tectonic regimes along the eastern, western and northern margin of the continental shelf. Local and regional variations in sea level had a great impact on the sediment deposition history of the area (Worsley, 2008). The stratigraphy and sedimentary facies development was significantly impacted by continental drift and also by the changes in climate.

The stratigraphy of Svalbard (figure 2.10) is a more or less continuous record over a period of the past 2.5 billion years, which traditionally have been divided into three depositional phases separated by major deformational episodes. These depositional phases along with major Stratigraphic groups are presented below:

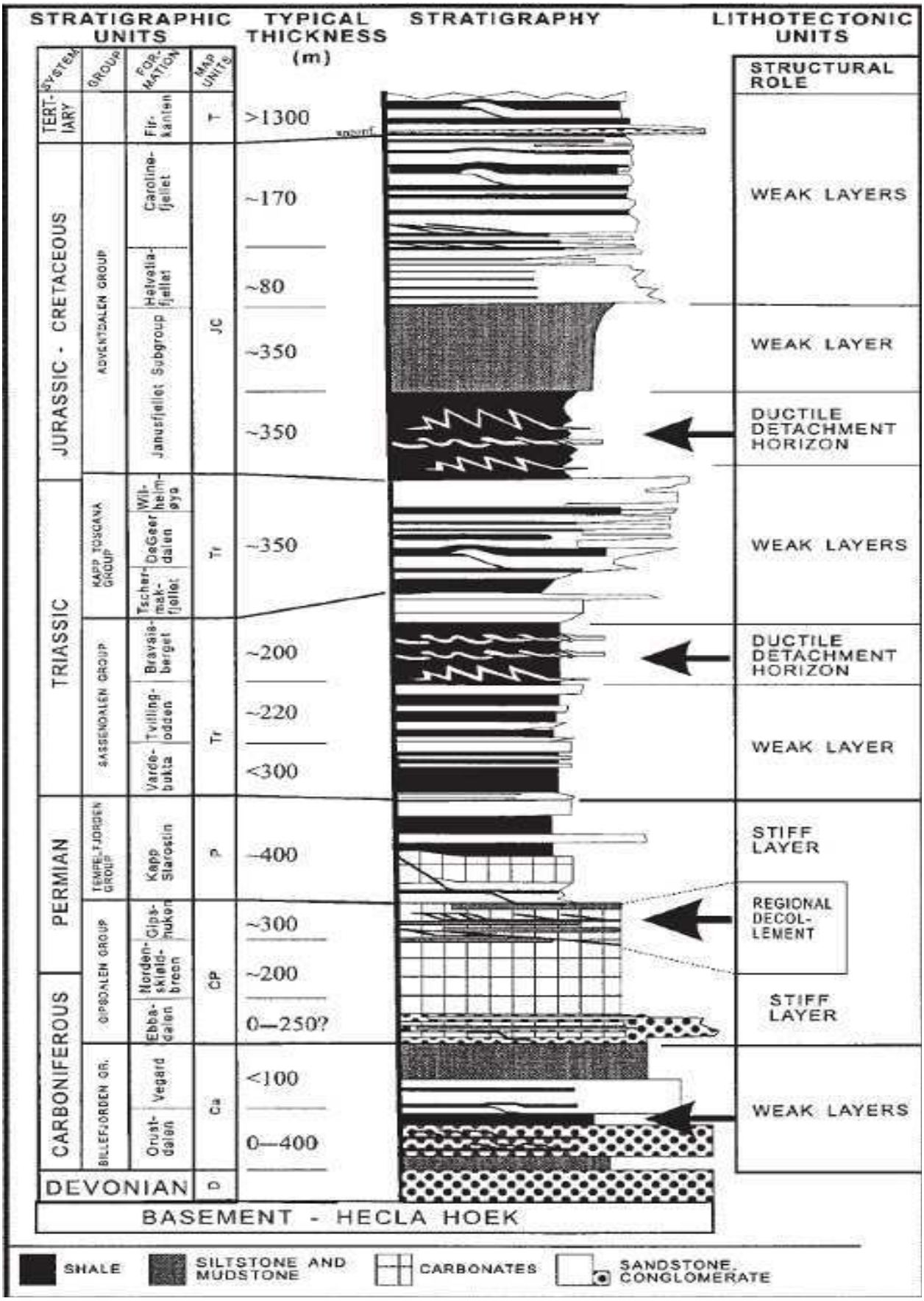

Figure 2.10: Stratigraphy column explaining the stratigraphy of Svalbard with age, group, formation names, thickness and structural properties (Braathen et al., 1999).

2.6.1 Pre-Caledonian sequence

Hecla Hoek-Pre Caledonian Group: The bed rock of Spitsbergen defines the deformed and metamorphosed sequence. This sequence can be distinguished from the overlying Paleozoic, Mesozoic and Tertiary sequences by an unconformity (Steel & Worsley, 1984).

2.6.2 Post-Caledonian including the old red Devonian sandstone

Old red Molasses group: These sediments were mostly deposited in grabens during a period of extensive erosion after the Caledonian orogeny. The thickest sequence is the Devonian of the Nordfjord –Block of central Spitsbergen (Steel & Worsley, 1984).

Billefjord group: This group consists of terrestrial rocks such as conglomerates, sandstone and shale. These sediments were deposited from late Devonian to late carboniferous period (Dallmann, 1999). Carbonate sediments with thickness up to 2 KM were deposited in braided rivers and on flood plains (Steel & Worsley, 1984).

Gypsum valley and Tempelfjorden group: This group consists of late Carboniferous to middle Permian carbonate and evaporate deposits. It is distinguished by a sharp erosive contact from the overlying Tempelfjorden Group that is mainly a carbonate and siltstone formation deposited from middle to late Permian (Steel & Worsley, 1984).

Sassendalen and Kapp-Toscana group: This group having rocks from Triassic age is divided in two groups, (1) Sassen Valley, (2) Cape Tuscany. The Sassendalen group consists mainly of marine shale with layers of silt and sandstone deposited from early to middle Triassic. It is characterized by coastal and delta depositional environment in the west while further east on Svalbard and in the Barents Sea it is characterized by mudstone with high content of organic matter (Steel & Worsley, 1984; Dallmann, 1999).

Adventdalen group: Adventdalen Group lies on the Cape Tuscany group having rocks from Jurassic and Cretaceous period. The Adventdalen Group can be divided into three subgroups, (1) Janus Mountain subgroup with lithology of shales deposited in open marine environment. (2) Helvetiafjellet formation that was deposited in deltaic environment mainly consists of sandstone. (3) Caroline Mountain Formation having alternating layers of shale, silt and sandstone (Steel & Worsley, 1984; Dallmann, 1999; Eiken, 1985).

2.6.3 Early Tertiary succession

Van Mijenfjorden group: The Van Mijenfjorden group mainly consists of sandstone, siltstone and slate deposits of Tertiary age in the central Spitsbergen (Steel & Worsley, 1984; Dallmann, 1999).

3. SEISMIC ACQUISITION METHOD

Seismic methods are widely spread to exploration problems involving the detection and mapping of subsurface lithological boundaries. These methods are well suited to the mapping of layered sedimentary sequences and therefore, it is widely used in search of oil and gas. The importance of the seismic methods over other geophysical methods as mentioned by Robinson & Coruh (1988) is due to its accuracy, resolution and presentation. In addition to oil and gas prospecting, the seismic methods are also employed for the:

- Measurement of the bedrock depth
- Ground water investigation
- Geotechnical purpose
- Investigation of lithospheric structures

3.1 Seismology vs seismic

The seismology science comes from the study of naturally occurring earthquakes. Today the understanding of the earth's mantle, crust, and core is based on the analysis of seismic waves that are produced by the earthquakes. Geologists and seismologists have also discovered that the man made seismic waves has more practical use: probing the shallow structure of the earth to help locating the underground water, minerals and hydrocarbon resources. Seismic data acquisition is just one stage of this, while the full process is known as seismic surveying that involves four stages: Planning and survey design, seismic data acquisition, data processing and data interpretation. This chapter deals with the fundamentals of data acquisition to gain the basic knowledge that is necessary to plan a survey. One must have a grasp of seismic wave's physics and data processing steps to understand the various techniques for data acquisition (Evans, 1997). The aim of seismic acquisition and processing is to deliver the products that mimic the cross-section through the earth. In order to fulfil this, correct type and amount of data is required. For the oil industry today it is highly unusual to drill the exploration wells before the seismic data being shot, processed and interpreted (Bacon et al., 2003).

3.2 Basic seismic reflection theory

Geophysicists use the same basic principle and physical properties for seismic surveying as the earthquake seismologists do. Usually low energy acoustic waves are mechanically generated and they are directed in to subsurface. The energy travels through the water and into the rock layers, some part of energy is reflected back to the surface from different layers of rocks beneath, due to acoustic impedance contrasts generally occurring where the lithology changes. The upcoming waves are captured by sensitive instruments called seismic receivers within a log cable towed behind the boat (figure 3.1). They record the strength of the waves and time it has taken to travel through the rock layers and back to the surface. These recordings are then taken to various adjustments done by computers, and the data are then transformed into visual images that give a picture of what the subsurface looks like beneath

the survey area. So the seismic survey is used to get a picture of the structure and the nature of the rock layers in the subsurface indirectly (Bacon et al., 2003).

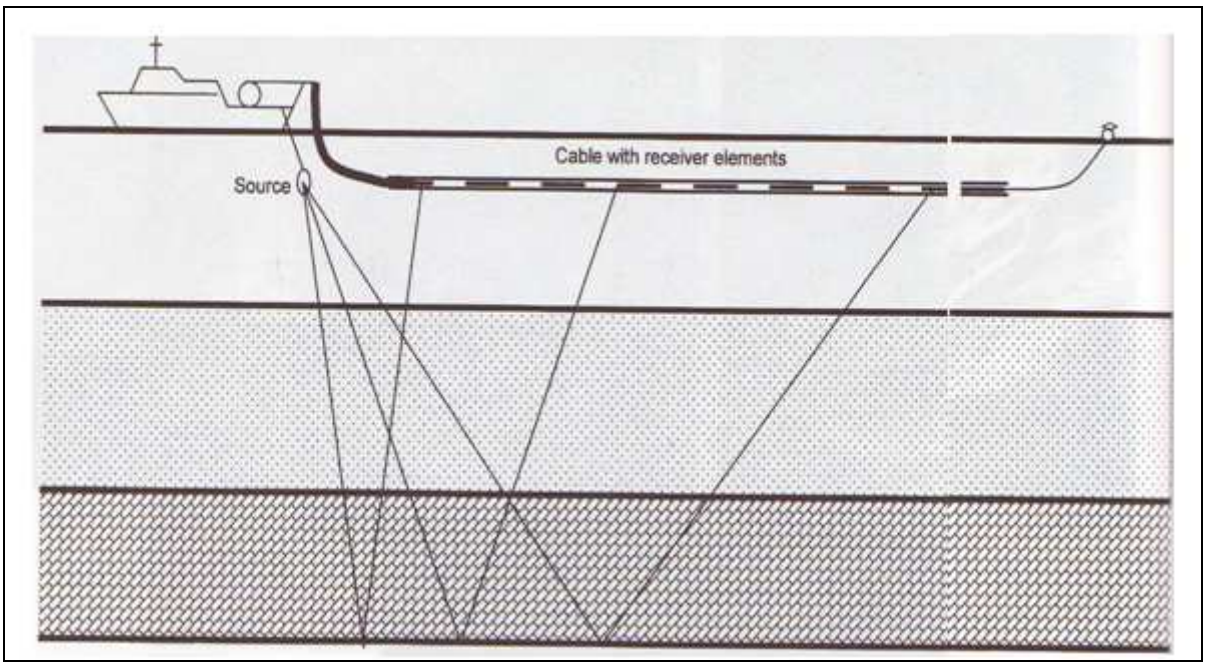

Example: Reflection points between the single shot and receivers.

Figure 3.1: The basic marine acquisition. The boat travels through the water and fires the source every 25-50 m (Bacon et al., 2003).

3.3 Marine data acquisition

Generally marine data acquisition is faster and simple than land acquisition. For standard marine seismic data acquisition a purpose-built boat is used to tow one or more energy sources and one or more cables with a group of hydrophones (figure 3.1) in a streamer (Bacon et al., 2003). The equipment is towed behind the vessel at a steady pace with the source closest to the vessel of approximately at 5 to 15 meter depth and streamer with an offset near source (Sheriff & Geldart, 1995). The seismic streamer detects the low level of reflection energy that travels from the seismic source through the water layer and rock layers in the subsurface and back to the surface where they are recorded by hydrophones. The hydrophones are pressure sensitive devices which convert these pressure signals into electrical energy, which are then digitized and transmitted along the seismic streamer to the recording system on the vessel where the data is stored on magnetic tapes for further processing.

3.4 Survey design and planning

The geological structures are easier to understand along the dip directions as compared with the strike directions when a 2D profiles are acquired. So the dip lines are more important than strike lines in 2D data recording. 2D Data recorded in the direction other than dip direction can be confusing to interpret. Consequently the general information about the basin, like basin shape, orientation or structure depends on the correct positioning of the lines. In a new area

the seismic lines should be recorded both in the dip and strike directions because while interpreting the data the conjunction of strike line with the dip lines helps making the coherent picture of geology of the area. The Line spacing depends on the nature and prospect of the survey (Evans, 1997).

The range of seismic surveys varies from tens of square kilometres to several hundreds or thousand of square kilometres for exploration purposes. To achieve this aim, the surveys are needed to be planned to cover the adequate area of interest. The actual recorded data must cover an area that is larger than the target area by migration aperture (figure 3.2). Also the trace spacing needs to be small in all directions to avoid aliasing. The subsurface coverage should be uniform with a consistency between the contribution of different offsets and azimuths (Bacon et al., 2003).

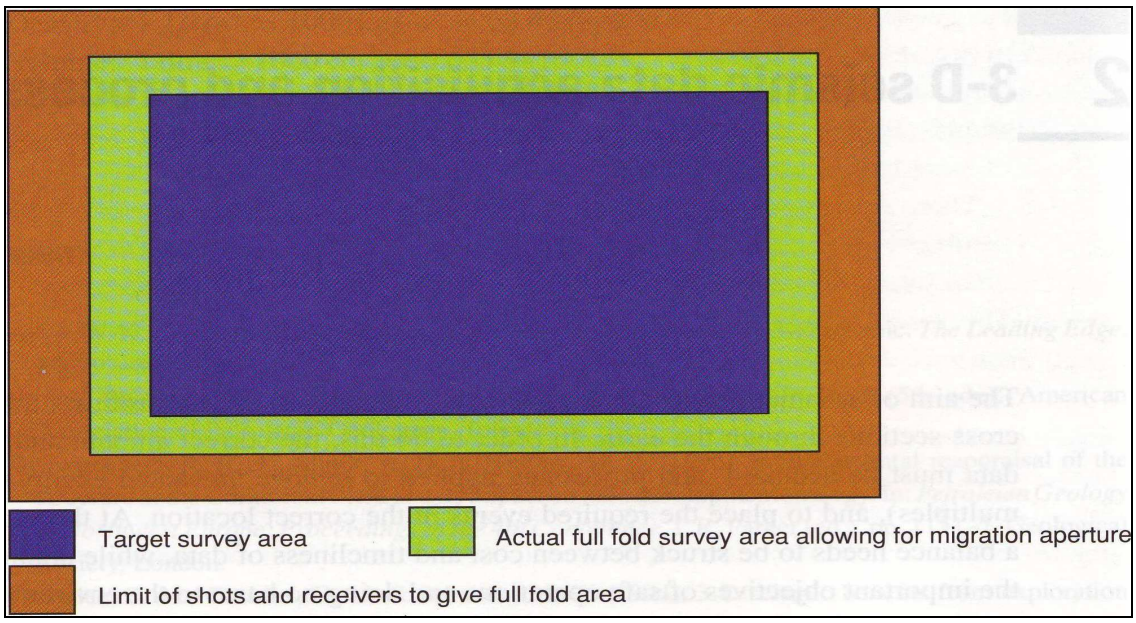

Figure 3.2: The relationship between the acquisitions and target area (Bacon et al., 2003).

3.5 2D and 3D seismic data acquisition

Seismic surveys operations can vary in complexity. There are two main types of seismic acquisition surveys, two dimensional or 2D explorations and three dimensional or 3D explorations. The 2D survey method may be considered as a basic, inexpensive and simple survey method that is still in use and very effective to find oil and gas. On the other hand 3D surveying is a much more accurate and complex method which involves greater investment and much more sophisticated equipment than 2D survey (IAGC, 2002).

3.5.1 2D acquisition

In 2D acquisition method, a single seismic streamer is towed behind the seismic vessel together with a single source. The subsurface reflections are supposed to lie directly below the sail line traversed by the seismic vessel. Seismic 2D lines are acquired typically several

kilometres apart over a large area. These days 2D method is used generally in frontier exploration areas before 3D method and drilling, to make the general understanding of the regional geological structures of the area.

3.5.2 3D acquisition

A 3D seismic survey covers an area that generally represents a known geological target from a previous 2D survey. Careful planning is undertaken to make sure that survey area is precisely defined. The detailed planning result will be a map defining the survey boundaries and direction of survey lines. The line separation in 3D surveys is of the order 200 to 400 meter normally. By using more than one source and many parallel streamers towed behind the vessel many closely spaced subsurface 2D lines can be achieved by a single sail line. A 3D survey is more efficient since it generates much more data than 2D surveys. 3D surveys have become a preferred method for providing geological subsurface information.

3.6 Seismic source and receiver

3.6.1 Seismic source

A number of seismic sources can be used for the collection of seismic data e.g. air-guns; water guns and marine vibrators. The source selection depends on the scale of the image. A collection with different volumes of air guns is used for imaging the upper few km of the crust. The air gun consists of two chambers with high air pressure; a control or upper chamber and discharge chamber (figure 3.3a).

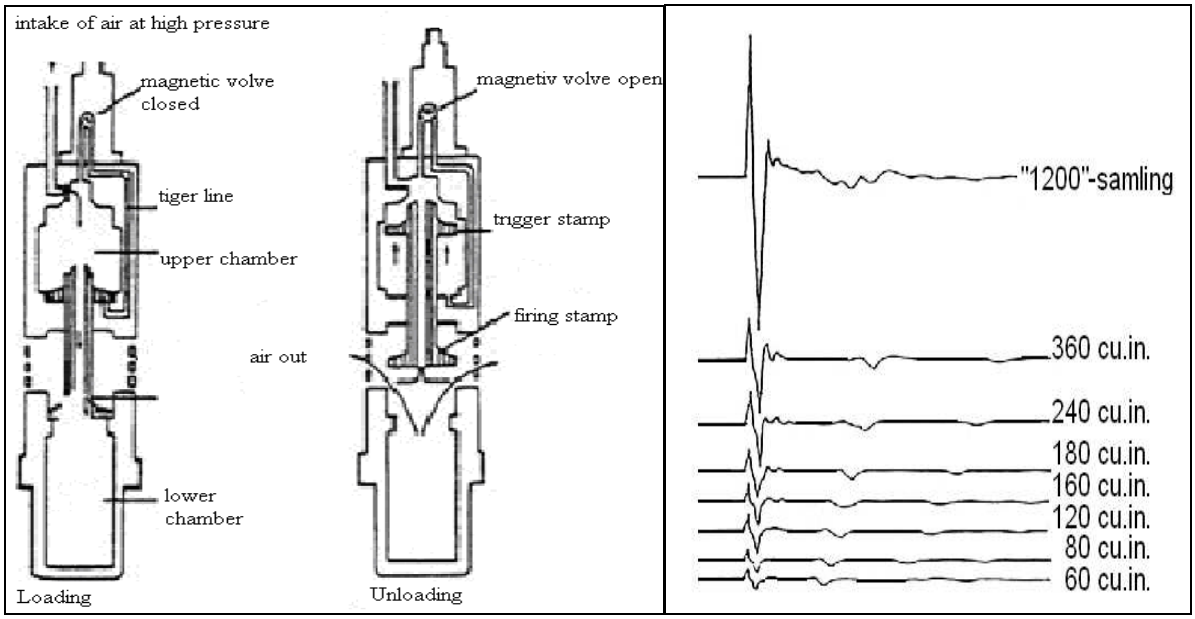

(a) (b)

Figure 3.3: (a) The functioning and parameters of air-guns. (b) A series of air guns with volume 60 to 1200 cu.in.source signal interfere in a constructive way to make the signal stronger and reduce the bubble pulse effect (Mjelde, 2003).

High pressure air is discharged into the surrounding water from the firing chamber, generating the air bubbles. These bubbles oscillate alternately, collapse and expand and rise to the surface where the recording devices record the pressure of these bubbles as input (Sheriff & Geldart, 1995). The amplitudes of the generated pulse can be increased by using a collection of air-guns. It also reduces the bubbles pulse effect, when the volume of the air-guns varies (figure 3.3b). Apart from that it also increases the directivity by using the collection of air guns. In marine data the ghost multiple is the energy that is reflected from the surface directly from the source. The source and receiver's depth is adjusted to create positive interference between down going wave and ghost, so that it could help to strengthen the signal.

3.6.2 Seismic receiver

In marine seismic data acquisitions, the device which is used to detect the seismic signal is called a hydrophone. The hydrophone consists of two piezoelectric plates in a copper cylinder. These plates are located opposite to each other with reverse polarity. If such a plate is placed in an environment experiencing changes in pressure, it will produce a voltage that is proportional to that pressure (Evans, 1997). So based on this principle these hydrophones record the pressure variations and convert them into electrical signals after summing. The responses of hydrophone plates to acceleration due to unsteady streamer towing and the pressure due to seismic signals are explained in the (figure 2.4). While acquiring the seismic data these hydrophones are mounted in a streamer and connected with a cable having a group length of 6.25, 12.5, 25 or 50 meters (Sheriff & Geldart, 1995).

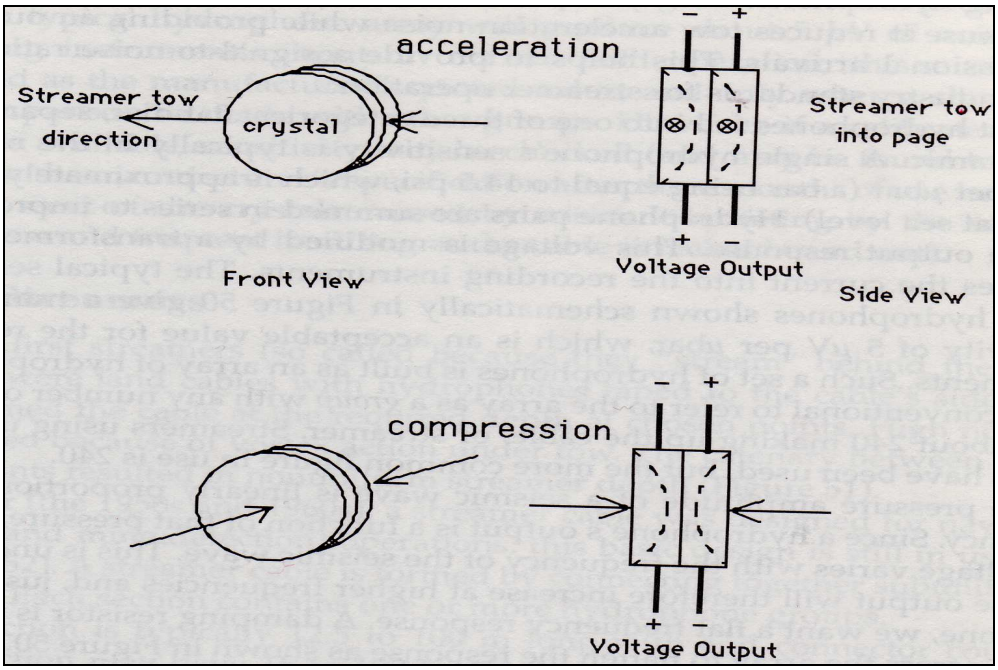

Figure 3.4: The hydrophone response to acceleration and compressional waves (Evans, 1997).

4. DATA ACQUISITION AND PARAMETERS

The following chapter describe the different parameters used to acquire the data and technical information about the data set used for this study project. The data set consists of nine multi-channel 2D seismic profiles (figures 1.3a & b) collected from Isfjorden, Svalbard in 2008, 2009 and 2010. All the collection parameters obtained from the acquisition fields reports (Mjelde, 2008, 2009, 2010). Profiles 27 and 29 were acquired in Aug, 2008, while the rest of the 7 profiles were collected during, 2009 and 2010, covering an area approximately 125 square km. Some of the profiles recorded in 2009 were just repeated in 2010.

4.1 Geophysical and acquisition parameters

Below are the acquisition and geophysical parameters, used to record the data for this study project.

Svalex, 2008; Profiles 27& 29

Table 4.1: Acquisition parameters for the seismic profiles in 2008 (Mjelde, 2008).

Vessels----------R.V. Håkon Mosby
Digital Streamer (Western Geco, Nessie 3) ----------2.9 Km
Shot- point interval----------50 m
Recording length----------12 second
Air-gun depth----------8 m
Tuned air-gun array----------Leg I &II: 6 Bolt air-gun, total volume: 1.406 inch3
Tuned air-gun array----------Leg III &IV: 4 Bolt air-gun, total volume: 1.256 inch3
Triac Recoding---------- (Western Geco)
Group length----------12.5 m
Streamer depth----------10 m
Distance from GPS antenna to center of source, leg I &II----------58 m
Distance from GPS antenna to center of source, leg III &IV----------62 m
Distance from GPS antenna to first active channel ----------154 m
Recording filter----------3Hz (18dB/octave), 180Hz (72 dB/octave)
Lacoste-Romberg gravity meter.
Marine proton magnetometer (digital).

Svalex, 2009, 2010: Profiles 16, 18, 20, 22, 24, 26 and 28

Table 4.2: Acquisition parameters for the seismic profiles in 2008 (Mjelde, 2009 & 2010).

Digital Streamer (Western Geco, Nessie 3) ----------3 Km
Shot- point interval----------50 m
Recording length----------12 second
Air-gun depth----------6 m
Triac Recoding---------- (Western Geco)
Four Bolt air-gun----------300+240+136+90 inch3=8766 inch3
Group length----------12.5 m
Streamer depth---------- 8 m
Distance from GPS antenna to center of source----------36 m
Distance from GPS antenna to first active channel ----------136 m
Recording filter----------3Hz (18dB/octave), 180Hz (72 dB/octave)
Lacoste-Romberg gravity meter.
Marine proton magnetometer (digital).

4.2 Geographical coordinates of profiles

Table 4.3: The geographical coordinates (latitude, longitude, easting, and northing and shot point) for the SOL (start of the line) and EOL (end of the line) for all the profiles used for this thesis project in data processing and for interpretation as well. All profile lie in the zone 33xWGS 84 (Svalex reports, 2008, 2009 & 2010).

Line	Shot number	Latitude	Longitude	Easting	Northing
ISF-16(SOL)	8	78.2921	15.4251	509630	8691006
ISF-16(EOL)	746	78.5915	14.7226	493876	8724394
ISF-18(SOL)	9	78.5823	14.7988	495555	8723363
ISF-18(EOL)	720	78.2936	15.4690	510624	8691174
ISF-20(SOL)	3124	78.3140	15.4724	510681	8693451
ISF-20(EOL)	3826	78.5892	14.8291	496226	8724126
ISF-22(SOL)	8	78.5608	14.9509	498913	8720952
ISF-22(EOL)	613	78.3144	5.5158	511663	8693509
ISF-24(SOL)	9	78.3241	15.5472	512361	8694599
ISF-24(EOL)	604	78.3241	14.9869	499710	8721526
ISF-26(SOL)	8	78.5588	15.0557	501234	8720729
ISF-26(EOL)	589	78.3211	15.5896	513323	8694277
ISF-27(SOL)	1019	78.3332	15.442	501737	8720766

ISF-27(EOL)	1593	78.1932	15.3659	513927	8694783
ISF-28(SOL)	7	78.3297	15.6319	514270	8695239
ISF-28(EOL)	588	78.5659	15.0859	501902	8721530
ISF-29(SOL)	1148	78.1956	15.6910	514681	8695548
ISF-29(EOL)	1723	78.3358	15.641	502465	8721574

The lines did not shot in sequence. This is done to avoid sharp turns that generate much noise in the receivers when the stream is flexed. Also sharp turns increase the chance that streamer gets out of position are cut off or interfere with the source. The sources are to some extent "wide": it is not directive in the input line-level, will to some extent reduce energy towards the sides. The following figure (4.1) shows the source configuration of source and receivers for Svalex, 2008.

Svalex, 2008

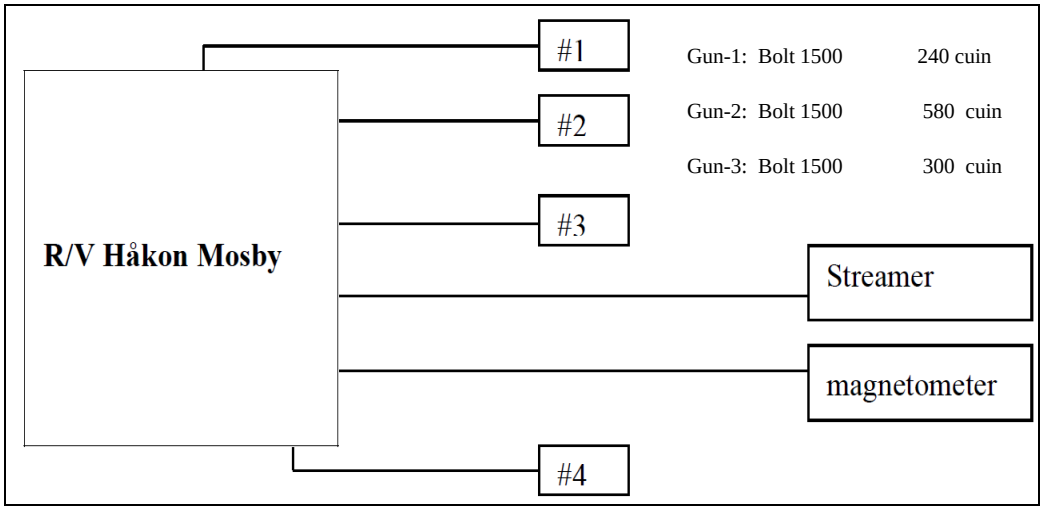

Figure 4.1: Source and receiver configuration for the profiles acquired during 2008 (Mjelde, 2008).

5. SEISMIC PROCESSING METHOD

5.1 Introduction

Data processing is an approach by which the raw data recorded in the field is enhanced to the extent that it can be used for geological interpretation. In other words data processing is a sequence of operations, which are carried out according to a pre-defined program to extract useful information from a set of raw data. Generally, the objective of seismic data processing can be summarized as follows:

- To enhance the signal to noise ratio of the raw data.
- To display the results in the form of seismic sections, from which geological information of the subsurface can be obtained.

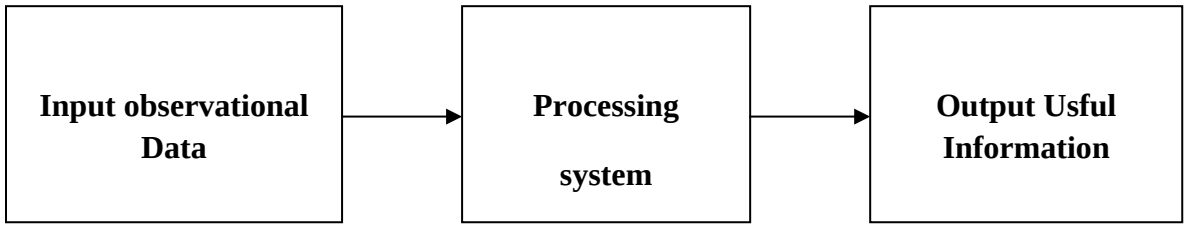

Figure 5.1: As an input - output system in which the input raw data go through the processing system to give useful output information.

The seismic reflections become weaker as the depth of the investigation increases, so these reflections are needed to be strengthened by digital processing of the data (Robins & Coruh, 1988). Seismic field recorders generally record the seismic data on magnetic tapes. These tapes are then transferred to the data processing centre where they are subjected to a sequence of computer programs for improving the signal to noise ratio. The strategies and results of seismic data processing are greatly affected by data acquisition parameters. The most widely used technique is common-midpoint (CMP) recording. Quality of the data also depends on the surface conditions, environmental and demographic restrictions. The main steps in seismic data processing are being discussed below:

5.2 Reformatting and editing

At this stage the data is normally stored in one of the designated industry formats to make the raw records form a basis for later processing possible. Reformatting includes converting the data from industry format into another format that the processing system uses.

Editing involves the removal of traces that are either dead or contains much noise, due to for instance technical problems in a hydrophone. Poor traces are removed as early as possible in the processing and replaced with interpolated traces or these poor traces are set to zero. Editing also means to reverse the polarity, if necessary (Bacon et al., 2003)

5.3 Designature

In marine seismic data, the output signals with a main peak are followed by smaller secondary peaks due to re-expansion of the air bubble. These bubble pulses are unwanted since every

reflection is followed by a smaller repetition of itself. The process of designature removes the secondary peaks and converts the wavelets in more compact form. At this stage it is decided whether the output data should be the minimum- phase or zero-phase (figure 5.2). A zero-phase wavelet is one which is symmetrical about its centre, while a minimum-phase wavelet is one which starts at time zero and has as much energy near the start as physically possible (Bacon et al., 2003).

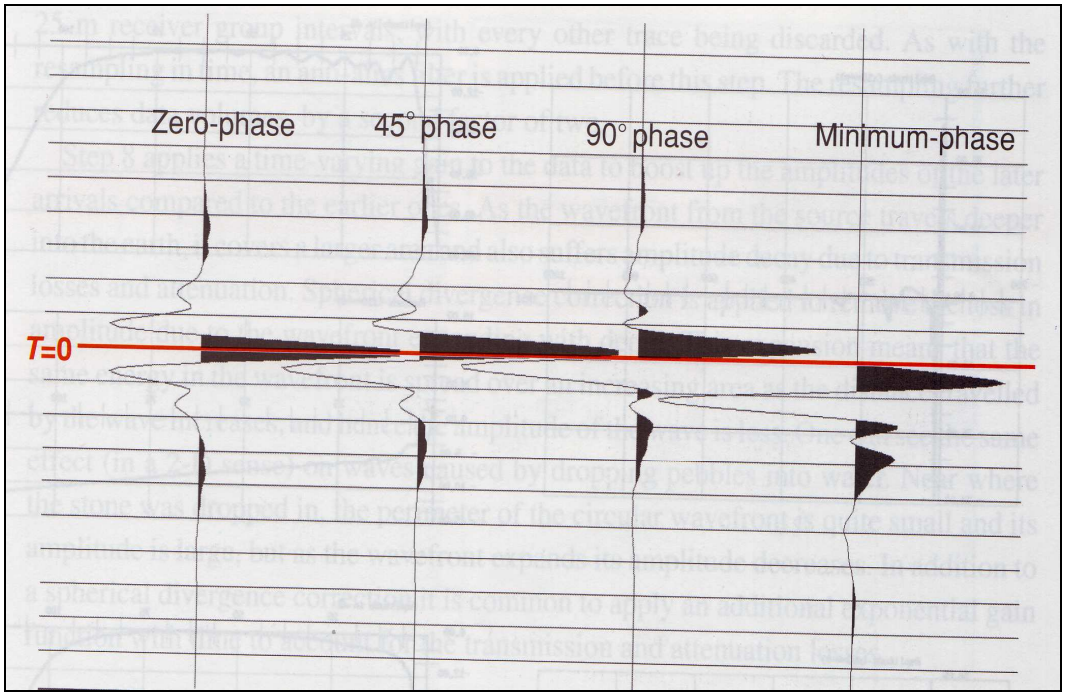

Figure 5.2: Comparison of zero phase and minimum phase wavelets. The zero-phase wavelet with their phase rotated by 45° and 90° are also shown. The desired output from the seismic data processing is usually a seismic section which represents the earth reflectivity convolved with a zero-phase wavelet, because such a wavelet has greatest resolution for any bandwidth (Bacon et al., 2003).

5.4 Gain recovery

Time-varying gain is applied to the data to boost up the amplitudes of the data at greater depth (later arrivals) when compared to the earlier arrivals. As the wavefront moves deeper into the earth it covers a larger area, and in addition it suffers from amplitude decay because of transmission losses and attenuation. To remove the loss in energy due to wavefront expansion with depth, a spherical divergence correction is applied (Bacon et al., 2003). If r is the radius of the wavefront, energy is given by the following relation:

$$\frac{E}{4\pi r^2}. \tag{5.1}$$

When the distance increases the energy will decrease with r^{-2} due to geometrical spreading. The amplitude is proportional to the square root of the energy so it decreases with r^{-1} (Sheriff & Geldart, 1995). The wave also loses energy every time it hits an interface, the energy splits into a transmission and a reflection. In addition to the spherical divergence correction, it is common to

apply an additional exponential gain function that accounts for transmission and attenuation losses (Bacon et al., 2003).

5.5 Filtering of the seismic data

Generally the aim of the seismic data processing is to increase the signal-to-noise ration and improve the vertical resolution of the individual seismic traces. The main types of waveform manipulation are frequency filtering and inverse filtering (deconvolution). Frequency filtering can improve the signal-to-noise ratio but it damages the vertical resolution, conversely the inverse filtering improves the resolution but decreases the signal to noise ratio (Kearey et al., 2002).

5.5.1 Frequency filtering

The data recorded by hydrophones contain not only the real reflections but also various forms of noise. The latter includes high frequency noise e.g. noise produced by electrical cables or heavy machines and low frequency noise produced by waves for example. To remove these types of noise, a frequency filter is designed and applied to allow a desired range of frequency (Yilmaz, 2001).The application of frequency-filtering requires the data in frequency domain (amplitude as a function of frequency), which is achieved using the Fourier transform. The frequency filtering is based on the Fourier transform. The operator usually takes an input image and filter function in Fourier domain. This input image is then multiplied by with the filter function given by the following expression (Hamming, 1983):

$$G(k,l) = F(k,l)H(k,l)\,, \tag{5.2}$$

where $F(k, l)$ is the input image as a function of wave number k and length l in the Fourier domain, $H(k, l)$ is the filter function and $G(k, l)$ is the filtered image.

The common types of filters used in the data processing are low-pass filter, high-pass filter, band-pass filter, band reject and notch filter (figure 5.3). A low-pass filter attenuates high frequencies and retains low frequencies. A high-pass filter, on the other hand, attenuates low frequencies. The band pass, band rejects and notch filters contain/suppress the frequencies within a specified frequency band (Sheriff & Geldart, 1995). Since, frequency decreases with increasing length of travel path due to the attenuation, so the characteristics of the frequency filters are normally varied as a function of reflection travel time. For example in 3s seismic trace, the first second might be band-pass filtered between the limit of 15 and 75Hz and the frequency limit for the third second might be 10 and 45Hz. The choice of the frequency band is made by inspection of the filter panels (Kearey et al., 2002). After applying the frequency filtering the data are again transferred from the frequency domain to the time domain by the inverse Fourier transform (Sheriff & Geldart, 1995).

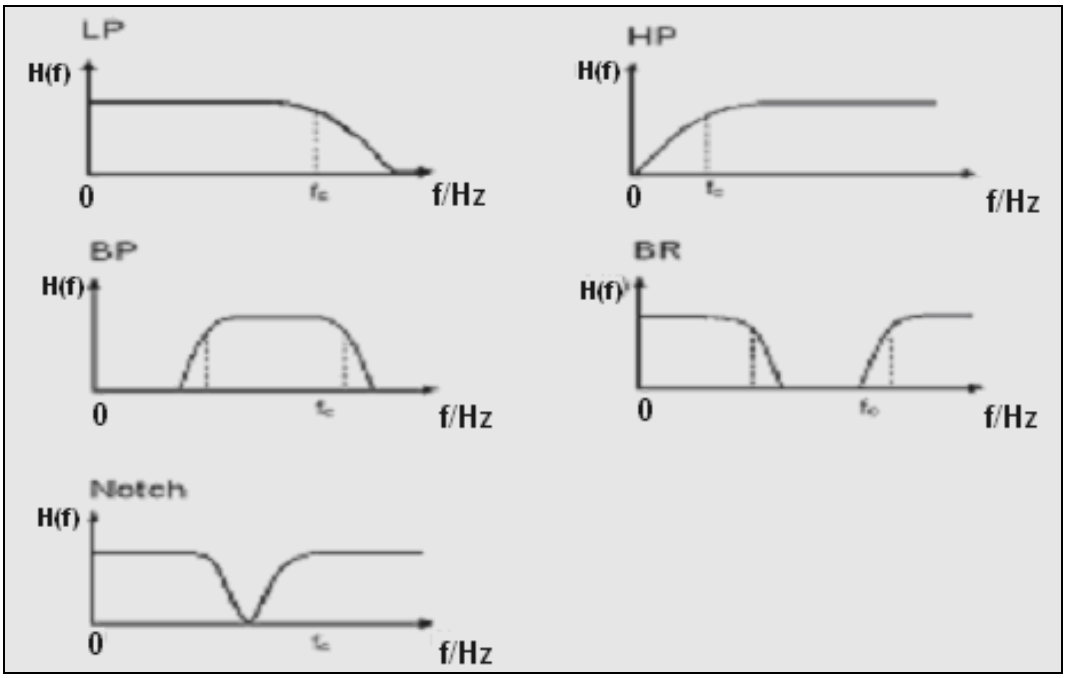

Figure 5.3: The frequency response H(f) for frequency in H(z) for various types of filters such as: band-pass (BP), high-pass (HP), low-pass (LP), band reject (BR) and notch filters (Kearey et al., 2006; Sheriff & Geldart, 1995).

5.5.2 Velocity filtering

The purpose of the velocity filtering is to remove coherent noise events from the seismic data on the basis of angles at which these coherent events dip. A seismic pulse travelling with velocity V at an angle α to the vertical propagates across the spread with an apparent speed given below:

$$V_a = \frac{V}{\sin\alpha}, \tag{5.3}$$

and each individual component of the pulse has an apparent wave number K_a, that is related to its individual frequency f, where

$$f = V_a k_a . \tag{5.4}$$

If the frequency f is plotted against K_a, it will give a straight line curve also known as f-k plot (figure 5.4b). A seismic events propagating across the spread is characterized by an f-k curve with a particular gradient determined by the apparent velocity. The overall set of curves containing reflected and surface events are shown in the (figure 5.4a). Different types of seismic events fall within different zones of f-k plot and this provides a mean to filters the unwanted events on the basis of apparent velocity. This method is known as f-k filtering. To perform velocity filtering seismic data is transformed from t-x domain to f-k domain, and then f-k plot is filtered by removing a wedge-shape zones or zones with unwanted events. Finally the data is transformed back to t-x domain (Kearey et al., 2002).

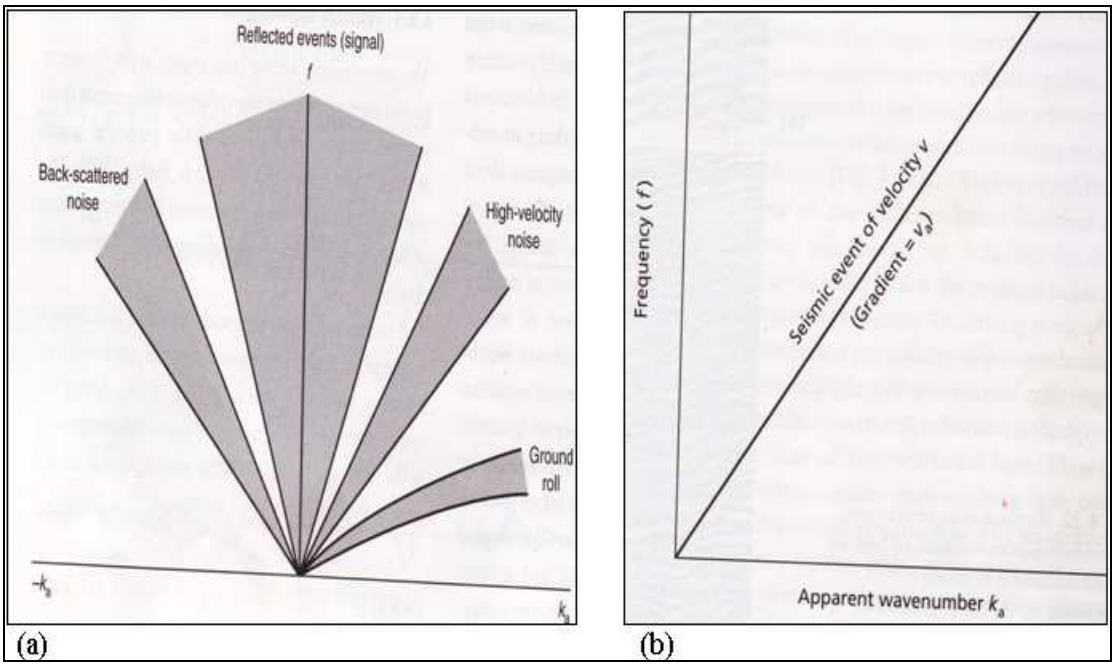

Figure 5.4: (a) An f-k plot for a shot gather decomposed in reflection events and different types of noise. (b) An f-k plot for a seismic pulse passing across the spread of receivers (Kearey et al., 2002).

5.5.3 Inverse filtering (deconvolution)

In the frequency spectrum of a reflected pulse, there are many components of seismic noise that can not be removed by frequency filtering. Inverse filters are able to suppress the noise that have the same frequency character as the reflected signal (Kearey et al., 2002).

Inverse filtering (deconvolution) is the analytical process that sharpens the wavelets and removes the short period reverberations. For this process a digital operator is designed for each trace and that operator is then convolved with each trace to remove the ringing. An operator is designed automatically based on the trace characteristics and then some parameters, like the operator gap, are modified by the processing analyst. The idea is that the operator will not change the wavelet from time zero to the end-time of the gap but try to remove periodicity at times beyond the end of the gap. Deconvolution may be either spiking or predictive. The difference between the two types is the length of the operator gap. In spiking deconvolution there is a very short gap that gives maximal wavelet compression, while in predictive deconvolution there is large gap (32 ms or more) in order to remove the periodicity that is caused by the multiples having period longer than the gap (Bacon et al., 2003).

Examples of inverse filtering to remove particular filtering effects include (Kearey et al., 2002):

- Dereverberations: this application removes the ringing effect associated with multiples reflection in the water layer.
- Deghosting: degosting removes the short path multiple that are associated with the energy travelling upward from the source and reflected back from the surface.
- Whitening: which equalize the amplitude of all frequency components within the recorded frequency band.

Figure (5.5) explains the difference between primary events and multiples. There are several methods or techniques used to remove the multiples based either on velocity move-out or on prediction based on geometry and timing of the cause of the multiple (Bacon et al., 2003).

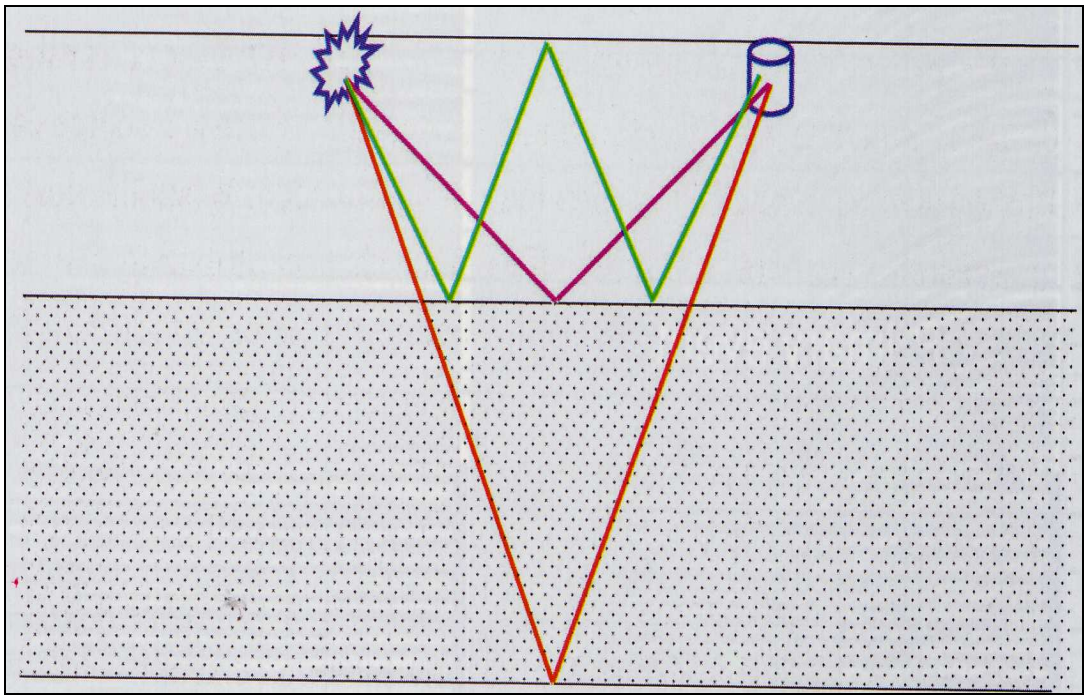

Figure 5.5: Primary and multiple reflections. The red and purple events are primary reflections, while the green events show the first order multiple reflections (Bacon et al., 2003).

5.6 Sorting the data from common shot point (CSP) to common midpoint (CMP)

Seismic raw data are usually sorted by common shot point (CSP) (figure 5.6a). The common practice behind common shot point (CSP) shooting is that a vessel is moving at constant intervals along a line, while shooting at regular intervals. In the subsurface the reflection from various shots depicting the same point is detected by different channels from shot to shot (common midpoint (CMP) (figure 5.6b). The seismic data is sorted to common midpoint (CMP) before stacking.

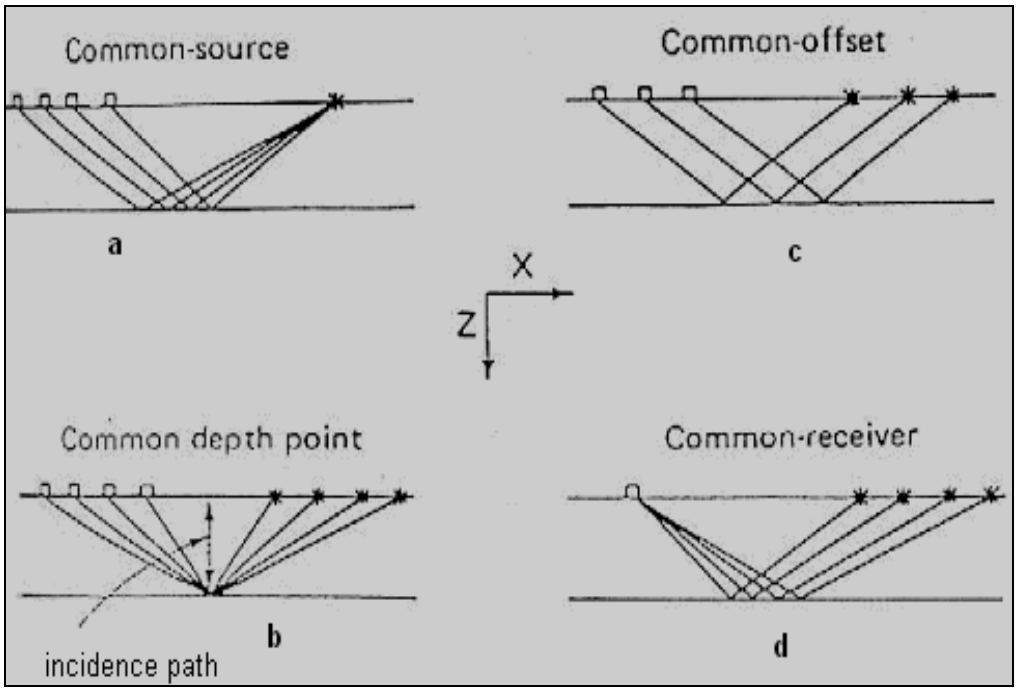

Figure 5.6: Geometry and ray path for different configurations of source and receivers (Sheriff & Geldart, 1995).

5.7 Seismic velocities

Good knowledge of velocities at all points along the reflection path is required for accurate interpretation of the reflections. The accuracy of the data reduction, processing and interpretation depends mainly on the correction of the velocity measurements. Principle objectives of the seismic velocity analysis are:

- Good stacking of the data, in order to increase the signal to noise ratio.
- Appropriate conversion of time section to depth section in order to have structural as well as lithological interpretation.

The most common concepts of velocity are the following (Robinson & Coruh, 1988):

Root mean square (RMS) velocity

When the subsurface layers are horizontal having interval velocities as V_1, V_2, ---, V_n and two way time to the respective interfaces as t_1, t_2, ---, t_n; then the Root Mean Square velocity (V_{rms}) for an n layer model is defined as:

$$V_{rms_n}{}^2 = \frac{\sum_{i=1}^{n}(V_1^2 t_1)}{\sum_{i=1}^{n} t}, \qquad (5.5)$$

V_{rms} may be derived approximately from CDP shooting.

Average velocity

Average Velocity (V_{av}), can be simply obtained by dividing depth (h_n) by its travel time (t_n), where *n = 1, 2, 3---, k.*

$$V_{av} = \frac{\sum_{n=1}^{k} h_n}{\sum_{n=1}^{k} t_n}, \tag{5.6}$$

V_{av} is also measured from the surface down to the reflecting surface.

Interval velocity

The velocity within a chosen time interval and may be expressed as:

$$V_{\text{int}} = \frac{h_n}{t_n - t_{n-1}}, \tag{5.7}$$

where *h* is the layer thickness and *t* is two way travel time. Dix's Interval Velocity is obtained by the Dix Formula (Dix, 1955) given by:

$$V\,\text{int}_{i+1} = \frac{\left[(T_{i+1} Vrms^2{}_{i+1}) - (T_i . Vrms^2)\right]^{1/2}}{(T_{i+1} - T)^{1/2}}, \tag{5.8}$$

T denotes two ways travel time to horizontal interfaces and V_{rms} is the Root Mean Square Velocity.

Stacking velocity

Stacking velocities is the velocity used in the application of normal move out (NMO**)** correction on common depth point (CDP) gathers. The travel time equation for a homogeneous two layer model with flat horizontal interface is written in term of horizontal distance between source and receiver (*X*), velocity (V_{NMO}) for zero offset two way time to the reflection (T_o).

$$T_x = \left(T_o^2 + \frac{X^2}{V_{NMO}{}^2} \right)^{1/2}. \tag{5.9}$$

The stacking velocity V_{NMO} obtained by the equation:

$$V_{NMO} = \left(X^2.(T_x{}^2 - T_o^2\right)^{1/2}. \quad (5.10)$$

Migration velocity

Migration velocity is the velocity that is used to migrate seismic data.

$$V_{mig} = V_{NMO}. Cos\alpha\ , \quad (5.11)$$

α is the angle of dip of the reflector.

5.8 Velocity analysis

Before stacking the correct velocity analysis and NMO correction are required. NMO correction is the correction of travel times of the traces in a CMP gather to make them zero offset. The correct velocity choice is very important, too high velocity results in under correction (bending downward) of the travel times whereas low velocity causes over correction (upward bending) of the travel times (figure 5.7).

Velocity analysis is an interactive tool used to estimate the stacking or NMO velocity on 2D and 3D pre-stack seismic data. The velocity analysis is usually done on CMP gathers where the assumption of hyperbolic move-out of reflections is often reasonable. The analysis procedure may involve comparing a series of stacked traces in which a range of velocities were applied. The aim of the velocity analysis is to find the velocity that flattens a reflection hyperbola and thus provides the best result when stacking is applied (Yilmaz, 2001).

5.9 NMO correction

When the offset (distance between the source and receiver) increases, the travel time for the larger offsets also increases. On the seismogram the effect of this delay in travel time is visible as a hyperbolic curve (figure 5.7a). After interpreting the stacking velocities, we apply the NMO correction, which is the difference in travel time for a receiver at some distance x from the source and the travel time t_o for zero-offset distance.

The receivers with large offset will detect longer travel-time than the traces that are recorded by the receivers close to the source (Yilmaz, 2001). The difference in time is called move-out and to remove this difference, a move out correction (NMO) is applied, where the final result ought to be a horizontal reflector (figure 5.7b). The NMO correction is given by the difference between $t(x)$ and t_o.

$$\Delta t_{nmo} = t(x) - t_o\ , \quad (5.12)$$

$t(x)$ is the two way travel time with a given offset (x) and t_o is the two way travel time with zero-offset.

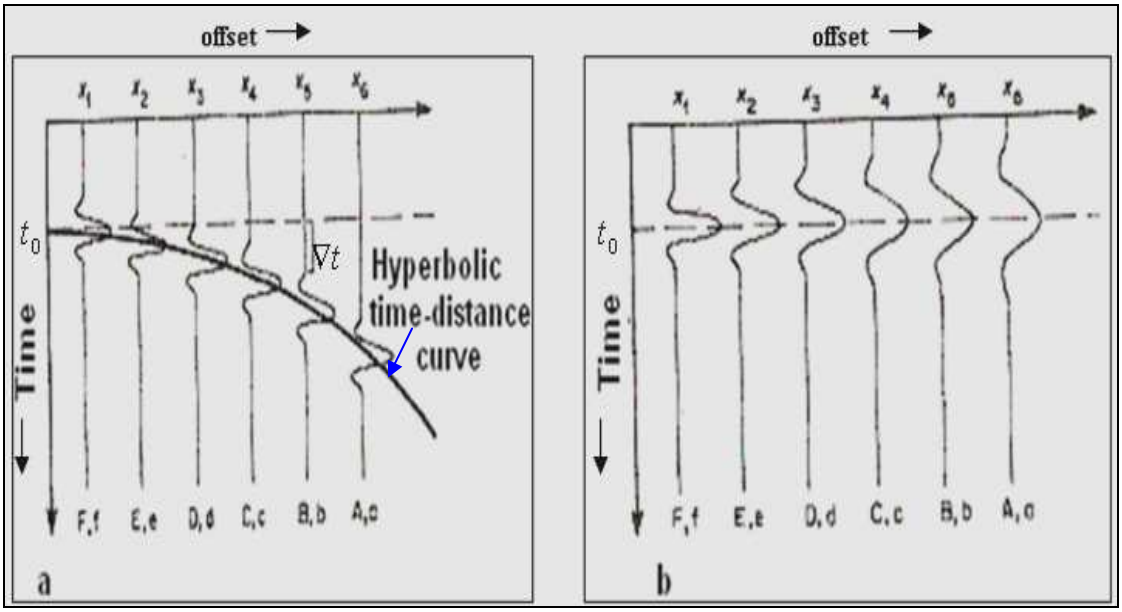

Figure 5.7: (a) The hyperbolic time distance curve. The travel time increases by a factor Δt with increase in distance from the source. (b) The hyperbolic move-out of the reflections is removed after applying the NMO correction (modified from Robins & Coruh, 1988).

5.10 Muting

After the application of the NMO correction the frequency distortion occurs and the traces normally get stretched. This happens particularly to the shallow arrivals with larger offset. This is called NMO stretching. Stretching is a frequency distortion in which the events are shifted to lower frequencies. Stretching is quantified by the following relation:

$$\frac{\Delta f}{f} = \frac{\Delta t_{nmo}}{t_o}, \tag{5.13}$$

Δf is the change in frequency. This stretch factor changes the pulse shape significantly. The V_{av} process of muting is applied to remove the most distorted part of section.

5.11 Stacking

The seismic data are stacked after the final velocity analysis and move-out correction is applied. All the traces with common midpoint (CMP) are summed up into one trace. Stacking the traces that contain the same reflection information improves the signal to noise and reduces the coherent noise such as multiples, which stack at different velocities from the primary events.

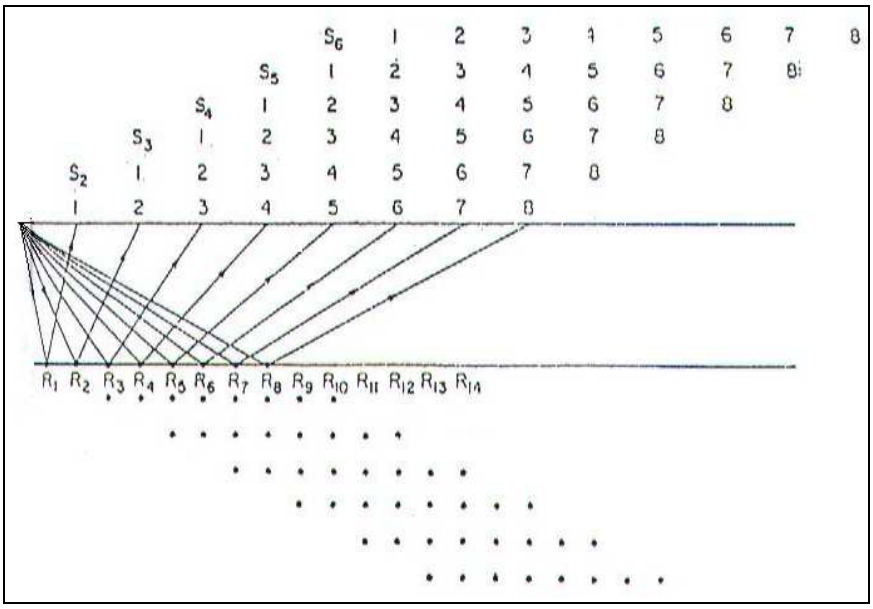

Figure 5.8: Stacking pattern chart (Dobrin & Savit, 1988).

5.12 Migration

Migration is one of the key steps in seismic data processing. Migration is a process in which a seismic section is reconstructed, so that all the seismic events are repositioned to their correct subsurface location with a corrected vertical reflection time (figure 5.9). The process of migration also improves the resolution of the seismic section by focusing all the energy spread over the Fresnel zone and collapses diffractions, thereby delineating detailed subsurface features such as fault planes (Kearey et al., 2002). The goal of migration is to make the stacked section appear similar to the geological cross section along the seismic line. Migration can be performed with time or depth as vertical dimension. If there is lateral velocity variation, the time migration can seriously dis-locate the events. To solve this kind of problems, depth migration is applied which correctly handles the velocity variation. But if the data come from an area with steep dips without large lateral velocity variation, pre-stack time migration is preferred (Bacon et al., 2003).

Two-dimensional survey data provide no information on cross-dip, so in the migration of two-dimensional data, reflection points migrated are constrained to lie within the plane of the section. The conversion of reflection times on a non-migrated sections to depths by using the one way travel time multiplying with appropriate velocity, yields reflector geometry of reflector also known as the record surface. When the reflectors are dipping, the record surface differ from the reflector surfaces and it gives a distorted picture of the reflector geometry The process of migration removes this distortion effects of dipping reflectors from the seismic section and their associated surface record. In diffraction migration all dipping reflection events are assumed to be tangential to some curve of maximum convexity. So the events are migrated back to their diffraction points by using a wavefront chart prevailing velocity-depth relationship (Kearey et al., 2002).

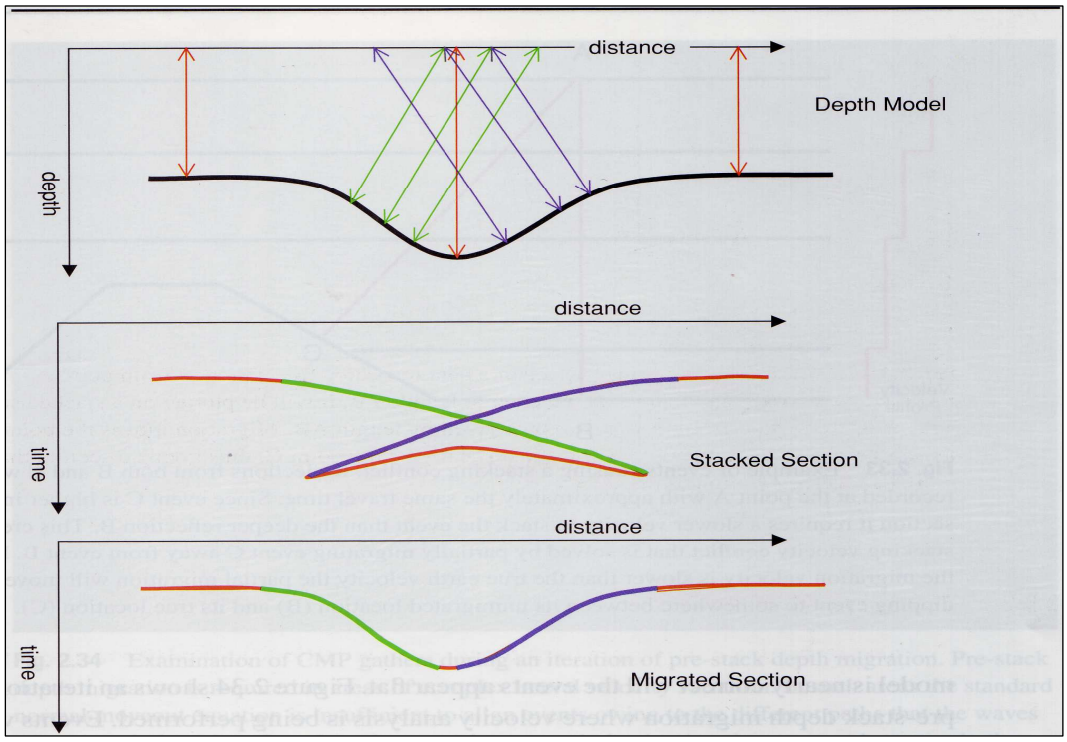

Figure 5.9: Seismic migration moves events from their recorded position to their true subsurface position. This diagram also explains the effect of migration on a syncline. The blue rays from the right side of the syncline are sometime recorded to the left of the green rays reflected from the left side of the syncline. This makes a bow tie pattern in the corresponding time section. The process of migration moves the events back to their true subsurface position (Bacon et al., 2003).

6. SEISMIC DATA PROCESSING (Results and Discussion)

The processing of the Svalex seismic data set 2008, 2009, 2010 is performed by use of the Geocluster (CGGVeritas, 2008) software. A total of nine seismic profiles from this data set are used for processing. The different processing steps performed on the data include reformatting and editing of the data, near trace gather generate (this step has been carried out to pick the water depth, in order to remove the multiples), filtering and deconvolution, sorting the data to CMP, velocity analysis and NMO correction, stacking, migration and display of data. For the purpose of illustration in this chapter, the seismic profile-22 is selected to display and describe the results in detail for each processing step. The results for the rest of profiles will be displayed in the appendix-I.

6.1 Geocluster (CGGVeritas)

One of the main applications of Geocluster is Seismic data processing. Geocluster offers a comprehensive set of processing modules and applications that deal with most aspects of seismic processing. The processing modules are designed to execute single or complex functions on seismic data. Geocluster runs both batch and interactive applications on PC/Linux systems. The processing is carried out by using a set of commands which are grouped in a seismic job. These jobs are created by using the XJOB graphic editor and then submitted for analysis and execution, which uses GSL (Geocluster Seismic Language of all processing commands) to build a seismic job (Geocluster, 2008). In what follows, a brief introduction about the main applications of the Geocluster used in the seismic data processing is presented below:

6.2 Main Geocluster applications used in data processing

6.2.1 Geopad

Geopad is one of the main applications that can be used to manage the Geocluster environment. This is a file manager and it provides a complete working environment for Geocluster, particularly in file management and launching applications. Geopad is started by typing a command (Geopad) in the text console window, and the Geopad main window appears (figure 6.1; Geocluster, 2008).

6.2.2 XJOB

Xjob is an interactive application of Geocluster which is used to create a seismic processing job flow (figure 6.2). A seismic job is basically a group of different modules or commands performed in a specific order. The job flows created on XJOB are linked through Geocluster processing modules to form a logical processing sequence through graphic editor in the main Xjob window (figure 6.2; Geocluster, 2008).

6.2.3 ChronoVista

Chrono vista is one of the major applications of Geocluster, which is used for interactive velocity analysis in the time domain. This application combines Geovel and Velpicker, which

allows the user to pick the stacking velocities in the time domain and after that to perform the QC and specific processing on the picked stacking velocities (Geocluster, 2008).

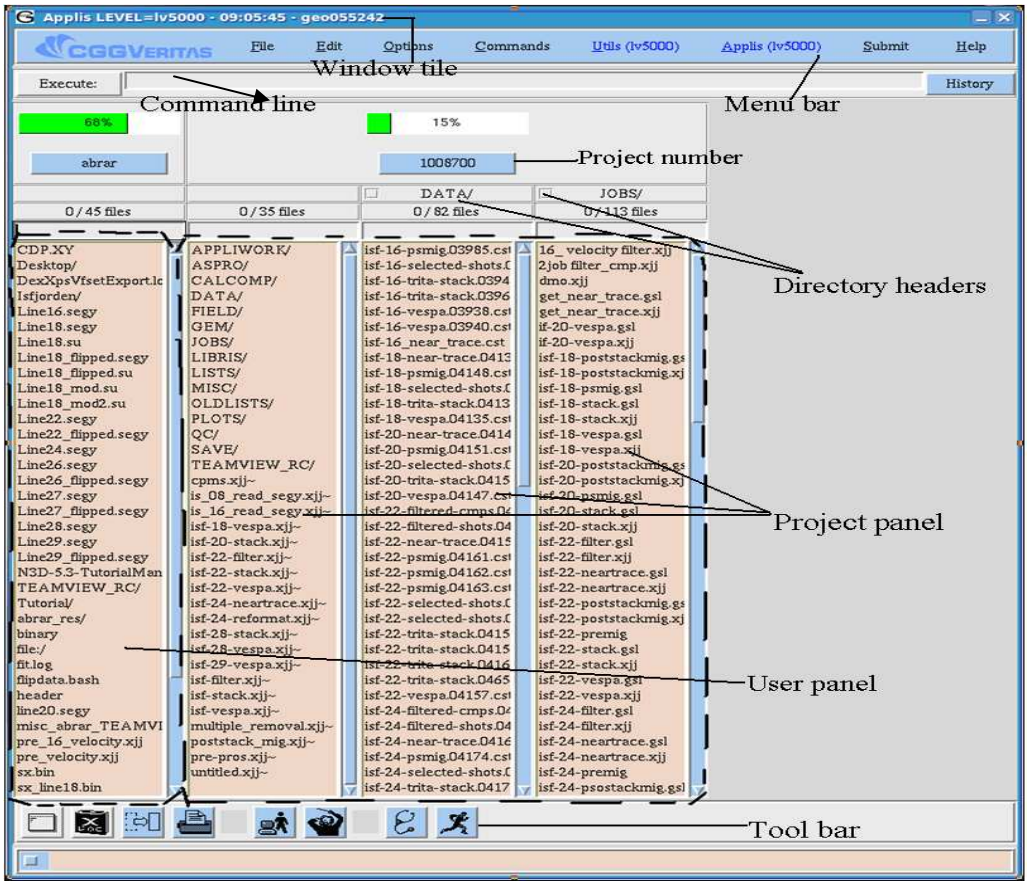

Figure 6.1: Geopad main window with different tool bars and panels.

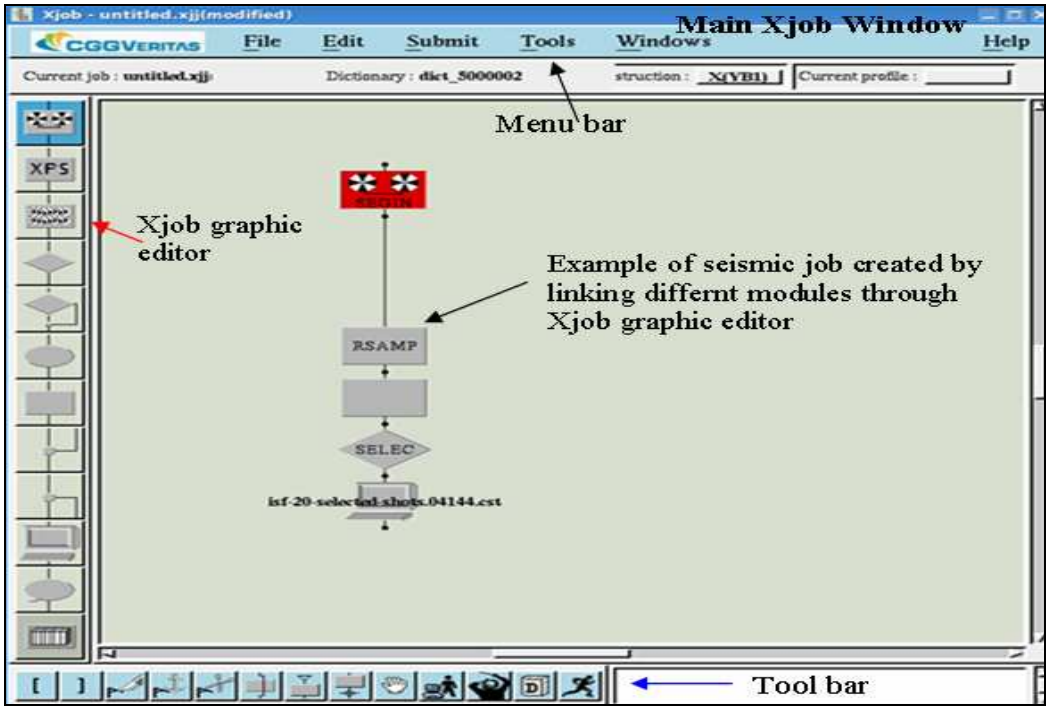

Figure 6.2: An example of Xjob (Geocluster) created by linking through different modules by the graphic editor.

6.2.4 XPS (eXtended Processing Support)

The XPS (eXtended Processing Support) system is a part of large database, which allows managing the auxiliary data in a simple and uniform way. In the XPS system the auxiliary data is managed in the form of small database. In this manner all the data is accessible with the same structure, and can be manipulated with the same tool. The XPS system is composed of several software elements, for example; XPS data base, XPS library and XPS modules.

6.3 Processing modules and processing flow chart

Table (6.1) summarizes the major Geocluster modules (Geocluster, 2008) used in the processing flow as following.

Table 6.1: Main Geocluster modules used in different processing jobs while processing of the Data.

Geocluster modules (Geocluster, 2008).	**Purpose**
FILTR (filtering module)	This program applies the filter operators stored in the filter libraries and perform time variant filtering. It also performs the spatial interpolation between libraries, if necessary.
FANMO (hyperbolic, non-hyperbolic or linear move-out)	This program uses the velocity library and optionally, mutes and water bottom libraries. Linear interpolation is used to obtain the velocity for all points in time
INPTR (trace input from disk or tape)	The function of INPTR is to read the tapes and traces selected by LIBRI TR and convert the input trace format into a unique processing format.
MODET (trace header modification)	MODET module is used to modify one or more trace header words.
MCDEC (spiking and predictive multichannel deconvolution)	This program performs multichannel processing by using a spiking deconvolution (DECON type) or a predictive deconvolution (TRITA type).
RSAMP (trace resampling)	This module is used for resampling of the data. The resampling phase is carried out by applying an interpolation filter whose frequency is adjusted by parameter FMAX (maximum frequency).
REFOR (time gain function)	The main purposes of applying this function are, to multiply the sample amplitude, converting the samples to absolute values, normalization and searching for maximum sample.
RECOV (amplitude recovery)	The function of this module is to perform amplitude recovery.
SPASM (spatial amplitude smoothing)	The aim of this function is equalize the input trace with respect to its neighboring traces considered for amplitude comparison (spatial window).

SPARN (random noise attenuation)	This module carries out projective filtering in the (f-x) domain, to attenuate the random noise SPARN uses the projective filtering instead of predictive filtering.
STAPA (seismic trace stacking**)**	The aim of this module is to stack a trace gather in an output buffer.
TRITA (predictive deconvolution)	Performs a time variant predictive deconvolution, generally used to remove the long period multiples.
TIKIM (Kirchhoff pre-stack time migration)	This module represents the Kirchhoff time migration for 2D and 3D migration.
BSORT (one–pass trace sorting)	This function is used to sort out the traces. First it defines the selection limits of the traces to be sorted, and then it defines the sorting and processing criteria.
FKFIL (F-K filtering)	This module is use to filter out a set of traces the FK domain by defining different options like; equalization of input traces, possibility of weighing the input traces and time variant filtering.
OUTBD (Trace output in Geocluster tape format)	In Geocluster this module is used for writing the traces onto tapes. It controls the output of seismic traces, in CGG format to tape and disk files on the bases of given information in the corresponding LIBRI BD.
VESPA (velocity analysis computation and composite plotting)	This module for velocity analysis works in four options; VV, CV, SH and TI. For the velocity analysis, the traces belonging to a group of traces are corrected using n velocity functions.

Figure (6.3) shows the processing flowchart with main steps carried out to process Svalex, 2008, 2009, 2010 seismic profiles. Table (6.2) summarizes all the important processing steps used in this study with their objectives.

Processing flow chart:

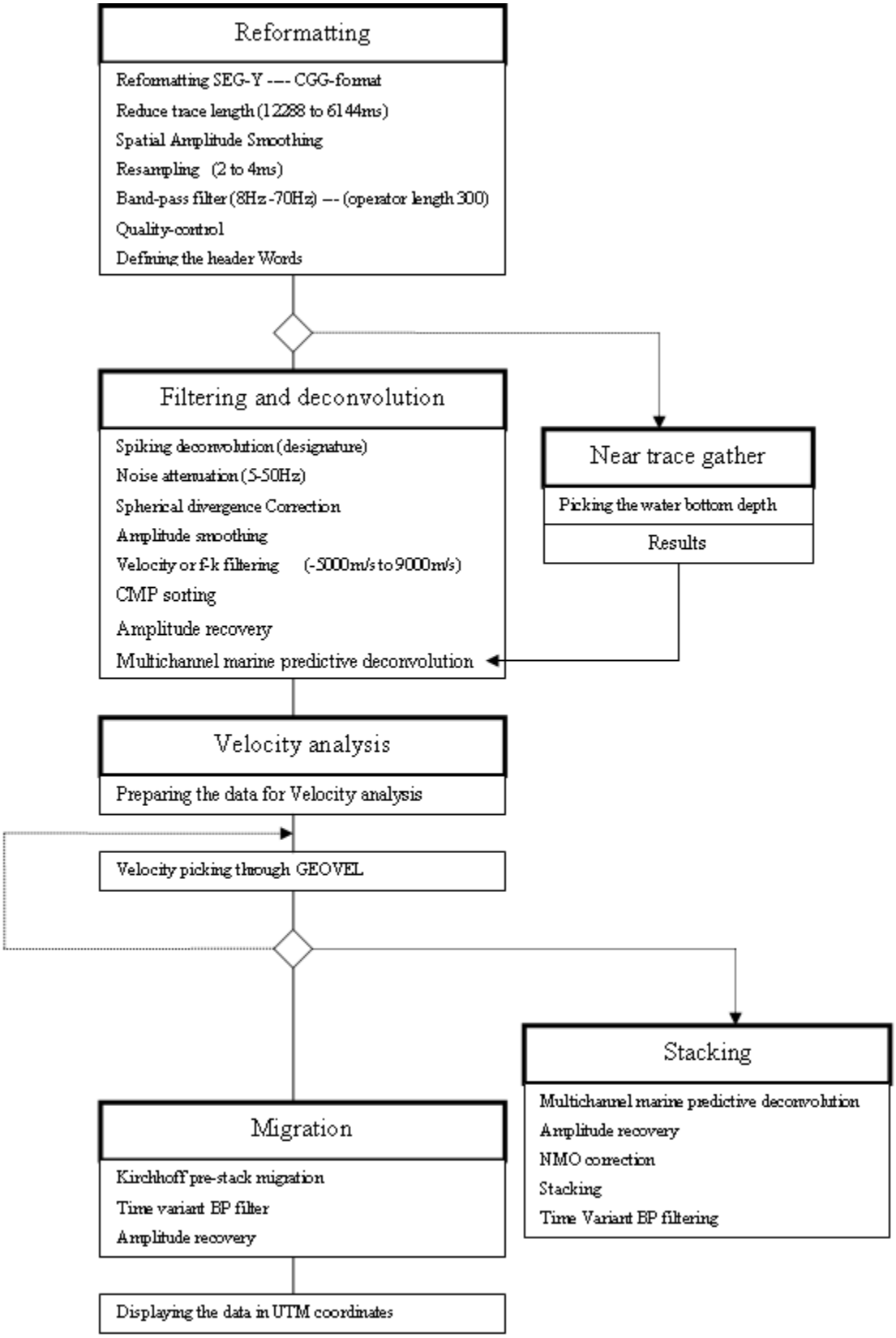

Figure 6.3: Processing flow chart, used to process the seismic data.

Table 6.2: Main processing steps carried out during the processing of seismic data against with their objectives.

No.	Processing steps	Objectives
1	Conversion of SEG-Y format to CGG format	Conversion the data to processing oriented file format.
2	Data viewing and editing and Muting	Removes the dead or noisy traces. The unwanted data are zeroed and replaced with interpolated values.
3	Data reduction (12844 ms to 6144 ms)	Reducing the trace length and volume of the data to speed up later processing sequence.
4	Band-pass filtering (8Hz-70Hz)	To remove the energy (frequency) out of defined range.
5	Resampling (2 to 4 ms)	Resampling the data from 2 to 4 msec to get max frequency up to 125 Hz.
6	Gain recovery	To gain the amplitude loss caused by the spherical divergence, absorption and transmission losses.
7	Near trace gather generate	To pick the water bottom depth (time values) in order to remove the long period water bottom multiples.
8	Deconvolution (spiking, Designature)	To remove the bubble pulse effect and water layer multiples.
9	F-K Filtering or Velocity filtering (f - k domain)	Reduces low velocity coherent noise. Velocity interval value (-5000m/s – 9000m/s)
10	CMP sorting	To sort the data from CSP to CMP for stacking purpose.
11	Deconvolution (predictive)	Removes multiples, specially the water bottom multiples.
12	Velocity spectrum analysis	Preparing the data for velocity analysis.
13	Velocity analysis	Obtain NMO-velocities and stacking velocities for NMO correction and stacking.
14	Normal move-out (NMO)	Corrects the difference in travel time due to increase in source-receiver distance.
15	Muting	Removes the bad traces and attenuates the NMO stretching effect.
16	Stacking before migration	Check the quality of the velocity models picked by velocity analysis.
17	Time variant band-pass filter (TVF)	Removes energy outside the given range.
18	Pre-stack Kirchhoff time migration	Repositions the dipping events to their correct location in the subsurface and collapses the diffractions from point sources.
19	Section scaling and visualization, automatic gain control	Repetition of some of the previous procedures to improve the quality of the data. Automatic gain control is used to enhance the amplitudes for deeper levels.

20	Time variant band-pass filter (TVF)	Applied for final section. Removes energy outside the given frequency band. Different band-pass filter values are applied for time windows of the data.

6.4 Reformatting and editing of the data

Seismic raw data recorded in the field was loaded to Geocluster in SEG-Y format, which is the common format used in the oil industry. The data is reformatted internally to the Geocluster format. Since the bottom half of the original traces (with total length up to 12288ms) contain very little information due to the relatively weak source. So, for this purpose the data was reduced by taking the information up to half of the trace length, which is 6144ms. To remove the noise burst and spikes particularly related to amplitude, the application of spatial amplitude smoothing (to smooth the amplitude) was done by using module (SPASM). The next step was to apply a band pass filter in a way to filter out the high frequency noise such as noise due to cables or machines,0, and low frequency noise such as noise produced by waves. For this purpose a frequency filter was designed with limits having low value of 8 Hz and high frequency value of 70 Hz to filter the frequencies below and above these values, respectively. The marine seismic data is usually recorded with 2 ms sampling interval with Nyquist frequency 250 Hz. The seismic data is then resampled from 2 to 4 ms with Nyquist frequency 125 Hz. The resampling of the data reduces the volume by 50% without any loss of data quality. This reduction in volume of the data also helps in speeding up all the later processing stages.

The next step was to obtain the common depth point (CDP) number, offset and position of the CDP's. The MODET module in Geocluster was used to define header words and to calculate the above parameters. The fold (the max number, a point in the subsurface is mapped), offset and CMP were calculated using the following expressions:

$$Fold = NR / (2*SS/RS). \quad (6.1)$$

$$Fold = 240/ (2*50/12.5) = 30 \text{ fold data} \quad (6.2)$$

SS is source spacing with value 50 m kept while recording the data, *NR* is number of receivers (grouped) with a value of 240, and *RS* is receiver spacing having value 12.5 m while recording. The offset was defined and calculated in the MODET by the following relation:

$$Offset = channel\text{-}number*12.5m + 90 \quad (6.3)$$

Offset = 102.5m for first channel and 3090 m for channel number 240

For profiles 16 - 28 channel-number ranges from 1 to 240, while for profiles 27 and 29 its value corresponds from 1 to 232. The CMP was calculated by the following relation:

$$CMP = (2*SS/RS)* SP – CHN + (?) \text{ or } – (?). \quad (6.4)$$

Where *SP* is shot number and *CHN* is the number of channels. The terms *+ (?)* or *– (?)* represents the values that were added or subtracted to keep the *CMP* value in certain range (1–9999), as defined during the data processing. As an example, *CMP* values defined and calculated for profile 22 with shot points ranging from (8 – 613) using the equation (6.4):

$$CMP = (2*50/12.5)* 8 – 240 + (?) \text{ or } – (?) \quad (6.5)$$

$$= \text{ -176 (with shot points of value 8)}$$

$$CMP = (2*50/12.5)* 613 – 240 + (?) \text{ or } – (?) \quad (6.6)$$

$$= \text{ 4664 (with shot points of value 613)}$$

Since these *CMP* values (-176 to 4664) do not exactly fall in the range (1 – 9999), so a value 200 was added instead of subtracting to keep the *CMP* values in that range.

$$CMP = (2*50/12.5)* 8 – 240 + (200) \quad (6.7)$$

$$= 24$$

$$CMP = (2*50/12.5)* 613 – 240 + (200) \quad (6.8)$$

$$= 4864$$

Now the new *CMP* values are from 24 to 4864, which lie in the range (1- 9999).

The data were then checked for quality control to make sure that all the traces were present, and the amplitude was enhanced by applying automatic gain control (AGC). The data were reformatted before display as each system requires its own format to display the data in that particular format. Figures (6.4 & 6.5) show the display of the selected shots with the observed events marked with different arrows. These events are:

- The amplitude attenuation at larger travel times due to spherical spreading, transmission losses and internal friction (figure 6.4).
- Different types of arrivals such as direct arrivals marked by black arrows (figure 6.5), refracted events marked by blue arrows (figure 6.5) and reflected events marked by red arrows (figure 6.5).
- Different types of noise e.g. multiples, marked by green arrows (figure 6.5).

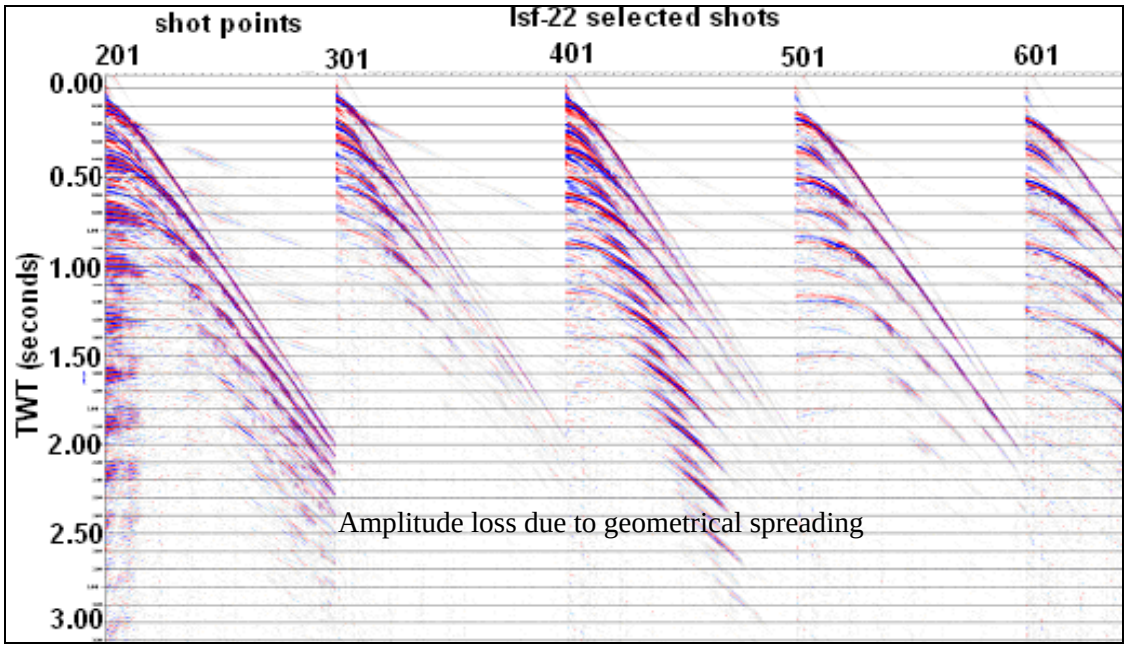

Figure 6.4: Display of some selected shots without amplitude recovery (AGC).

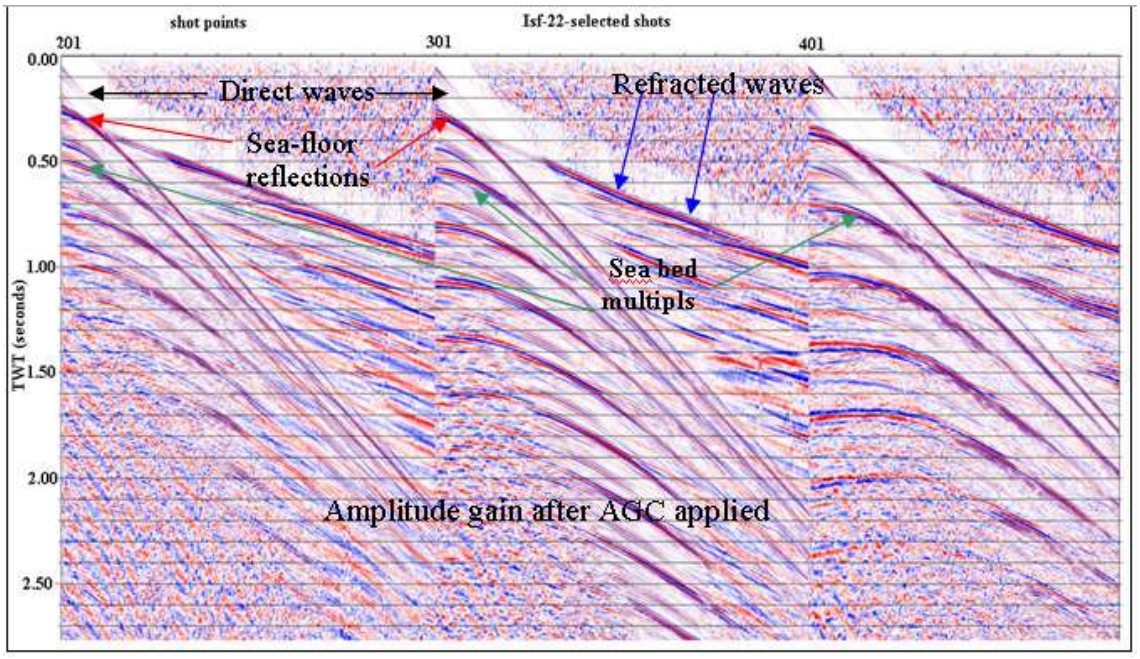

Figure 6.5: Display of some selected shots after amplitude recovery (AGC) was applied.

6.5 Near-trace gather stack

A near-trace gather was generated (figure 6.6) by using the raw traces corresponding to the receivers that are nearest to the air gun array. To make sure that weak reflections were also observed in the near-trace gather display, REFOR (time gain function) function was applied. The main purpose with generating a near trace gather is to pick the water depth (time values), in order to remove the water bottom multiples and to improve the data quality. After generating the near trace gather, the data were displayed in Teamview and water depth was picked along the sea bed (blue line; figure 6.6). The time values of the water bottom

reflections picked in this manner were exported to the XPS data base in Geocluster to create a water bottom library. These time values of the water bottom reflections are used to compute the operator gap (prediction distance), which is used to remove multiples by applying predictive deconvolution filter.

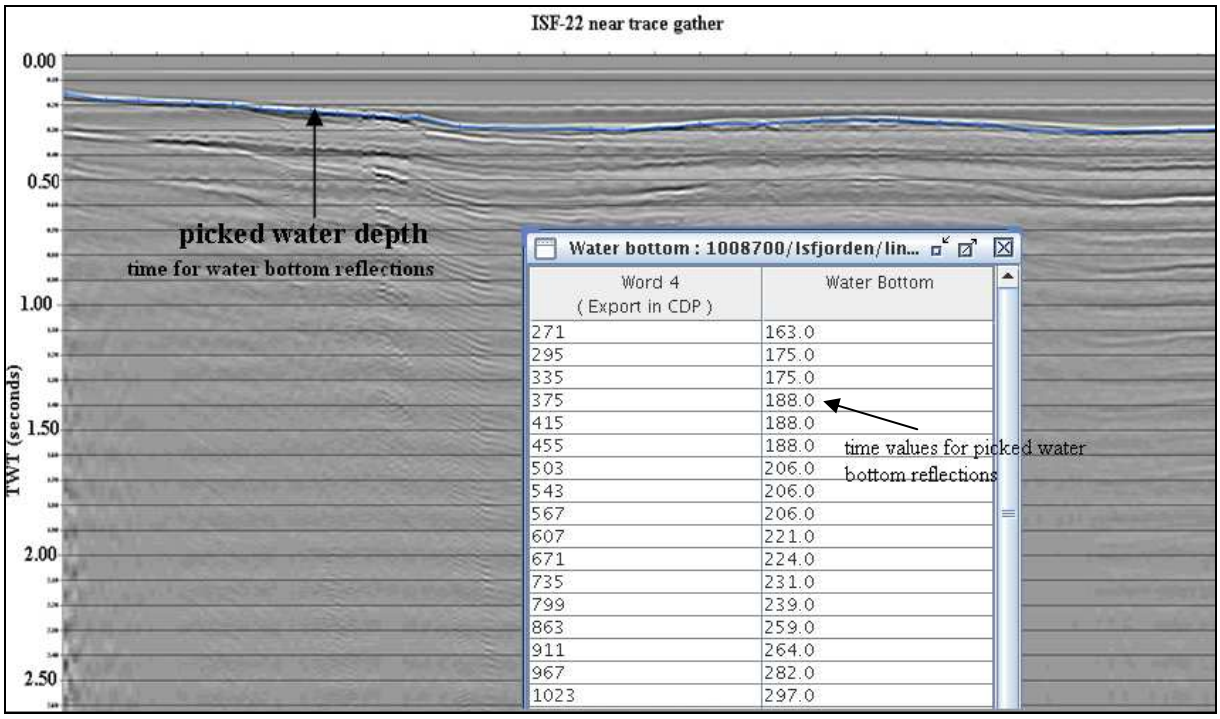

Figure 6.6: Display of near trace gather with picked water bottom reflections (blue line), inset window shows the time values for picked water depth.

6.6 Spiking deconvolution and velocity filtering

A primary task in the data processing was to remove coherent noise and strong multiples, which mask the actual reflected arrivals. Multiples presented in the seismic data were usually generated as a result of high velocities in the seabed. The velocity in the seabed was estimated to be around 3000 m/s or more, obtained from analysis of data on the Teamview display in Geocluster.

6.6.1 Spiking deconvolution

The output from the reformatted job was read in the module to perform spiking deconvolution and filtering function. The Spiking deconvolution module MCDEC (spiking multichannel deconvolution) removes the source pulse effect, bubble effect and attenuates the water layer short period multiples. It is common for all arrivals to have bubble pulse regardless of the offset.

In spiking deconvolution, the input traces are divided into windows, and each window is convolved with respect to signal variation in time domain by using the Wiener-Levinson algorithm (W-L deconvolution), describes as follow:

$$S = C * R + N, \tag{6.9}$$

where S is the seismic signal, C is the seismic pulse (wavelet), R is the earth reflectivity and N is the noise.

The main purpose is to find the inverse of C from the seismic data and then to apply the inverse to remove the effect of C in order to bring out the reflections. The key to W-L deconvolution is the separation of the effective seismic pulse from the reflectivity by spectral decomposition. Separation of C and R is accomplished in the time domain by selecting a window from the seismic data of length N, auto-correlating the window, and truncating the correlation function to length L much less than N. The calculation window while designing the deconvolution filter was kept from 2500 - 6000 ms with an active operator length of value 325 ms.

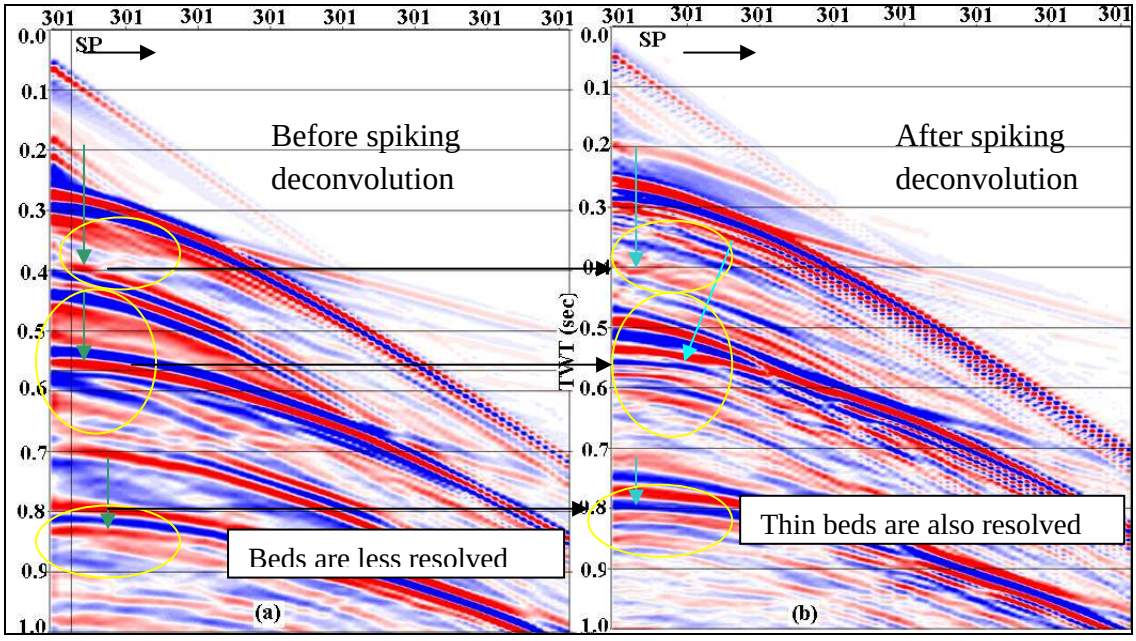

Figure 6.7: (a) Display of the selected shots zoomed at shot point 301, before the spiking deconvolution applied. (b) Display of the selected shots zoomed at shot point 301, after the application of spiking deconvolution.

It is obvious in (figures 6.7a & b), that the effect of bubble pulse has been attenuated and the wavelets get sharpen after the application of spiking deconvolution. The application of spiking deconvolution increases the vertical resolution of the data by decreasing the wavelength and resolves the beds at smaller scale, which were not visible in the data display before the application of spiking deconvolution.

$$Vertical\ resolution = \frac{\lambda}{4} = \frac{v}{4f}\ , \tag{6.10}$$

λ is the wavelength, v is the velocity and f is the frequency. Smaller the value of λ greater will be the resolution.

The incoherent noise (water-wave noise) was removed using the SPARN function (a low cut frequency filter with upper limit up to 50Hz). The amplitude recovery and smoothing were done by applying REFORM and SPASM modules (also equalization of amplitudes of the traces).

6.6.2 Velocity filtering

Frequency-wave number filtering also commonly known as F-K filtering or velocity filtering is used in order to remove the coherent noise (direct and head waves) from the data. Before the application of F-K filtering, the data is converted from the time domain to the frequency (f) wave number (k) domain. The apparent velocity can be found by the following relation:

$$V_{ap} = \frac{f}{k} \ . \tag{6.11}$$

$$V_{ap} = \frac{v}{\sin i} . \tag{6.12}$$

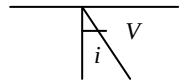

Where V_{ap} is the apparent velocity, V is the true velocity, f is the frequency, k is the wave number and i is the angle of incidence with respect to vertical. The velocity is measured along the slope in the F-K plot (figure 6.8) by the Teamview display.

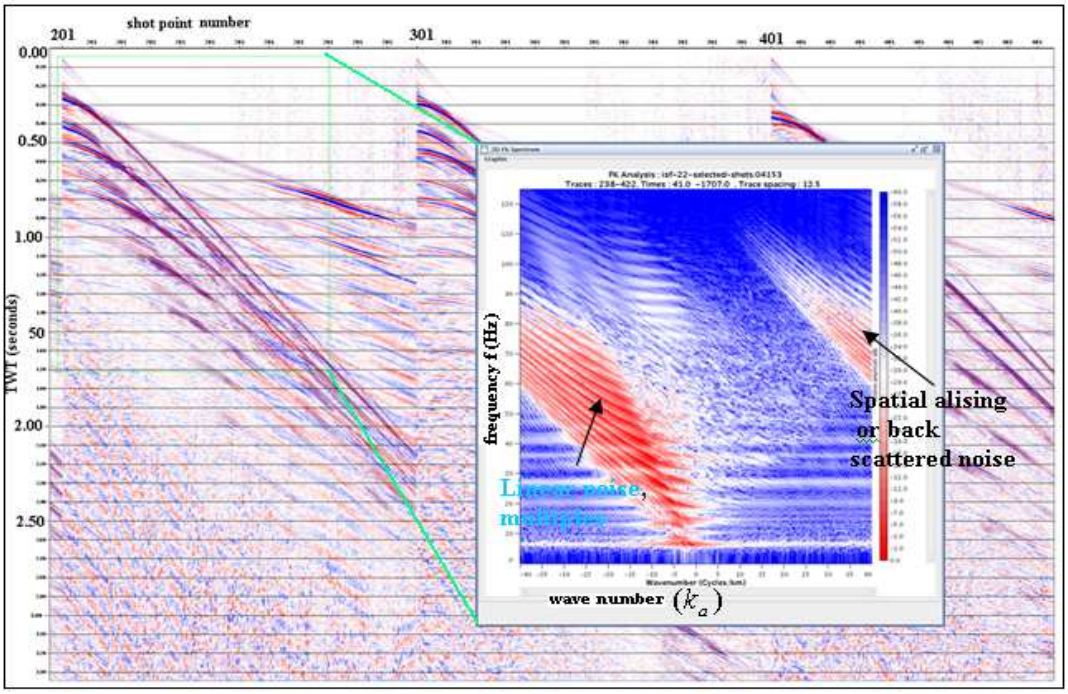

Figure 6.8: Display of frequency - wave number plot (inset) for some shot collections. Linear events in the F-K plot with spatial aliasing effect can be observed.

The main idea behind the velocity filtering function is to measure the apparent velocity for all seismic events that fall in different zones in F-K plot. This velocity is measured graphically along the slope in the F-K plot, and the data is then decomposed spectrally on the basis of this measured apparent velocity. The unwanted events are filtered out easily on the basis of gradient, which is actually measured by using the apparent velocity values (eq. 6.12).

The velocity of the wave propagating along seabed in Isfjorden is estimated to be around 4000 m/s. So a velocity filter was designed with a certain range of velocities -5000 to 9000 m/s with a maximum frequency limit of 115Hz. So the recorded linear events (critical refractions and direct waves) are supposed to be attenuated by applying a velocity filter. The data is then again displayed to see the effects after the velocity filtering process (figure 6.9).

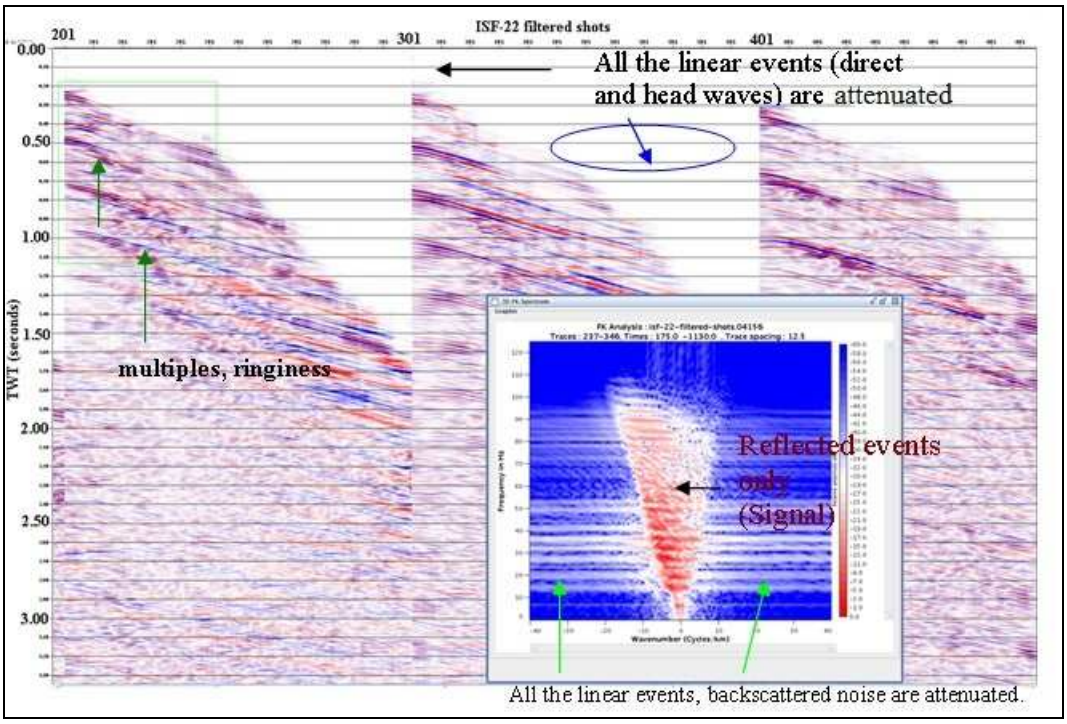

Figure 6.9: Display of the data after Velocity filtering with frequency - wave number plot (inset) for some filtered shot collections.

By making the comparison of figure (6.9) with figure (6.5), it can be clearly observed that all the linear events, direct waves (black arrows; figure 6.5) and refracted waves (blue arrows; figure 6.5) presented in the data have now been attenuated after applying the velocity or F-K filtering.

6.7 Sorting the data to common midpoint (CMP)

The next step is to sort the data from CSP (common shot point) to CMP (common midpoint). Seismic data acquisition with multifold coverage is done in shot-receiver (s,g) coordinates. Seismic data processing on the other hand, is conventionally done on mid-point (y,h) coordinates. CMP sorting is a coordinate transformation from (s,g) to (y,h). Those traces with the same midpoint are grouped together, making a CMP gather.

To sort the data to CMP, the BSORT (sorting according to two or three header words) module was applied. Once the data is sorted to CMP it is read to OUTBD (writing of traces onto tapes). After sorting to CMP some traces are selected and displayed (figure 6.10).

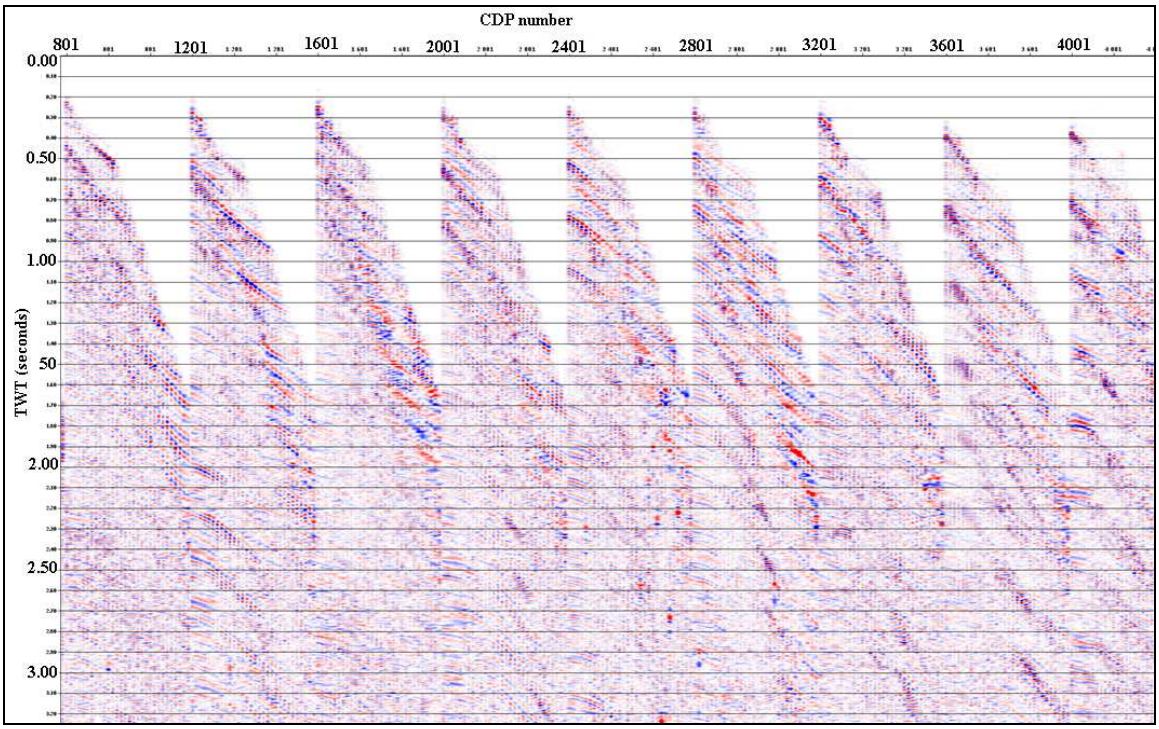

Figure 6.10: Display of data after sorting to CMP.

6.8 Multiple removal and data preparation

6.8.1 Predictive multichannel deconvolution (TRITA)

Removing multiples was one of main challenge in data processing and these multiples were attenuated by the deconvolution process. The output data from the CMP gather was again read to the INPTR module. To remove the multiples a TRITA (predictive multi-channel deconvolution) module was applied which perform the time variant predictive deconvolution. This deconvolution module is similar to the MCDEC module, which is a spiking deconvolution and removes the source and bubble pulse effect. It also removes the water layer short period multiples, while the rest of the multiples were removed by applying TRIRA application.

The TRITA module uses a gapped operator consisting of one impulse at zero time, followed by a series of zeroes with an active portion of length LAR (active operator length). The Parameter IQ (operator position) is the time between the origin and center of the active part. This corresponds to the period of the undesired multiples. This period can be defined by user or the program itself, or can read it from the water bottom library LIBRI FD (file of water bottom data, read data from XPS). A deconvolution filter was estimated by using the defined computation windows from 150 - 3500 ms with an active operator length of value 150 ms.

Certain amount of white noise was added in order to avoid dividing by zero values. In the TRITA module, the picked water depth data is read from the XPS water bottom library with a given particular version name, when picked in the near-trace gather. The deconvolution process extends the frequency band which makes the signal narrow and increases the bandwidth. So the frequencies above and below the seismic signals are tempered by band-pass filter.

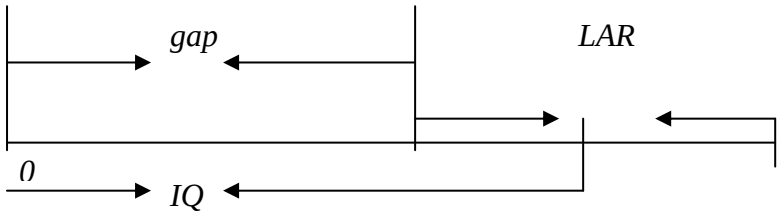

$$gap = IQ - \frac{1}{2} LAR \ . \tag{6.13}$$

6.8.2 Data preparation for velocity analysis

The data were then prepared for velocity analysis by computing a velocity spectrum using the VESPA module with an increment in percentage by 4. Time - velocity pairs were defined with different values of time and velocities shown in table (6.3). The RECOV (amplitude recovery) job was performed to recover the amplitude and to increase the dynamic range of the data. The data were displayed after predictive deconvolution and data preparation (figure 6.11).

Table 6.3: Values for velocity-time pairs used for the velocity analysis. The value for average interval velocity was kept at 5000 m/s.

No	Time (ms)	Velocity (m/s)
1	144	1485
2	200	2280
3	275	2835
4	435	3550
5	1200	4300
6	1875	4650
7	2850	4900

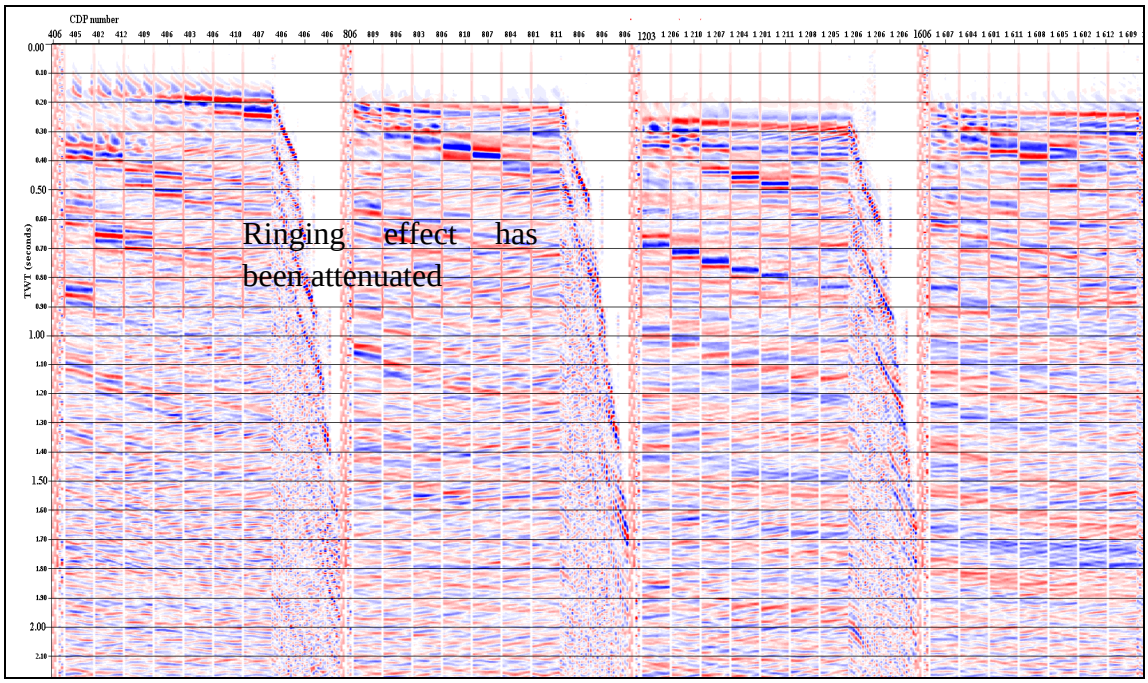

Figure 6.11: Display of data after preparing as an input to the velocity.

Comparing figure (6.11) with figure (6.5), it can be seen that sea bottom multiples seen in figure (6.5) have been attenuated to large extent after applying the predictive multichannel marine deconvolution (TRITA).

6.9 Velocity analysis

After preparing the data for velocity analysis, then next step was to perform the velocity analysis job. The velocities are picked using the Geocluster application Chronovista through Geovel (figure 6.12). A variety of graphic functions are used to estimate the stacking velocities which gave the best possible result. Under the Geovel in the velocity analysis viewer window we have several windows like velocity spectrum, interval velocities, central gather stack before and after NMO correction and mini-stack. When the velocities are picked in the velocity spectrum the effect can be seen in the NMO corrected stack with the flattening of the hyperbola (figure 6.12). The interval velocity stack shows a velocity curve corresponding to the velocities picked in the semblance plot. There is a considerable increase in the value of interval velocities for shallow travel time and then a slight increase with increasing depth can be observed (figure 6.12). The NMO corrected plot shows the results for the velocities picked in the semblance plot, while the mini stack shows the pattern of velocities (increasing or decreasing). Interpolation is used in between velocities picked for a particular CDP. Figure (6.13 shows the values for RMS velocity picked in velocity analysis.

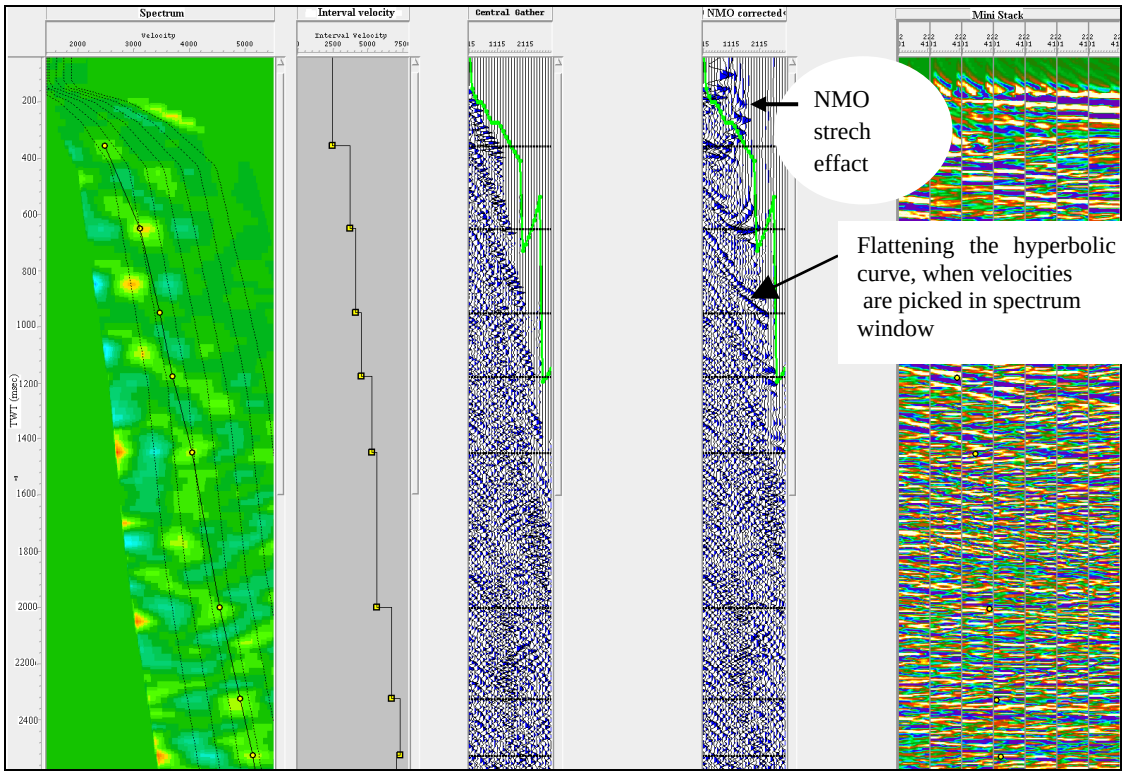

Figure 6.12: Geocluster application Chronovista, velocity picking process through Geovel. From left, the semblance plot, interval velocity plot, central gather plot, NMO corrected plot and mini stack.

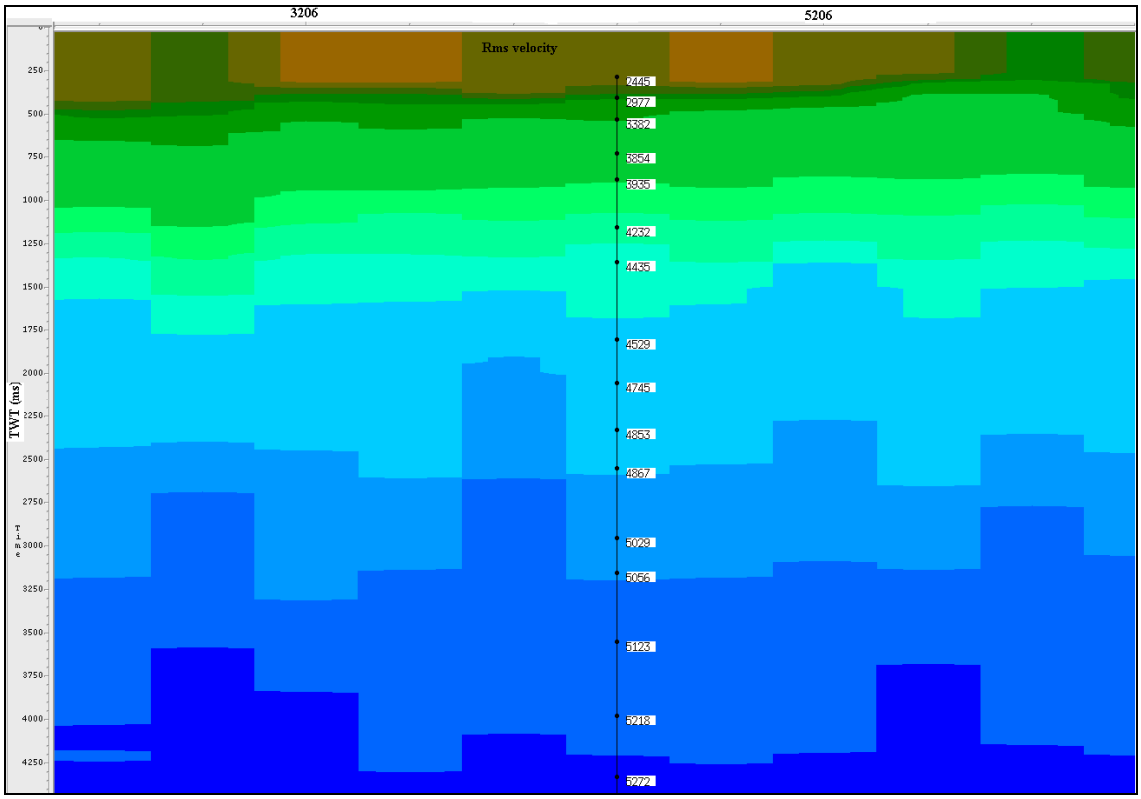

Figure 6.13: Shows the values of the RMS velocity picked during the velocity analysis (showing approximately 22-km of profile).

The velocity values estimated in this manner are supposed to be around 4000 m/s in upper 1sec and it is close to 5000 m/s below 1 sec. The interval velocity values are ranging from 2500 m/s to 6000 m/s. Once the velocities are picked, these velocities were exported to the XPS library. These values were used further in stacking and migrating the data.

6.10 NMO Stretch muting

After NMO correction a frequency distortion occurs and the traces get stretched. This happens particularly to the shallow arrivals with greater offset. This is called NMO stretching. Stretching is a frequency distortion in which the events are shifted to lower frequencies. This effect was partially removed by using a time variant band-pass filter (values used are shown in table 6.4). The time variant band-pass filter was designed and applied such that it removes the low frequency in the upper part. In figure (6.14a), it can be observed (black arrows) that the data gets distorted as a result of NMO correction. The data were again displayed in order to see the results after NMO stretch muting application (figure 6.14b).

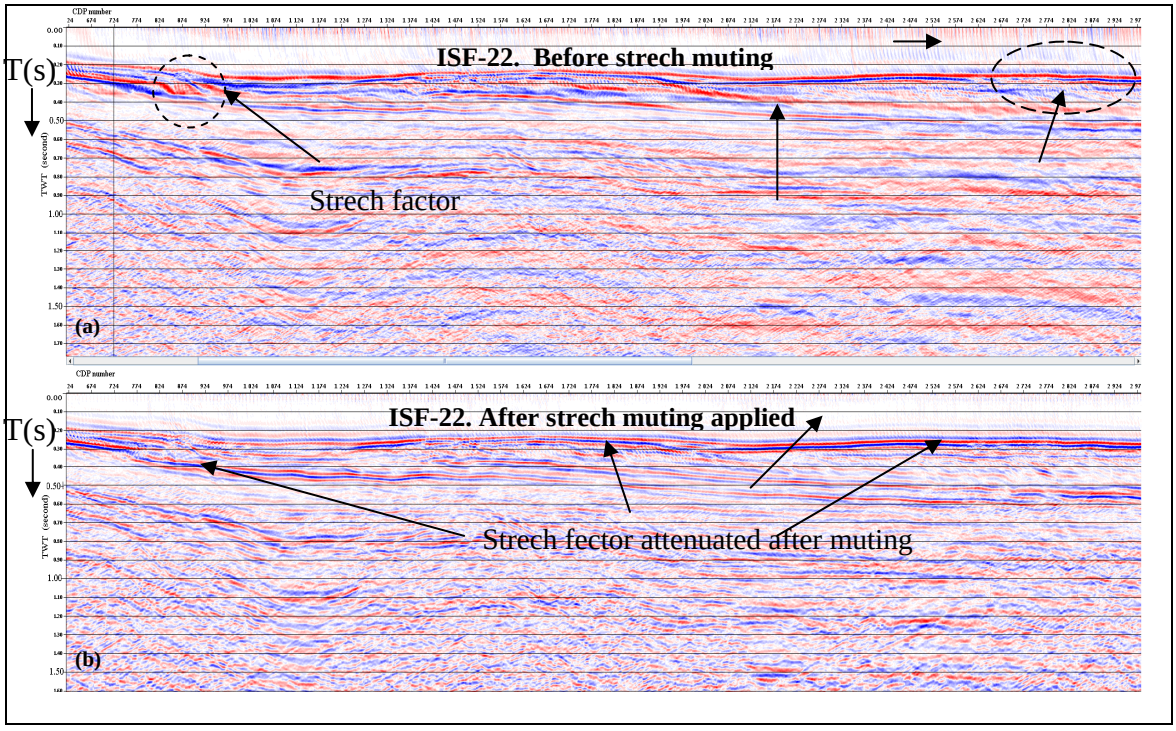

Figure 6.14: Display of the data, (a) before the NMO muting and, (b) after the NMO muting applied.

Comparing figure (6.14a) with figure (6.14b), it is clear that the effect of frequency distortion have been removed efficiently by applying muting (time variant band-pass filter).

Table 6.4 below shows the values used for time variant band-pass filter for NMO muting.

Table 6.4: The values for time variant band-pass filter.

Filters	(f) (Hz)	(f) (Hz)	(f) (Hz)	(f) (Hz)	Application window (start) ms	Application Window (end) ms
1-filter limits	**10**	**20**	**70**	**90**	**0**	**3 00**
2-filter limits	**8**	**16**	**65**	**80**	**600**	**900**
3-filter limits	**7**	**14**	**50**	**70**	**1200**	**1700**
4-filter limits	**5**	**10**	**40**	**55**		

6.11 Fast stacking

Once the velocities were picked, the data were stacked to check the quality of the velocity models picked by velocity analysis. The output of data from the velocity analysis job were read by INPTR (trace input from disk or tape), and the TRITA (predictive multi-channel deconvolution) module was again applied to remove the multiples, if any. The velocities used for the NMO correction and stacking were read from the XPS library through FANMO (dynamic correction NMO) module. The data were stacked by using STAPA module (total stack). After that, the amplitude was recovered by plot equalization, using RECOV (amplitude recovery).

The resolution of the stack was investigated using scaled values of initially picked velocities with an increase or decrease of 5% (figures 6.15a & b). This is performed in order to obtain a good quality stack. When the initially picked velocity values are increased by 5%, the data showed the better resolution (figure 6.15a) as compared to a decrease of 5%.

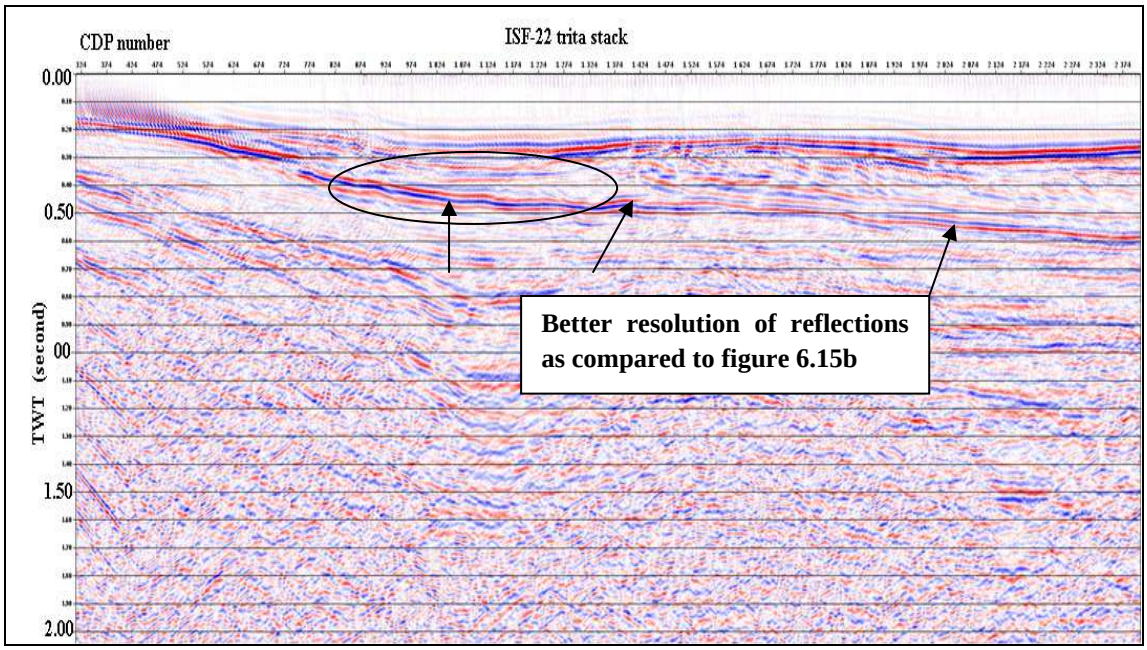

Figure 6.15 (a): Display of Trita stack (zoomed) with 5 % increase in initial velocities pick (black arrows show better resolution for the reflections).

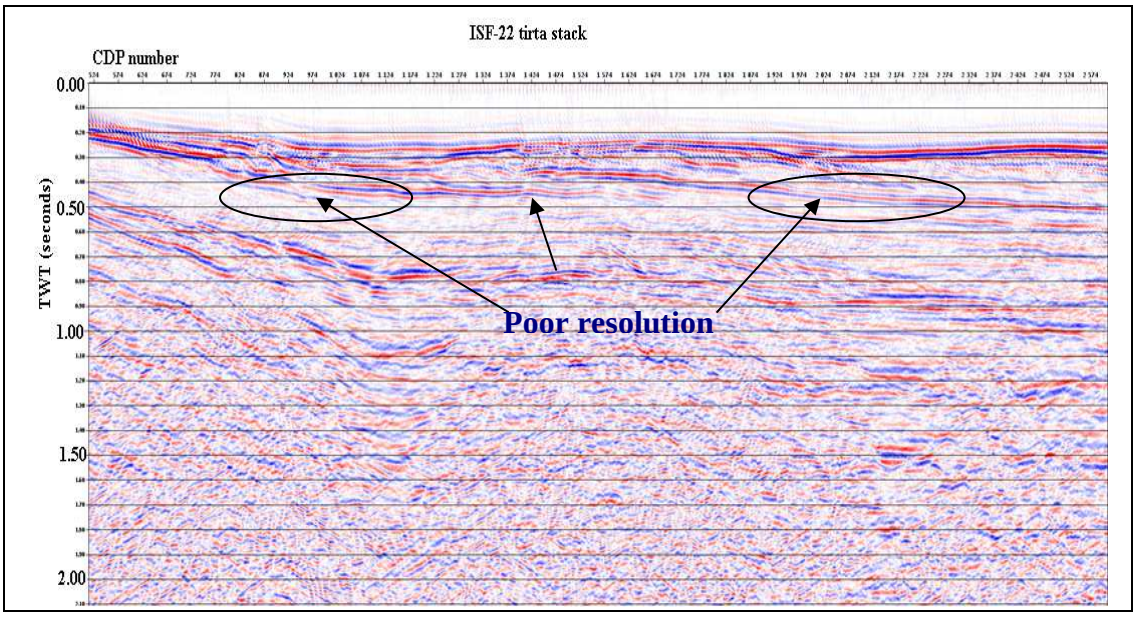

Figure 6.15 (b): Display of Trita stack (zoomed) with 5% decrease in initial velocities pick (black arrows show poor resolution for the reflections).

6.12 Muting and pre-stack migration

The final step performed on the data after the velocity analysis is the pre-stack migration related to repositioning of the reflection events. The application of migration requires muting to be applied to remove the NMO stretch factor. Migration was performed by using the modules TIKIM, which performs the Kirchhoff time migration for pre-stack 2D and 3D data. The Kirchhoff algorithm is a trace-by-trace migration, which treats each output sample as the

apex of a diffraction curve. Input samples are summed or spread along the diffraction curve characterized by a locally defined 1-dimensional RMS velocity function. Constructive interference builds the image of the reflector. The velocities are defined from the XPS velocity library. A limit is defined for the steepest gradient of the layers (DIPLIM) and the values above this limit are muted by the operator.

Data was also operated with the TRITA (marine multichannel deconvolution) module to remove the remaining multiples and the amplitudes were recovered by the RECOV (recovery factor to gain the amplitude loss).

6.13 Display of pre-migrated stacked section

The data is stacked after the migration. But before the data is stacked and displayed finally, a time variant band-pass filter is applied to remove the noise, particularly low frequency in the upper part and high frequency in the deeper part. High frequencies are kept at shallow time while low frequencies are kept in deeper part at larger travel times. Table (6.5) shows the values for band-pass filter used.

Table 6.5: The values for time variant band-pass filter.

filters	(f)	(f)	(f)	(f)	Application window (start)	Application Window (end)
Filter limits:1	10	20	80	90	0	300
2	8	16	65	85	600	900
3	7	14	50	75	1200	1700
4	6	12	40	60		

Section scaling, visualization and Automatic gain control were applied finally, as well as repetition of some of the previous procedures (SPAM, RECOV) to improve the quality and dynamic range of the data. Automatic gain control with window length (400) was used to enhance the amplitudes at deeper levels.

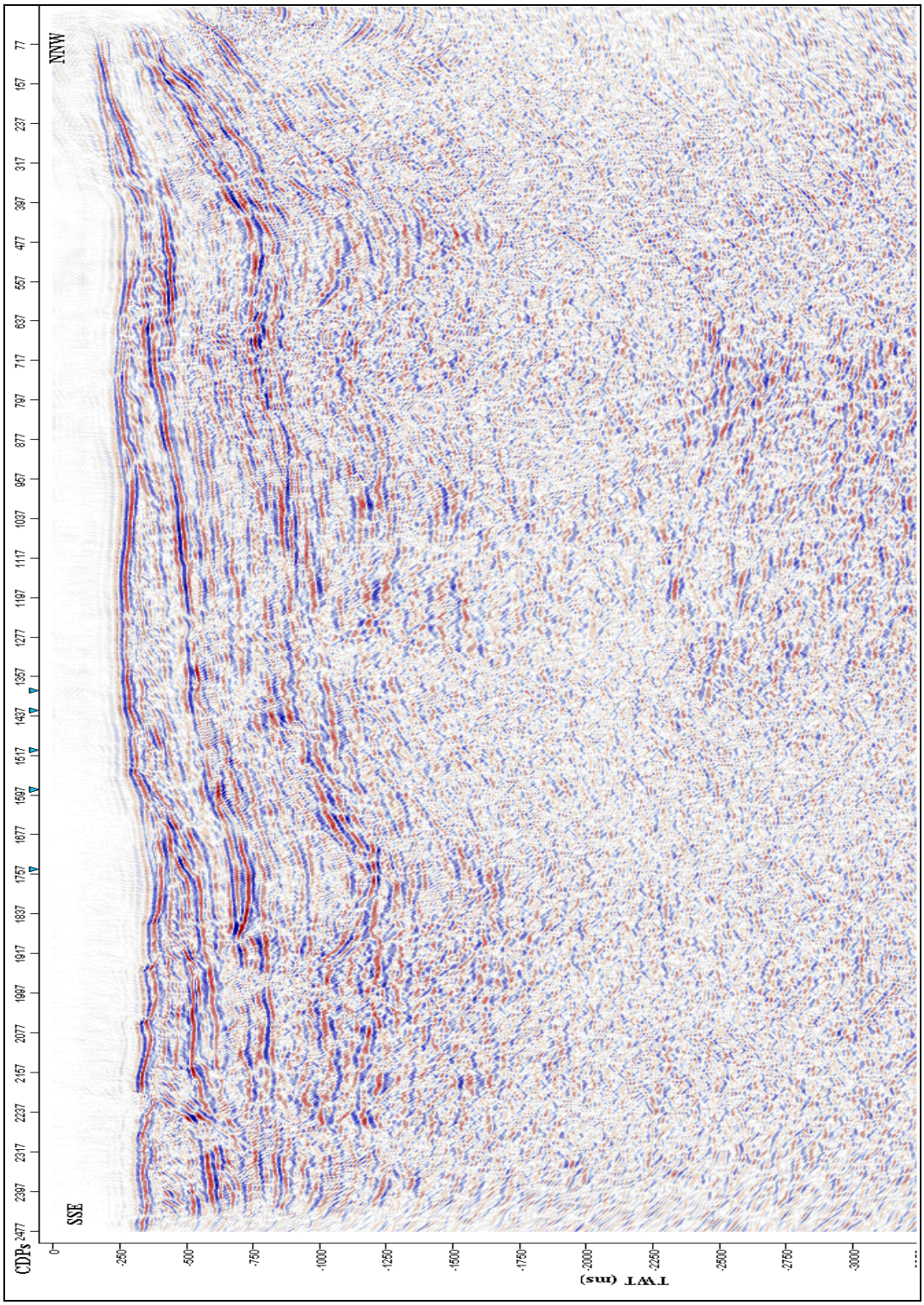

Figure 6.16: Display of final pre-migrated stacked section.

In the final presentation or display of the data, it can be seen that all linear events (direct waves, head waves), all types of noise, multiples, NMO effect and dipping events presented in the seismic raw data, have been attenuated effectively after processing the data with the sequence described in figure (6.3). The seismic data can now be used for the interpretation.

7. SEISMIC DATA INTERPRETATION METHOD

7.1 Introduction

The seismic data interpretation has been given many different meanings to geophysicists who handle seismic reflection records and by geologists who put the information to use. Seismic data interpretation involves prediction of structures with their geological properties or determining a model based on some geophysical measurements (Sheriff & Geldart, 1995). After a seismic map is constructed, an important thing is to interpret the seismic section by using the geologic information from surface and subsurface sources e.g. fault traces or geologic contacts. This involves identifying reflectors and making tie to the wells or surface features. All this depends upon the amount of information available. In seismic method, physical measurements are made at the surface. These measurements are then evaluated and interpreted in terms of what might be possibly in the subsurface, the position and property of interfaces. The resulting information is then combined into cross sections, which represent the structure of geological interfaces responsible for the reflection events.

The seismic reflection interpretation usually consists of calculating the position of geologically concealed interfaces or sharp transition zones from seismic pulses returning to the ground surface by the process of reflection. The influence of varying geological conditions is eliminated along the profiles to transform the irregular recorded travel times into acceptable subsurface models. This is very important for confident estimation of the depth and geometry of the bedrock or target horizons (Dobrin & Savit, 1988). The acoustic impedance, which is one of the rock properties that governs reflections, is the product of velocity and density, calculated by the following relation:

Acoustic impedance = interval velocity *density

$$Z = V.\rho \,. \tag{7.1}$$

Seismic reflections arise at boundaries across which the acoustic impedance changes. No reflection occurs if the impedance does not change even there is a lithology change. The reflection will be strong when there is greater difference in the acoustic impedance across the layer. The amplitude change in impedance is defined by the reflection coefficient (RC), which is the ratio of amplitude of the reflected wave to the incident wave or how much energy is reflected. The reflection coefficient can be expressed as:

$$R = \frac{(\rho_2 V_2 - \rho_1 V_1)}{\rho_2 V_2 + \rho_1 V_1)} \,. \tag{7.2}$$

Here ρ_1 is the density of the medium 1, ρ_2 is the density of the medium 2, V_1 is the velocity of medium 1 and V_2 is the velocity of medium 2. Typical values of "*R*" are approximately -1

from water to air, meaning that nearly 100% of the energy is reflected and none is transmitted; ~ 0.5 from water to rock; and ~ 0.05- 0.2 for shale to sand.

7.2 Seismic section

A seismic section is simply a diagram of cross section of earth or display of seismic data along a 2D line. A seismic section consists of numerous traces with location given along the x-axis and two-way travel time (TWT) or depth along the y-axis. The variation in these scales enhances the physical appearance of the seismic section. The section is called a depth section if the section has been converted from time to depth and a time section if this has not been done. Each seismic section has its own header, having the basic information about the acquisition and the processing of seismic section. A combination of the wiggles (one of the display pattern of traces) extending laterally is called horizon. The main objective here is picking of the horizons. Normally the horizons are named on the basis of the check shot survey and/or on the basis of VSP data. Synthetic seismogram can also be used to name the horizons accurately to some extent.

7.3 Interpretation of seismic section

The interpretation of the seismic data is done by defining the horizons and faults along the seismic section, determining the layer boundaries of interest. These horizons are followed either by positive or negative amplitude, which represents respectively a decreasing or increasing acoustic impedance. These horizons only represent the structure in two dimensions. In 2D seismic data the structures can be interpreted more accurately if several lines are shot in lattice pattern, with less distance between them. The orientation of the lines should best depict the structures, which is also important for the best possible interpretation. While interpreting the seismic data, well log data and result from previous geological surveys and studies of the region are often used in connection with the seismic data (sheriff & Geldart, 1995).

7.4 Approaches to the interpretation of a seismic section

There are two main approaches for the interpretation of a seismic section.

1 - Structural analysis.
2 - Stratigraphic analysis.

7.4.1 Structural analysis

Structural Analysis is very suitable for areas where most of the hydrocarbons are extracted from the structural traps. In structural interpretation, the most important aspect is to understand the cause of structuring. To understand the geology, correct interpretation of the structure is fundamental. Structures can be grouped into three categories at a basic level (Badley, 1985):

- Primary structures caused by deep crustal process e.g. basin margin faults, strike-slip faults.

- Secondary structures, these are direct consequence of the primary structures, for example, development of folds in sedimentary cover over fault basement blocks and subsidiary faults related to stress developed.
- Passive structures, developed as a consequence of, or an after effect of primary and secondary structures.

Most structural interpretation schemes use two way reflection times, from which depth and time structural maps are constructed to display the geometry of selected reflection events. Discontinued reflections clearly indicate faults and undulating reflections reveal folded beds (Dobrin & Savit, 1988).

7.4.1.1 Seismic interpretation of structures

Fold and flexures: Fold and flexures are the types of structures which are easily observed in the seismic section and identifiable from the dip changes of the reflections. These structures can be found at all scales, from hand-specimen size to the size of kilometers across. They are developed under a variety of conditions e.g. regional compression, subsidence and frictional drag associated with faults. Fold and flexures can be categorized in to following groups:

- Folds associated with compression on a regional scale, due to major crustal process.
- Smaller scale folds due to local compression e.g. anticlinal features associated with strike-slip faulting.
- Fold and flexures related directly to the faulting e.g. rollover anticline.
- Folding due to rise of the underlying features e.g. salt and shale domes, igneous intrusion.

Different fold styles within the same sequence can be produced when there is ductility contrast between different materials. Folds are described by their amplitude, wavelength, plunge and axial trace (Badley, 1985).

Interpretation of faults: Faults can be difficult to observe in the seismic data and faults plane reflections are rarely observable in seismic sections. Their location and geometry can be inferred by the reflection termination, diffraction and dip changes (Badley, 1985).

Normal faults: A normal fault is a fault with dip-slip is dominant and the hanging wall has moved down relative to the foot wall. These occur particularly in all types of basins and can be recognized easily in the seismic section as compared to thrust and strike-slip faults. Planar normal faults (figure 7.1) are the most common types of faults in most basins. Planar normal faults are recognized by different features e.g. an approximate fault plane, normal drag against the fault plane and antithetic faults. The listric normal faults (figure 7.1) have curved fault planes, which cause the hanging block to rotate. These faults are recognized by the differential tilting of the hanging and foot wall blocks, common development of reverse drag of reflectors in the hanging wall block and syn-fault sedimentation (Badley, 1985).

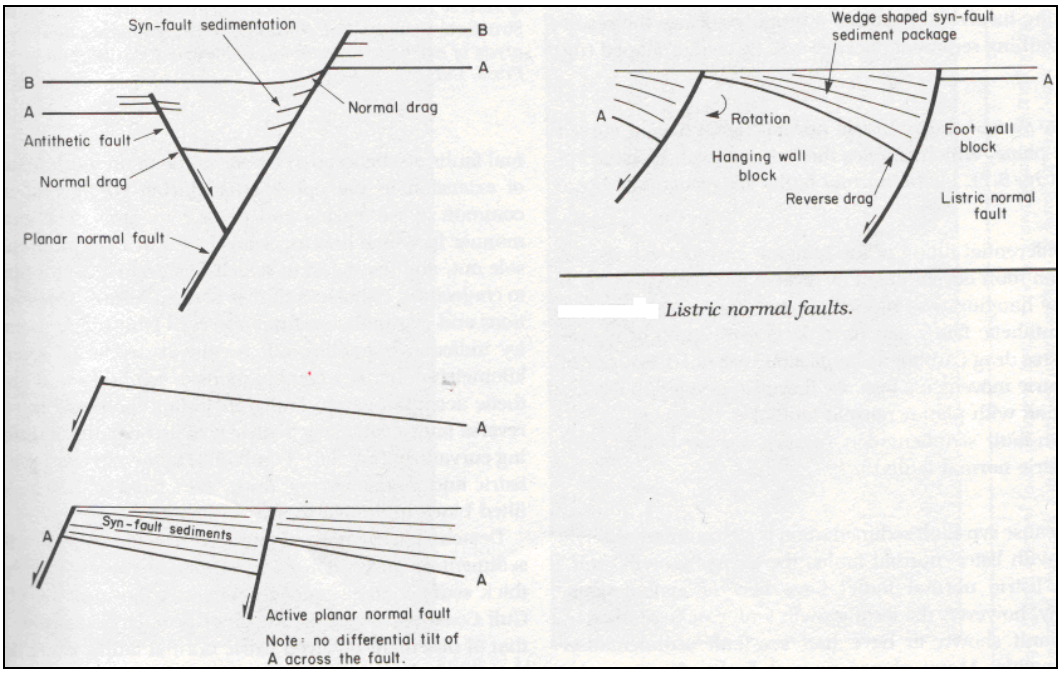

Figure 7.1: Basic fault terminologies, planar normal faults and listric normal faults (Badley, 1985).

Reverse faults and thrusts: A reverse fault is a dip-slip fault with the hanging wall moved up relative to the foot wall. Reverse faults can be either high angle or low angle. They are also called copressional faults as they are formed where the plate margins are converging, under a compressional stress system (figure 7.2). Low angle reverse faults are called thrust faults and the term reverse are used for high angle faults (Badley, 1985).

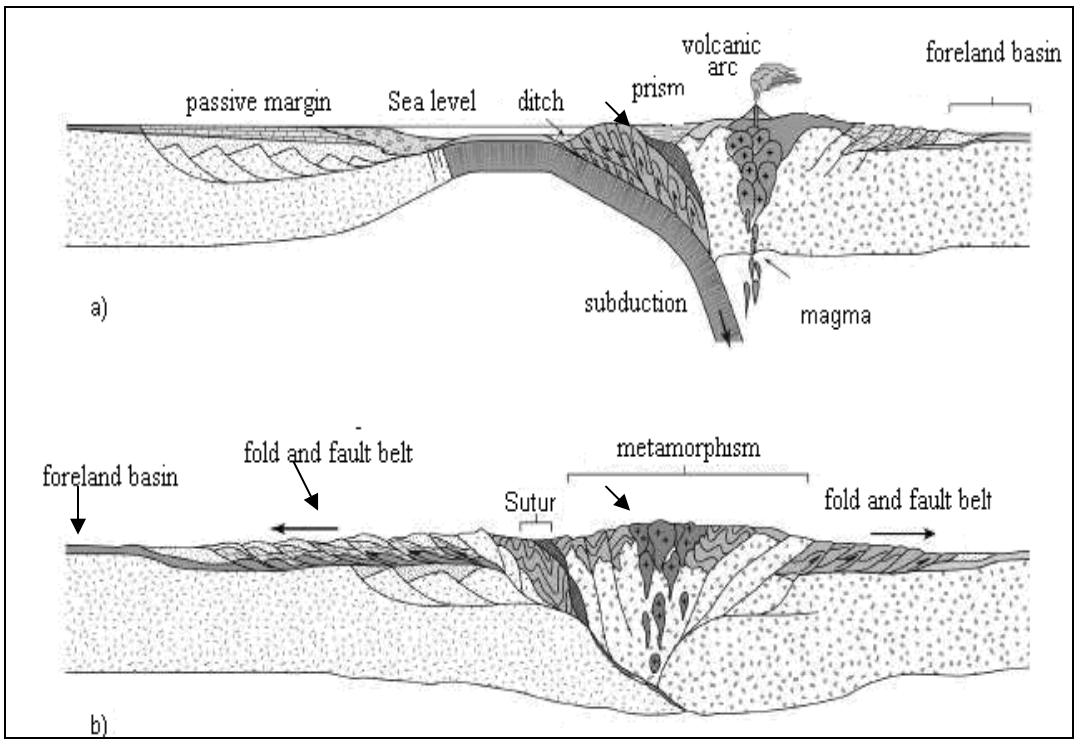

Figure 7.2: Contractional margin, formation of fold and fault belt, thrust faults and foreland basin (Pluijm & Marshak, 2004).

Reverse faults can be identified by the repetition of the strata. A complex array of structures commonly associated with thrusts, may be difficult to see in the seismic section. For instance duplex zones structures (figure 7.3) frequently figured in geological cross-sections are some time described as schematic, rather than an accurate depiction of the duplex-zones structures. Duplex zones are inferred from the thickening of the particular lithological unit.

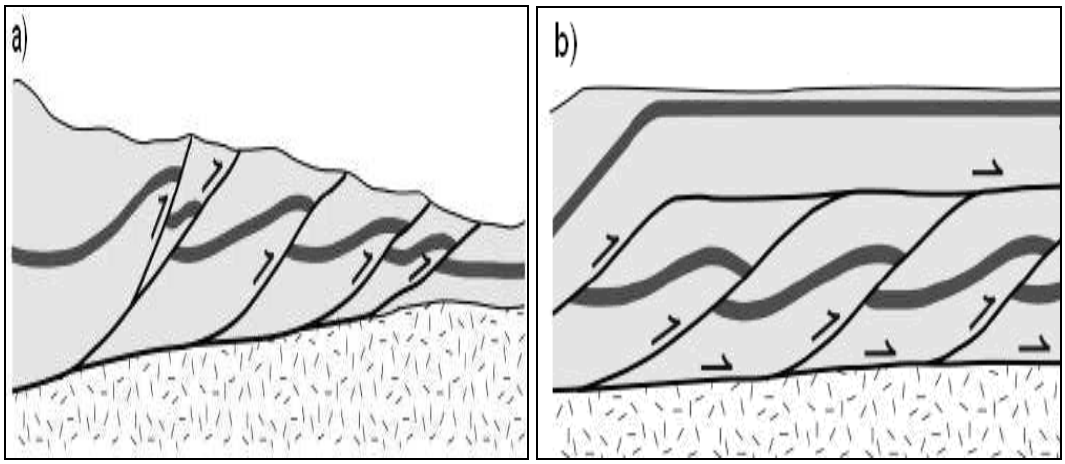

Figure 7.3: (a) Imbrications, (b) Duplex fault structures (modified from Pluijm & Marshak, 2004).

Seismic sections in low-angled thrusts terrains are often difficult to interpret because lateral and vertical velocity variations make it make it very difficult to collect good seismic data. However oil discoveries in the Rocky Mountain thrust belt have given great impetus for seismic investigations in recent years. Thrust faults occur both as basement involved and detachment faults (Badley, 1985).

7.4.2 Stratigraphic analysis

The interpretation of seismic stratigraphy is based on the identification of seismic sequences and on seismic facies analysis. This type of analysis is helpful in determining huge reservoirs of hydrocarbons. Stratigraphic analysis involves the subdivision of seismic sections into sequences of reflections, which are interpreted as a seismic expression of genetically related sedimentary sequences (figure 7.4). The principles behind this seismic sequence analysis are of two types. Firstly, reflections are defined in chrono stratigraphical units, since the type of rock interface that produce reflections are strata surfaces and unconformities. Secondly, genetically related sedimentary sequences normally comprise a set of concordant strata that exhibit discordance with underlying strata (Badley, 1985).

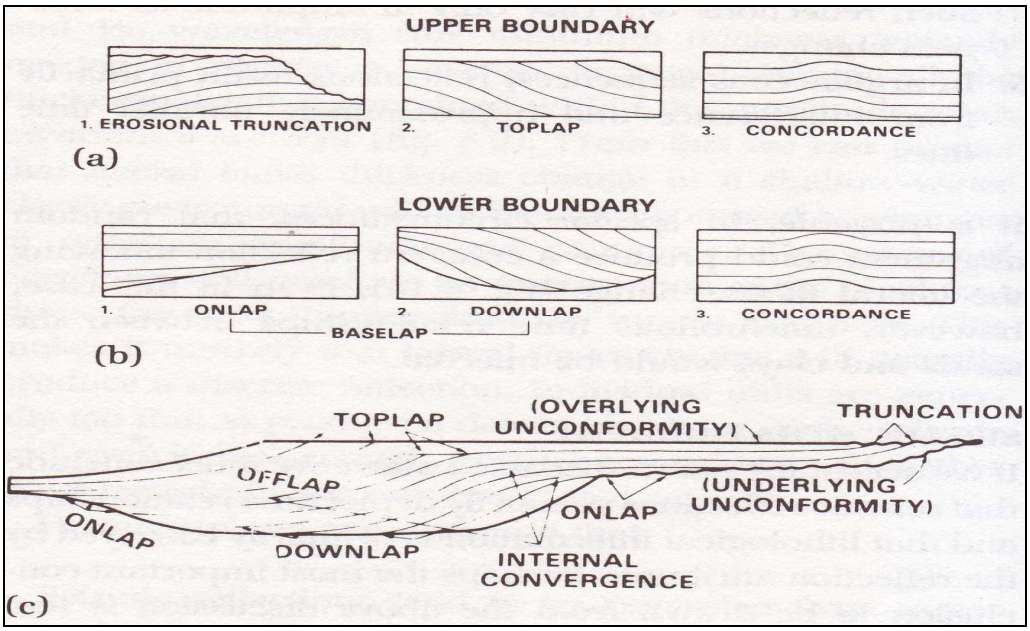

Figure 7.4: Reflection relationships; (a) Relationships at the top of the sequence, (b) Relationships at the base of the sequence, (c) Reflection relationships within an idealized seismic sequence (Badley, 1985).

7.5 Seismic facies analysis

Seismic facies represent a group of seismic amplitude variations with characteristics that distinctly differ from those of other facies. A seismic facies is the manifestation of the underlying geologic facies or structural feature in the seismic amplitude data. These can be searched and identified from the seismic data by different approaches. These could be based on analysis of either the seismic waveforms or the seismic attributes. Seismic facies analysis consists of the parameters and reflection configuration studies, which determine a seismic sequence (figure 7.4). The main idea behind the facies analysis is to interpret reflections with respect to lithology, stratification, and the characteristics of the depositional environment (Capron, 2005).

The meaning of seismic interpretation is to detect and differentiate among various stratigraphic packages, and that is done by identifying the unconformities and variations in seismic character within the sedimentary units. Mitchum et al. (1977) established a general method for the reflection configuration of seismic facies. These configurations include parallel, sub-parallel, divergent, and chaotic seismic pattern etc (figure 7.5). This is only based on the theoretical category, as the real seismic data may be R combination of several different patterns.

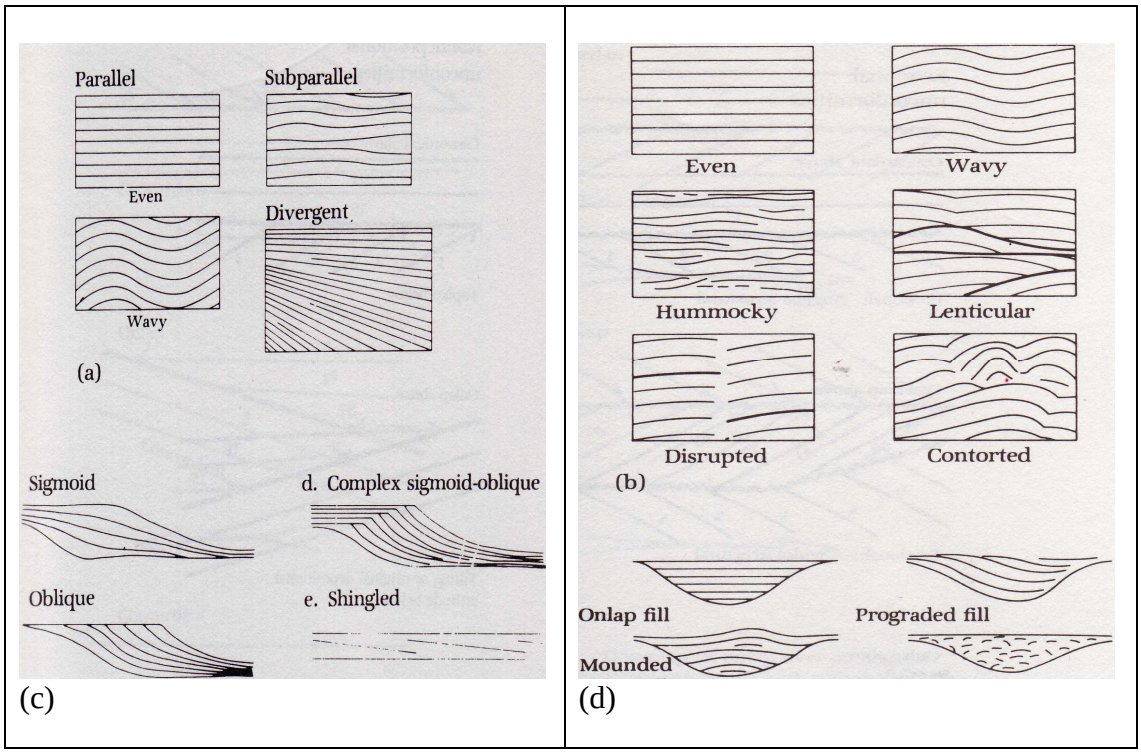

Figure 7.5: Reflection configurations for different seismic facies (from Mitchum et al., 1977; Badley, 1985).

7.6 Seismic resolution (Seismic data quality)

Seismic resolution is a measure of how large an object need to be in order to be seen in seismic. In seismic data, depth is normally measured in two-way travel time in milliseconds or seconds. This is the time the sound waves use from it leaves the source until it hits the reflector and return to the receiver. With the increase in depth the frequency of the signal will decease while the velocity and wavelength will increase. This means that with increase in depth the seismic resolution gets poorer. The high frequencies are reflected from shallow reflectors, while the low frequencies reach further down. The velocity of the sound increases with increasing depth as the sediments are gradually more compacted with increasing depth. The seismic resolution can be categorized in two types, such as vertical resolution and horizontal resolution. Both vertical and horizontal resolution depends on the signal bandwidth (Rafaelsen et al., 2002).

7.6.1 Vertical resolution

The smallest distance in time or depth between two layers where they will appear as a separate reflection is called vertical resolution. The vertical resolution is derived from the wavelength of the sound waves and the layers can be discerned when their thickness is below 1/4 wavelength. Vertical resolution is defined by the wavelength and frequency of the seismic signal. For two reflections, from upper and lower boundary, respectively, the limit for how close they may be is calculated by following expression (Rafaelsen et al., 2002; Yilmaz, 2001).

$$\lambda = \frac{V}{f}. \tag{7.3}$$

The vertical seismic resolution is given by $\lambda/4$, where λ is the dominant wavelength, V is the seismic velocity and f is the seismic frequency.

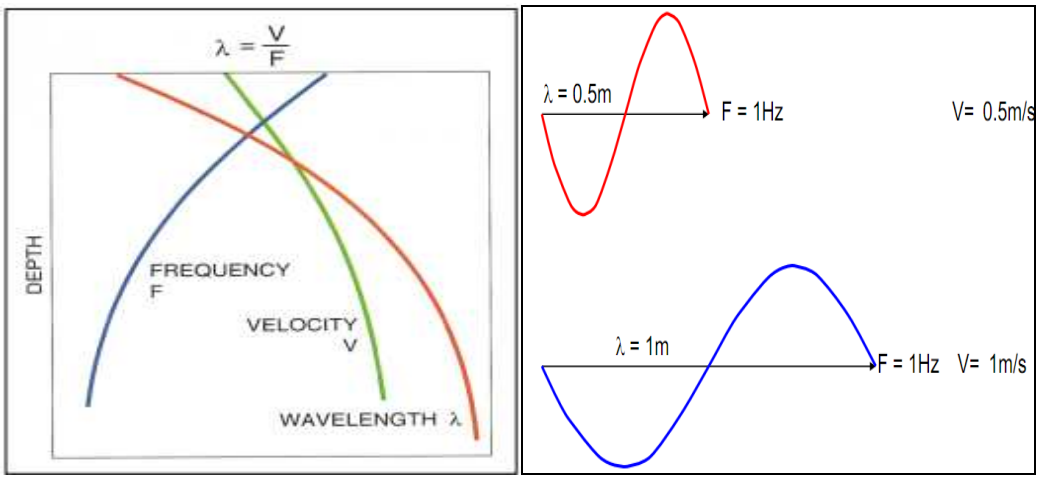

Figure 7.6: The relationship between wavelength, frequency and velocity of the seismic signal, there is direct relationship between wavelength and velocity while the frequency is inversely proportional to the wavelength (Yilmaz, 2001).

- Increasing depth causes an increase in velocity (in general).
- Increase in depth causes an increase in wavelength.
- Increase in depth causes a decrease of the frequency.

7.6.2 Horizontal resolution

Horizontal resolution is the minimum distance between two reflection points that will give two separate reflections. The sound waves sent out from the source move in three dimensions and spread out over a large area. The horizontal resolution is derived from the fresnel-zone (figure 7.7), the part of a reflector covered by the seismic signal at a certain depth (Rafaelsen et al., 2002).

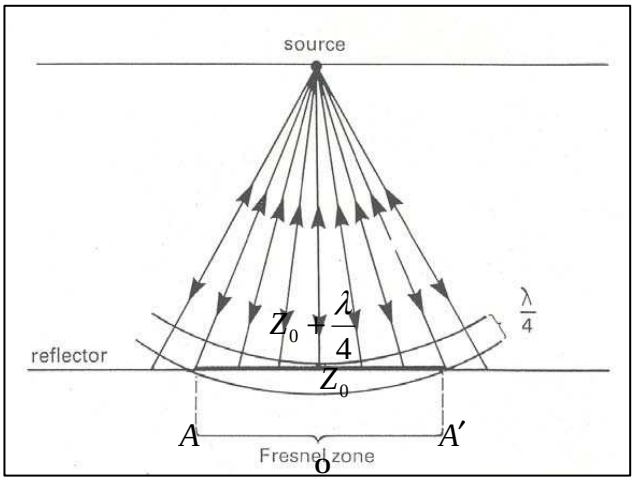

Figure 7.7: Defining a Fresnel-zone A- A' (Yilmaz, 2001).

Figure (7.7) shows the wavefront that hits the plane reflector; O is the point to be imaged. The travel time for energy reflected from O is $t_o = \frac{2z_o}{V}$, when the wave has moved from A to A' then $t_1 = (z_o + \frac{\lambda}{4})$. The total energy for this interval is called the fresnel-zone and the energy will interfere constructively. Migration of the data collapses the fresnel-zone by focusing the energy in a single point. In 2D seismic data, because of migration, the fresnel-zones get elliptical and will not correct the energy which is outside the plane. Figure (7.8) explains the effect of migration for the fresnel-zone.

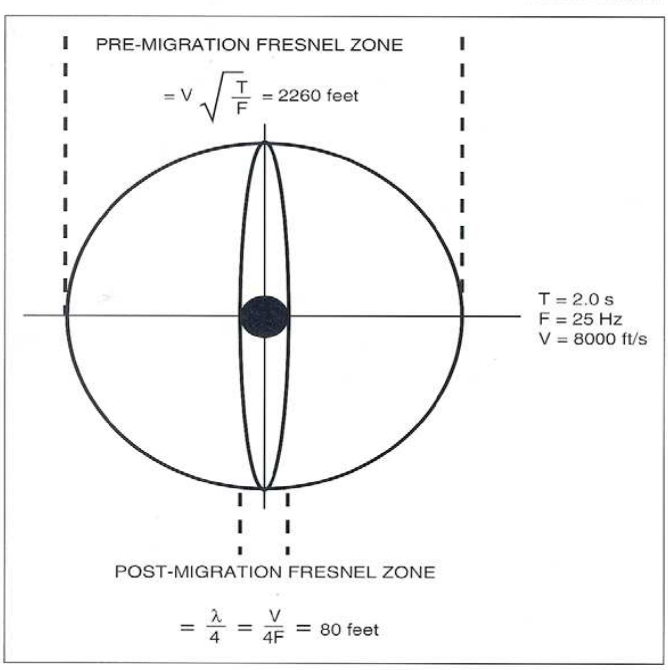

Figure 7.8: The effect of migration on the Fresnel zone. The example illustrates how migration reduces the width of zone at 2 s (TWT) (Brown, 1999).

8. SEISMIC DATA INTERPRETATION

The following chapter describes the interpretation of the seismic data from Isfjorden. A general interpretation was carried out to provide an overview of the prominent horizons and sedimentary packages along with the interpretation of some structures present in the subsurface. A total of nine seismic profiles (figure 8.1) were interpreted and some profiles with better resolution were selected to present the interpretation results.

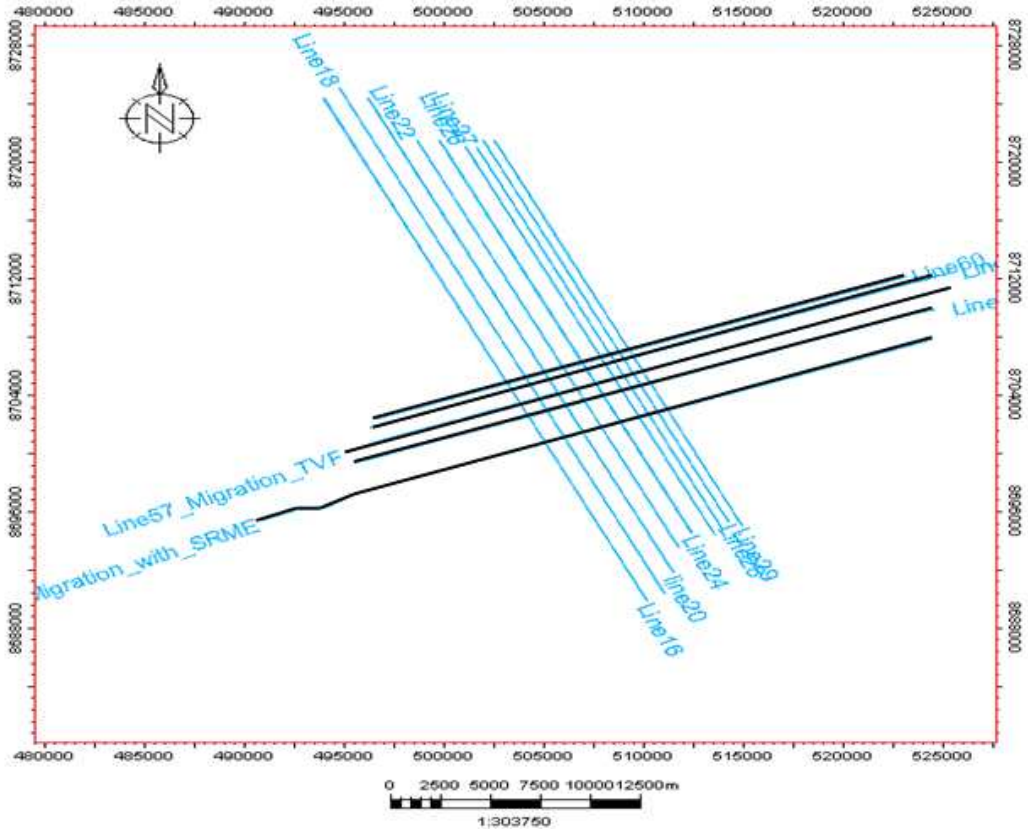

Figure 8.1: Location and orientation (with respect to coordinates) of the seismic profiles used for interpretation. The lines shown in black were only used for correlation and for support in interpreting the horizons.

8.1 Basis for interpretation

Schlumberger's Petrel 2010.2 visualization and reservoir modeling software was used as a tool for interpreting the seismic data. A set of nine seismic lines was imported into Petrel in SEG-Y format. A new seismic survey folder was created in petrel to store the lines. To get a 3D view of the 2D profiles the 3D window was used. A plan view of the area with the seismic lines included could be seen in the 2D windows. Both 2D and 3D windows were used in combination with the interpretation window for seismic interpretation.

8.2 Formation velocities from Svalbard

Formation velocities from Svalbard have been estimated from different seismic reflection and refraction surveys conducted in the area. On the basis of these studies the velocities for

Permian, Triassic and tertiary formations were estimated. Eiken (1985 & 1981) performed reflection and refraction studies in eastern part of Isfjorden, while Johansen et al. (1994) and Johansen et al. (2007) did laboratory measurements for rock samples collected from different places on Svalbard and compared the result of these samples with logs from the well logs. The velocities measured from these studies are presented in figure (8.2) below:

	Group/ formation	P-velocity km/s Eiken (1981)	P-velocity km/s Johansen et al., (1994)	P-velocity km/s Johansen et al., (2007)
Tertiary	Eocene			2.5 – 3.7
Triassic	Sassendalen Group	4.0–4.5	3.7 – 4.3	
	Upper kapp		4.9 , 5.1	
Permian	starostin FM	4.6–5.6		
	Middel kapp		5.2 , 5.4	
	starostin FM			
	Lower kapp		5.4 , 5.6	
	starostin FM	6.0 -6-7		
	Gibshukem FM		5.8 , 5.9	

(a)

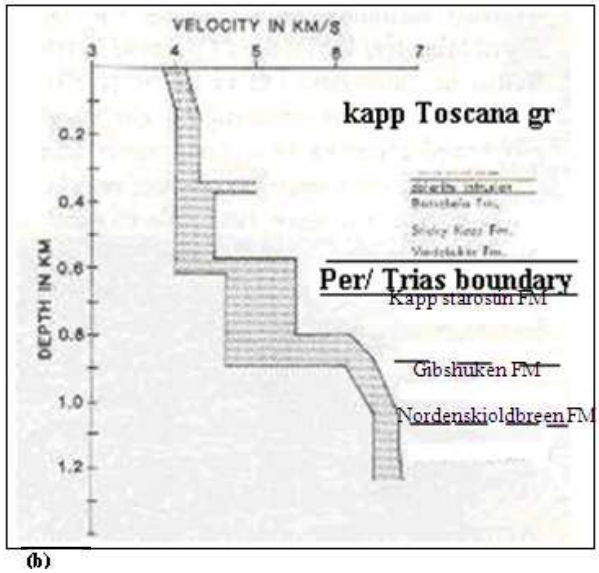

(b)

Figure 8.2: (a) Table shows the values for approximate P- wave velocities from Svalbard, (b) An estimation of velocity distribution and their geological correlation (from Eiken, 1985; Johansen et al., 1994 & 2007).

The formation velocities are supposed to be comparable with the formation velocities in Isfjorden.

8.3 Data for correlation

The seismic reflectors present in the subsurface of the study area were identified on the basis of seismic reflectivity contrast and seismic stratigraphic signature without any well control. The correlation was done on the basis of several previous studies done in that area along with the literature described in chapter 2. Below are some studies, used for the correlation of horizon's interpretation:

- Seismic Atlas of Western Svalbard (Eiken and Austegard, 1994), which includes the presentation of several seismic profiles.
- Results from Blinova et al., (subm), which include analysis of structural trends of sub-bottom strata in the area of West Spitsbergen Fold - and - Thrust Belt (Isfjorden) based on marine seismic data.
- Results from Bergh et al. (1997), where they interpreted multichannel seismic data from Isfjorden collected by Statoil (1988).
- Results from Eiken (1985), which include seismic mapping of the post Caledonian data in Svalbard.

- Results from Faleide et al. (2010), which describes geology of the Norwegian Continental Shelf (results from profiles interpreted in Isfjorden and Van Mijenfjorden).
- Results from Strømme, (2010), which describe the processing and interpretation of multi-channel seismic data from Mijenfjorden.

8.4 Data quality

The quality of the data in the study area depends on several factors. The sedimentary rocks that make up the subsurface in Isfjorden have high velocities causing large acoustic impedance contrast at the sea bottom. As a consequence of this we have strong water bottom multiples, which are a major challenge in seismic data processing. High reflection coefficient because of hard sea bottom means that a lot of energy from source is reflected back from the transition between water layer and seabed, and therefore less energy is penetrating in the subsurface. The presence of dolerite sill intrusions may also mask the underlying reflectors and affect the quality of the data. Water depth also is a problem for data quality because the short period between multiples masks actual arrival of the data. Another reason for low quality of seismic data is that the contractional structures beneath Tertiary Central Basin may also cause internal reflection disturbance. The diffractions and the velocity change both vertical and laterally in thrust terrains may also make it impossible to acquire good seismic data (Badley, 1985). The noise in the outer edge of the line and high frequency noise above the ocean floor represents a challenge when it comes to interpret and follow reflectors to the edges of the lines.

Structural geometries

Some of the structural features (Tertiary sequence) in the study area present complex structural geometries. They seem to dip in both directions. The reason can be that, some lines were shot SSE to NNW and some were shot from NNW to SSE. So while shooting in one direction it images the structures dipping in one side and shooing from other side caused the imaging the structures dipping in other side (may depend on the directivity of receivers array).

8.5 Interpreted horizons and seismo-stratigraphy

In seismic data interpretation, identifying the main key horizons is a natural starting point. A brief description of identified key horizons is presented under this section. However there is certain level of uncertainty in interpreting the data, as poor quality and resolution of the seismic data particularly at greater depth prevented from interpreting deep reflectors & successions, basement and structures precisely. Particularly in profiles 28 & 29, due to poor quality and bad imaging, it was difficult to interpret the sedimentary sequences below base Helvetiafjellet formation. Some of the key reflectors, identified on the basis of seismic reflectivity pattern, acoustic impedance contrast along with the correlation of some previous study done in that area (section 8.3) are presented below:

8.5.1 Sea-bed

Sea-bottom reflector was interpreted as peak due to increase in acoustic impedance contrast between the sea-bottom rocks and water layer. The sea-bottom is made up of rocks from Tertiary age in the south-east part of the study area, while in north-west part of area rocks from Cretaceous age make up the sea bottom (figure 8.3).

8.5.2 Base Tertiary

Base Tertiary reflector was interpreted as an unconformity and is supposed to lie in a transparent zone (0.6 – 0.7 sec TWT) above and below continuous strong reflections (figure 8.3; Bergh et al., 1997). The strong reflections below this zone are associated with sandstone in Adventdalen group.

8.5.3 Base Helvetiafjellet Formation (Cretaceous)

Base Helvetiafjellet formation was interpreted as the base of strong reflections (0.8 – 09 sec TWT) in the Cretaceous sandstone (figure 8.3; Blinova et al., subm).

8.5.4 Top Triassic (base Adventdalen Group)

Top Triassic boundary was interpreted as a strong reflector (1.1 – 1.2 sec TWT) that represents large acoustic impedance between the sandstone of Kapp Toscana Group and the overlying shale (Janusfjellet sub-group) of Jurassic age (figure 8.3; Bergh et al., 1997). Another reflector which marks the contrast between the sandstone of kapp Toscana group and the underlying shale of Sassendalen group with a prominent contrast in acoustic impedance was marked as base of kapp Toscana group, but this was interpreted with lower level of confidence.

8.5.5 Top Permian

Top Permian was supposed to be identified (1.6 - 1.7 sec TWT) as a strong impedance contrast between the high velocity carbonates of kapp Starostin formation and the overlying low velocity shale of Sassendalen group (figure 8.3; Bergh et al., 1997). This reflector is best depicted in the middle of some profiles.

8.5.6 Base Carbonate

Base carbonate boundary was interpreted (approximately 2 - 2.1 sec TWT) above the weak discontinuous reflections, a transparent zone representing the Devonian strata. Base carbonate reflector was marked with some uncertainty because of the bad resolution at this depth (figure 8.3).

8.5.7 Basement

A strong reflector at depth from 2.5 to 3 sec (TWT) was interpreted as top of the basement. This boundary was marked, a strong impedance contrast between the overlying weak and diffuses Devonian strata and underlying metamorphic basement (figure 8.5; Blinova et al., subm).

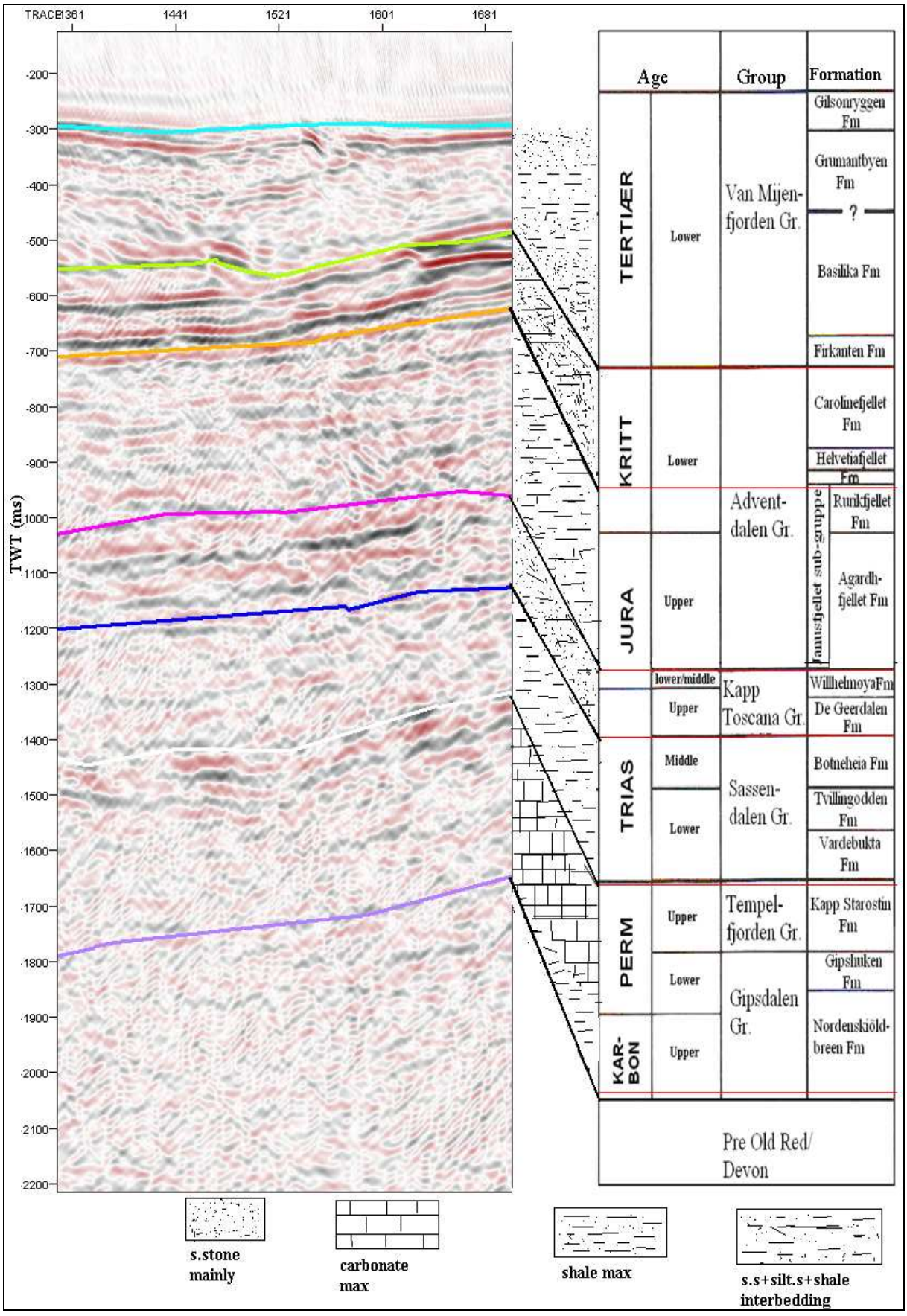

Figure 8.3: Correlation of seismic units interpreted form profile ISf-16 (centre of profile) and stratigraphic units in Spitsbergen (modified from Eiken and Austegard, (1994)).

8.6 Sea-bed

The top reflector was interpreted as sea-bottom in all profiles, and is displayed as peak due to increase in acoustic impedance from sea-water to sea-bottom. The sea-bottom is mostly smooth. Tertiary rocks from the Central basin make up the sea-bottom towards the south-east part of all the profiles, while in north-west part, the sea-bottom is made up of rocks from Cretaceous age. The shallowest area in the fjord is in the north-west, with a water depth approximately 125 ms (~ 93 m). The deepest area in the fjord has water depth approximately 350 ms (~ 260 m). Figure (8.4) shows the time surface map for sea-bed.

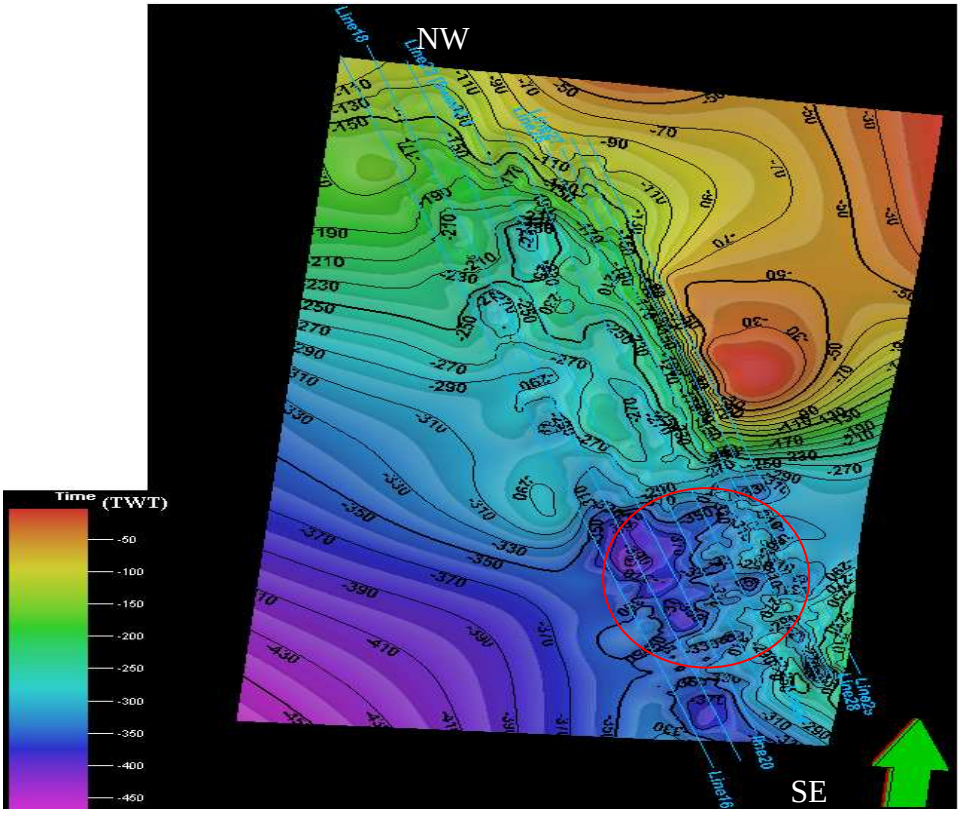

Figure 8.4: Surface map of ocean bottom with depth-scale in two-way time. Green arrow marks the north direction. It can be seen from the map that the deeper part in the study area (red circle) exists towards south or south-west.

8.7 Stratigraphic analysis (Interpreted successions)

The Paleozoic - Tertiary sedimentary strata unconformabley overlays the Devonian strata, and appears in the upper 2 sec (TWT) of the seismic section as layers with a shallow dip towards SSE or S. The seismic profile-16 has been used for the presentation of interpretation results. Figure (8.5) shows the example of the seismic data interpretation. Isochrone maps were generated at different stratigraphic levels. Thickness for some succession has been estimated by using the time values taken along vertical axis in petrel and average velocity values e.g. 1500 m/s in water layer, 4000 m/s in base Tertiary layer and around 5000 m/s for other layers. These values are measured during data processing as well as velocity values described in section 8.2. These are only rough estimates and there could be certain margin of error.

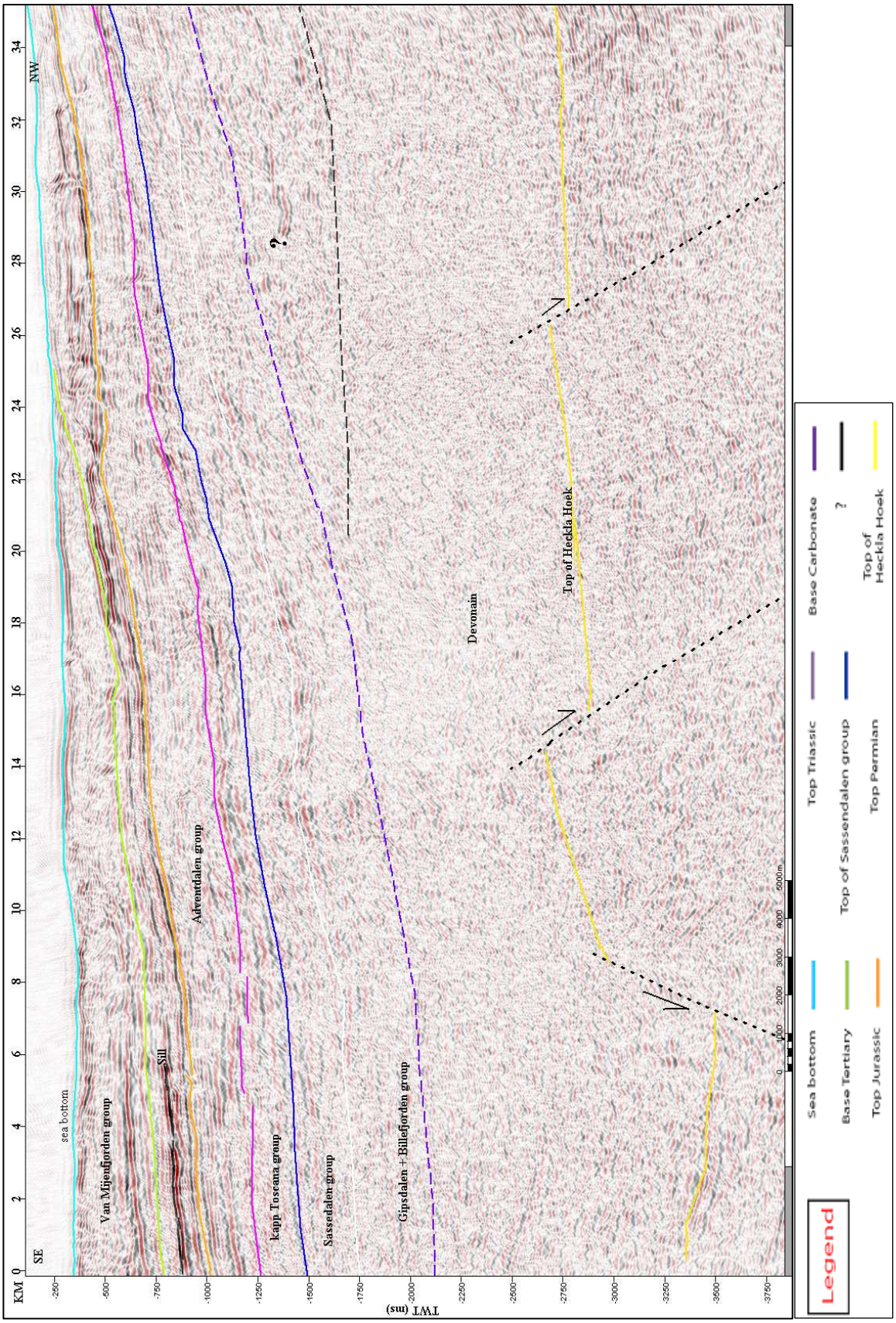

Figure 8.5(a): Shows the interpretation of identified horizons, sedimentary successions and faults for profile-16 (shot from SE to NW). Dashed line in Cretaceous sequence shows the sill (dolerite intrusion) resulting in very high amplitude reflections.

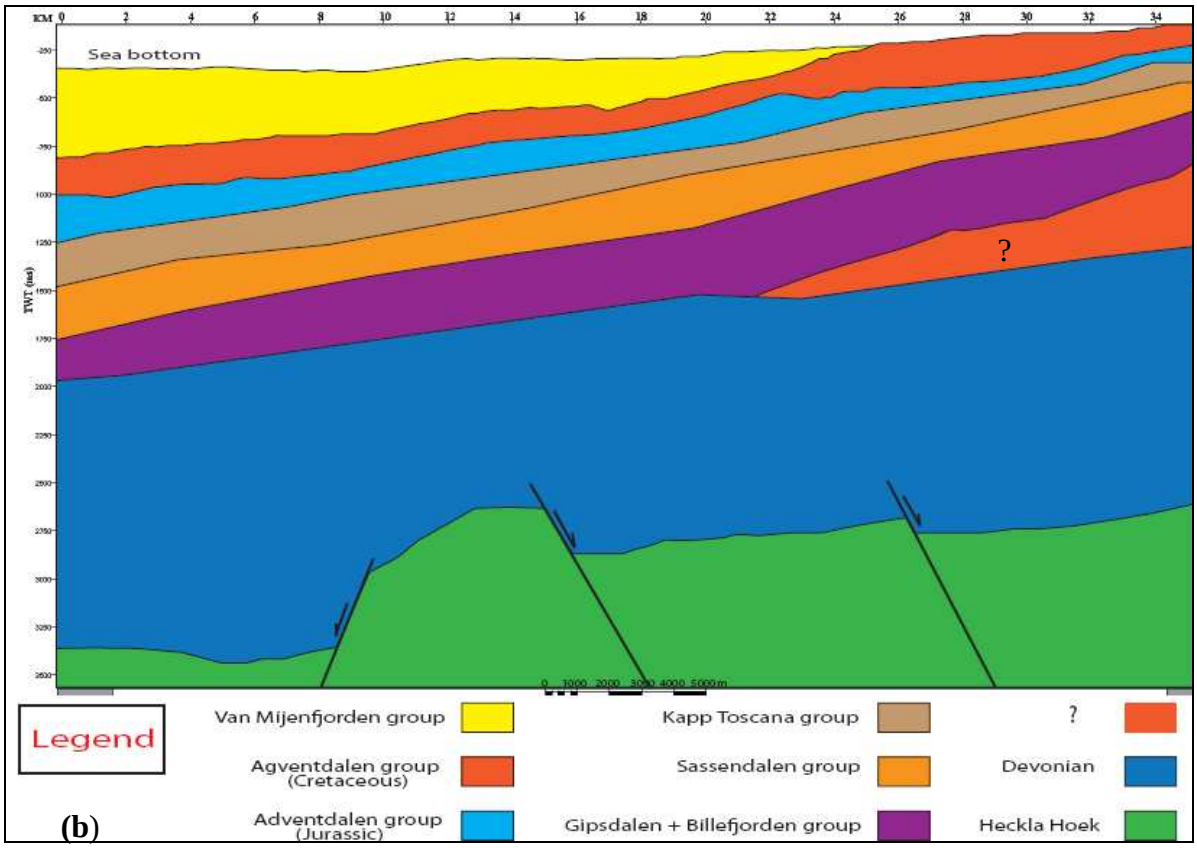

Figure 8.5(b): Shows the cross section of the interpreted stratigraphic successions.

8.7.1 Tertiary (Van Mijenfjorden group)

The Tertiary succession represents an asymmetrical syncline, interpreted as deposits from Tertiary age, named as Van Mijenfjorden group. Top cover of Tertiary rocks in Central Tertiary Basin was interpreted as the sea-bottom for all profiles (16-29). Base Tertiary makes the lower boundary of Central Tertiary Basin. Base tertiary reflector was interpreted, a reflector in the transparent zone, which lies below a strong double reflection and above a series of continuous reflections (Bergh et al., 1997). These strong reflections are related to the sandstone deposits in upper Adventdalen group of Cretaceous age (figures 8.3 and 8.5). The Tertiary deposits includes alternate sequences showing strong reflections (figure 8.6), which can be interpreted to represent the sandstone units in Van Mijenfjorden group. The top sequence of sandstone has thickness of apximately 75 - 100 ms (~200 m), while the lower sequence has thickness of approximately 100 - 125 ms (~225 m). Between these layers, there is a thick layer (average thickness ~ 100 - 125 ms, (~250 m) with more transparent character (comparatively weak reflections).

The Tertiary package defines an approximately 375 - 400 ms (~750 - 800 m) thick asymmetrical basin in the deeper part of study area and this thickness decreases towards the north-west direction. The Tertiary unit is deformed and is marked by some thrusts, backthrusts, folding of sea bottom and decollements.

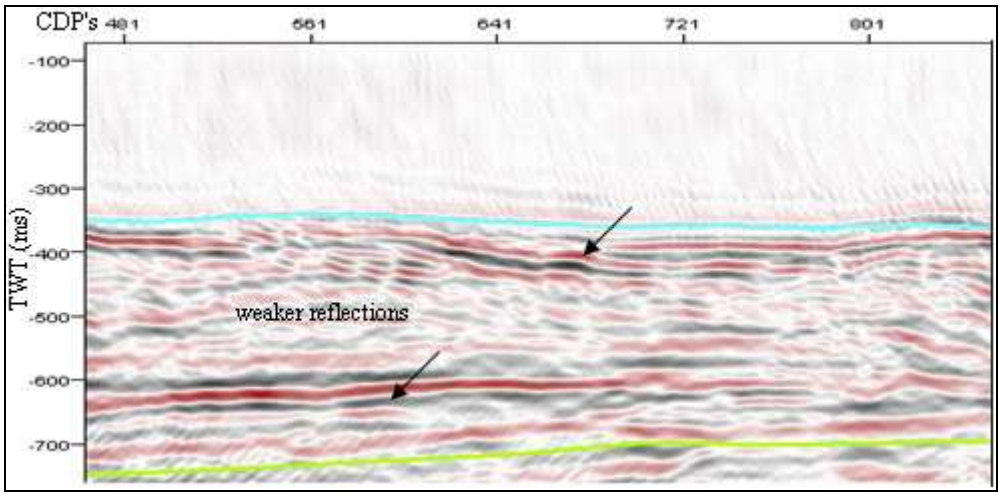

Figure 8.6: Display of the section from the profile-16, defining the sedimentary sequences in Tertiary package. The green line represents the base tertiary reflector and the marine blue line is sea-bottom reflector. The black arrows mark the strong reflections (probably sandstone packages deposited in early and late Tertiary period).

8.7.2 Cretaceous (Adventdalen group)

The Cretaceous succession represents several high amplitude reflections because of sandstone composition. The base of these strong reflections was marked as lower boundary (base) of Helvetiafjellet FM because of the contrasting reflectivity between the two seismic units and a sharp impedance contrast was observed between low velocity shale of Janusfjellet sub-group and the overlying high velocity sandstone of late - Cretaceous Helvetiafjellet Formation. The Cretaceous unit is defined approximately the range from 750 - 1050 ms (TWT) in the deeper part of the study area. The unit is more or less uniform in south with thickness 300 ms (~ 700 - 800m). In the middle of the line, probably some reverse faulting caused a piling up of strata resulting in the thickening of the sequence (figure 8.7). The upper part of the package represents weak reflections and chaotic behavior in the north-west part. The Cretaceous succession is shallower in north-west part and this is shown by an isochrone map generated at base level of Helvetiafjellet FM (figure 8.8). The Cretaceous sequence was interpreted to make up the sea bottom rocks in north or north-west part of the study area.

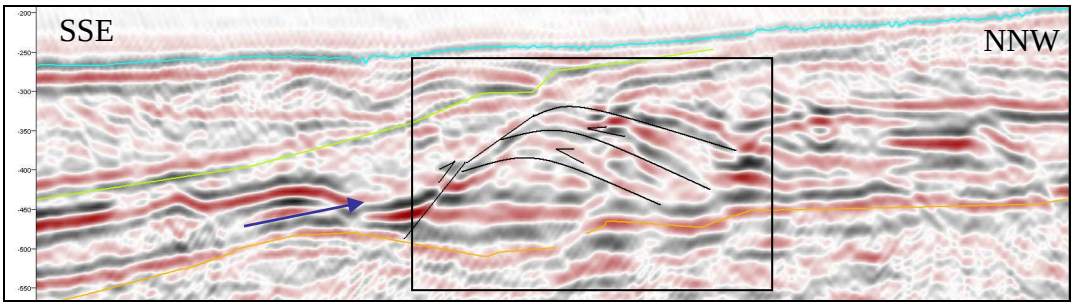

Figure 8.7: Display of zoomed section from the profile-16, marked green line (base Tertiary) and orange line (base Helvetiafjellet FM). Blue arrow directs towards the thickening of the Cretaceous succession probably caused by the thrust and backthrusts, during the Tertiary deformation (?).

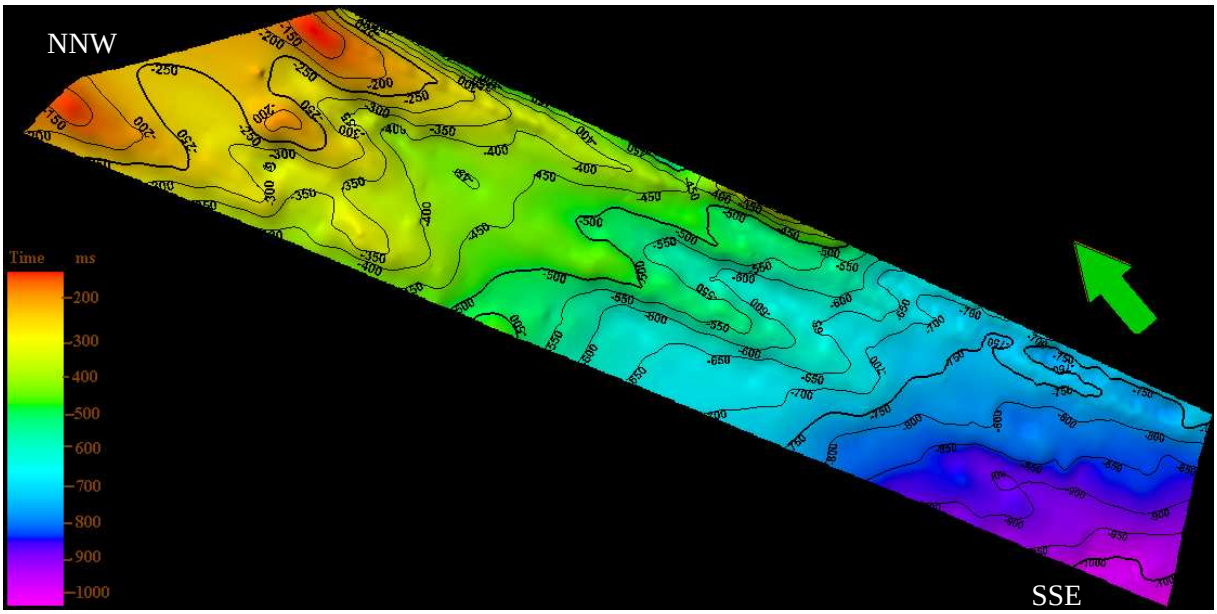

Figure 8.8: An isochrone map at Base level of Helvetiafjellet FM. Green arrow marks the north direction. It is obvious from the map that this unit is shallower in north or north-west side as compared to south and south-west part of the study area.

Sill

Very high amplitude reflections were observed in the southern and northern part of study area. These were interpreted as dolerite intrusions. This dolerite intrusion seems to terminate reflections at various levels from Triassic up to Tertiary successions, but it was found to be more prominent in Cretaceous succession in the southern part of the study area (figure 8.9).

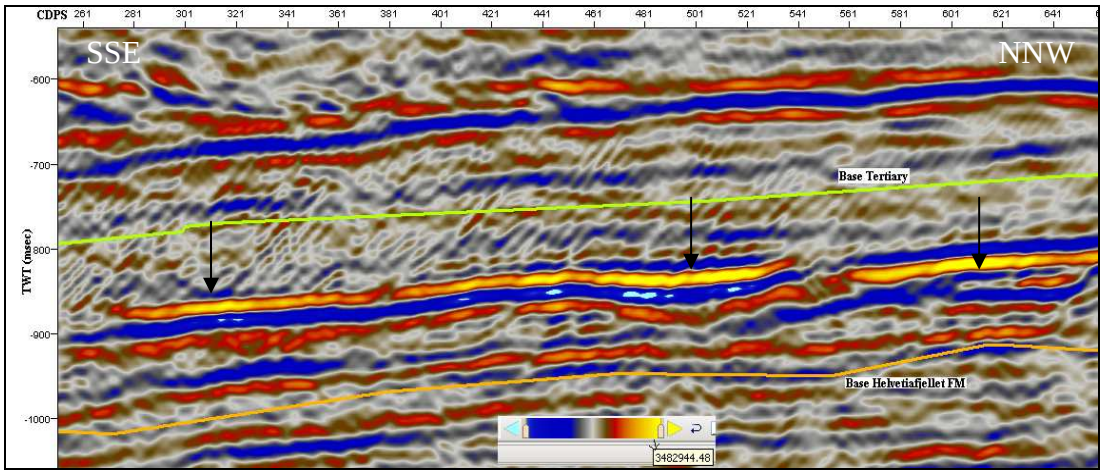

Figure 8.9: A section from profile-16, black arrows mark the very high amplitude reflections probably showing a sill (Dolerite intrusion) in the Cretaceous succession.

8.7.3 Jurassic (Adventdalen group)

This unit was interpreted as deposits from Jurassic (sandy-shaly sequence) in Adventdalen group, based in lower Jurassic and the upper limit defined by lower Cretaceous. The upper boundary was defined by the reflectivity contrast because of the overlying sandstone deposits

(Helvetiafjellet FM) of lower Cretaceous age. The lower boundary was marked by the reflectivity contrast between the underlying sandstone of Kapp-Toscana group and overlying Jurassic shale. The seismic character in Jurassic unit shows weak (low amplitude) and continuous reflections due to the shale deposits of Janusfjellet sub-group of Jurassic age. The thickness of the Jurassic package is approximately 300 ms (~700 m) in deeper part of the study area (figure 8.10). The thickness of the package changes with slight thinning towards north or north-west with sloping upward.

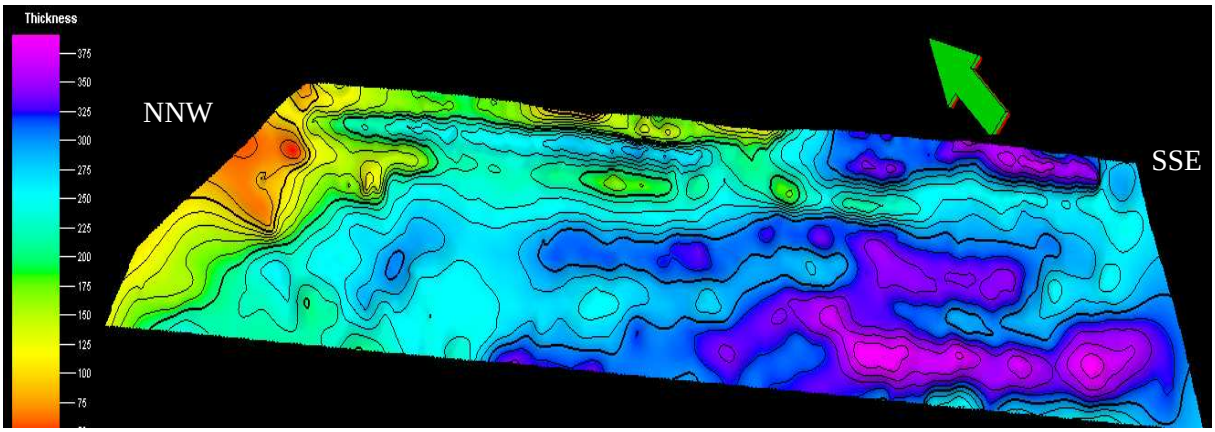

Figure 8.10: Thickness (in time) between Base Helvetiafjellet FM and top Triassic surface (Jurassic package). The unit is thicker in southern and western part of the study area with a continuous thinning towards north and north-east. Green arrow marks the north direction.

The minimum thickness for this unit is measured approximately to 100 m and maximum thickness measured is approximately 700 m. So the average thickness for this unit can be defined up to 300 - 400 m. The unit is thicker in southern and western part.

8.7.4 Triassic (Kapp-Toscana and Sassendalen group)

This sedimentary package was interpreted as deposits from Triassic age. Triassic deposits consists of kapp-Toscana group of upper Triassic age and Sassendalen group of middle and lower Triassic age, bounded by top Permian and lower Jurassic. The upper part of the unit presents strong reflections which are probably because of the sandstone composition, while the lower part of the unit expresses weak (low amplitude) discontinuous reflections, interpreted as shale deposits of Sassendalen group. The top of kapp-Tosscana group was identified and marked as a strong impedance contrast between the high velocity sandstone of kapp-Tosscana group and overlying shale of Jurassic age (Janusfjellet sub-group). The top of the Sassendalen group was marked as a result of reflectivity contrast between sandstone of upper Triassic and the shale of middle and lower Triassic age. The thickness of the Triassic unit in the deeper part of the study area has been estimated to be 400 ms (~700 - 800 m). An isochrone map was generated at top Triassic level for surface analysis (figure 8.11).

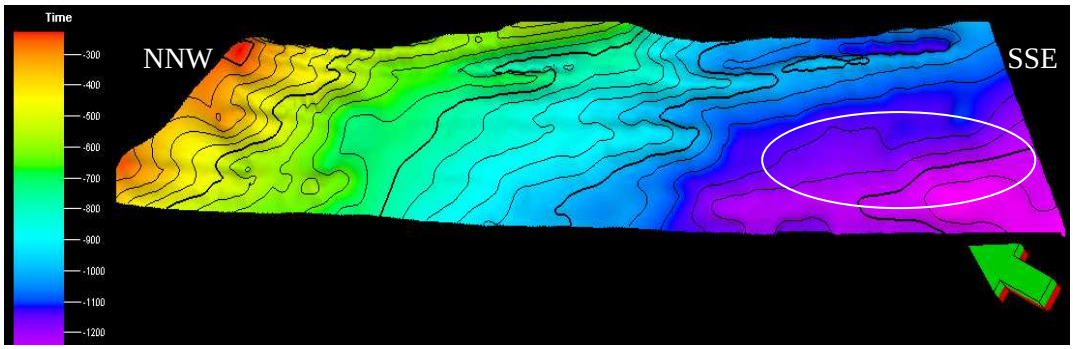

Figure 8.11: An isochrone map at top Triassic level. Green arrow marks the north direction. This unit is deeper (white circle) in the south-west part of the study area and it becomes gradually shallower moving towards north or north-west.

8.7.5 Permian and Carboniferous (Tempelfjorden and Gipsdalen group)

This unit was interpreted as deposits from the Permian and Carboniferous with the upper limit associated with the transition between low velocity shale of Sassendalen group and the high velocity silicified carbonates deposits of Cape Starostin Formation (figure 8.3). Top Permian reflector is supposed to be a strong reflector and is comparatively well identified in the middle and SE of profiles-16, 18, 22, & 26. This succession was identified at approximately 1.6-1.7 sec (TWT) in the deepest part. The Permian – Carboniferous carbonate package is characterized by folded, sub-parallel continuous reflections with low amplitude and locally discontinuous signature. This level corresponds to the unconformity between Devonian and Paleozoic sedimentary cover. Base Carboniferous reflector was interpreted with uncertainty due to poor resolution of the data at this level. Figure (8.12a) shows the isochrone map at top Permian level and time thickness map (figure 8.12b) for carbonate succession.

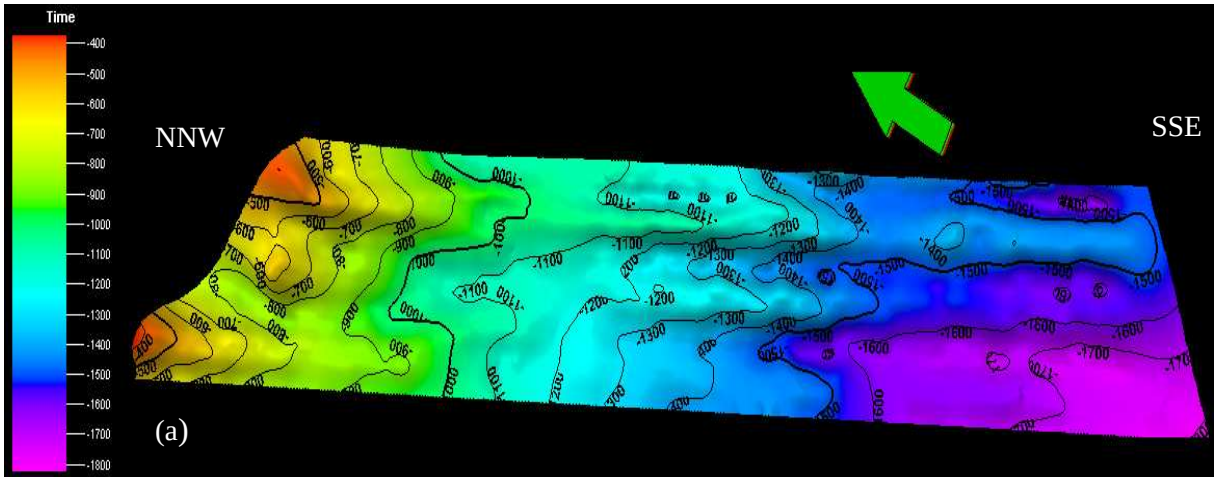

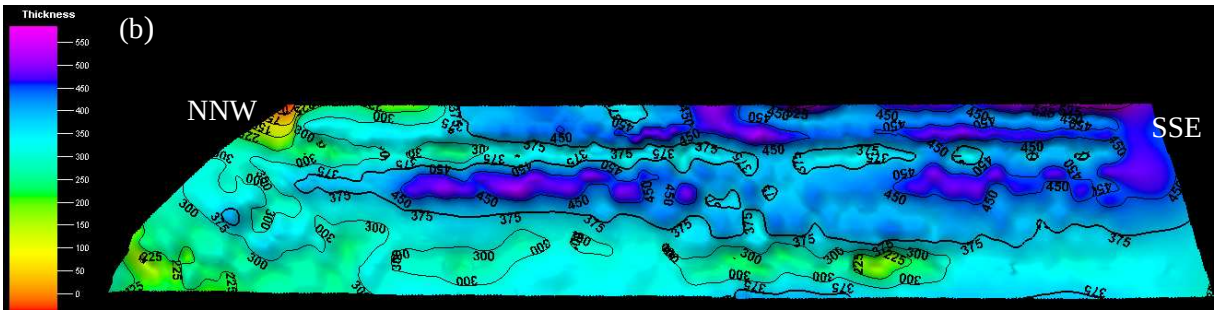

Figure 8.12: (a) An isochrone map at top Permian level, (b) Thickness map showing the thickness (in time) between top and base of carbonate package. Green arrow marks the north direction.

The base carbonate boundary was marked with lower level of confidence and uncertainty as a result of very poor resolution. So this thickness map may be a rough estimate.

The Devonian to early Carboniferous strata is characterized by chaotic, weak discontinuous seismic reflections. This unit presents mostly transparent seismic character with some weak reflections and has varying thickness because of the underlying faulted and uplifted basement. The sediments in Devonian were mainly deposited in the down faulted structures within the basement.

8.7.6 Basement (Hecla Hoek)

A strong reflector approximately at 2.5 to 3 second depth was interpreted as top of metamorphic basement (Hecla Hoek) and was defined as the boundary between strong and weak reflectivity pattern. This stronger reflectivity Caledonian unit is underlying a Devonian sedimentary section with weaker reflections and mostly transparent seismic character. However this interpretation is uncertain as this reflector is not clearly visible on some profiles or on parts of several profiles, where the reflectivity is scattered and diffused. The top basement reflector is best identified on profile-26, where it was interpreted on the whole profile (figure 8.13a). The seismic reflectivity pattern within the basement was found to be scattered with strong irregular reflections (figure 8.13b). This strong reflectivity scattered pattern may be due to varying acoustic impedance because of varying degree of metamorphism within the basement. The top of Hecla Hoek reflections is an irregular pattern which defines a ridge/basin type configuration visible on some profiles, best defined on profile-16. An isochrone map of top Hekla Hoek was generated, which shows the position of ridges and basins generated as a result of faulting (figure 8.14).

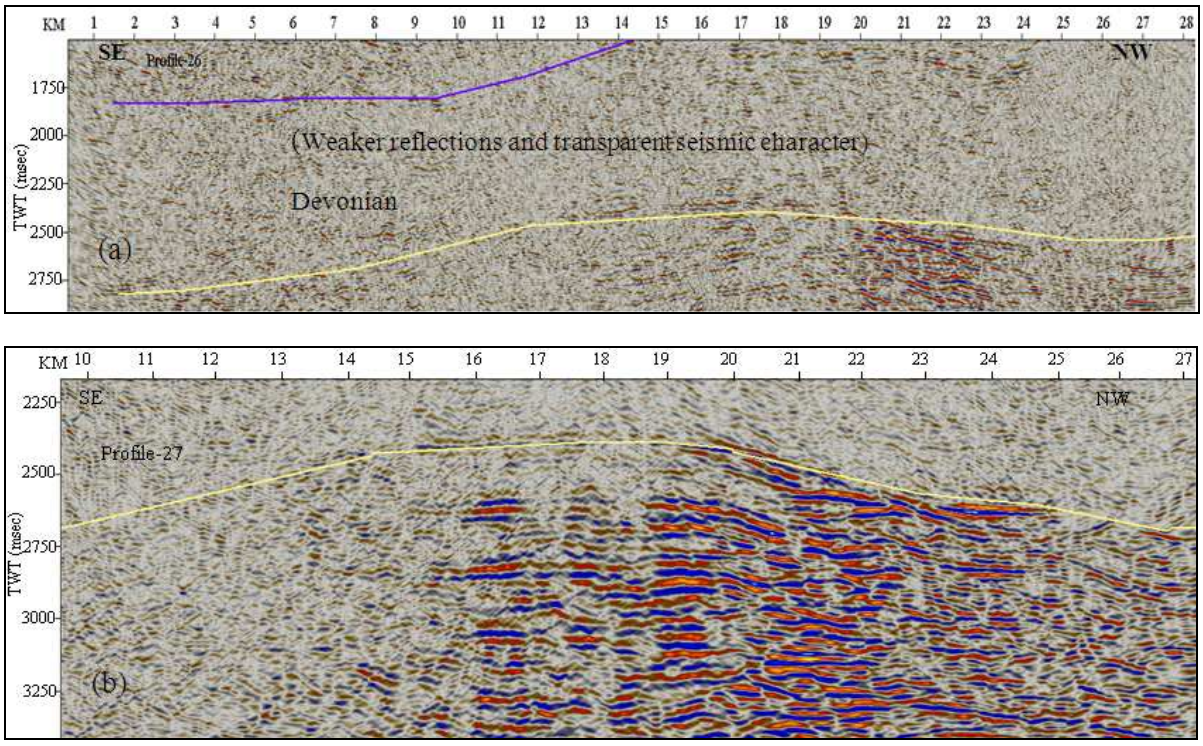

Figure 8.13: (a) Top Hekla Hoek marked with yellow colour, interpreted along the whole profile-26, purple colour is the base carbonate reflector; (b) Shows the strong reflectivity pattern within the metamorphosed basement in profile-27.

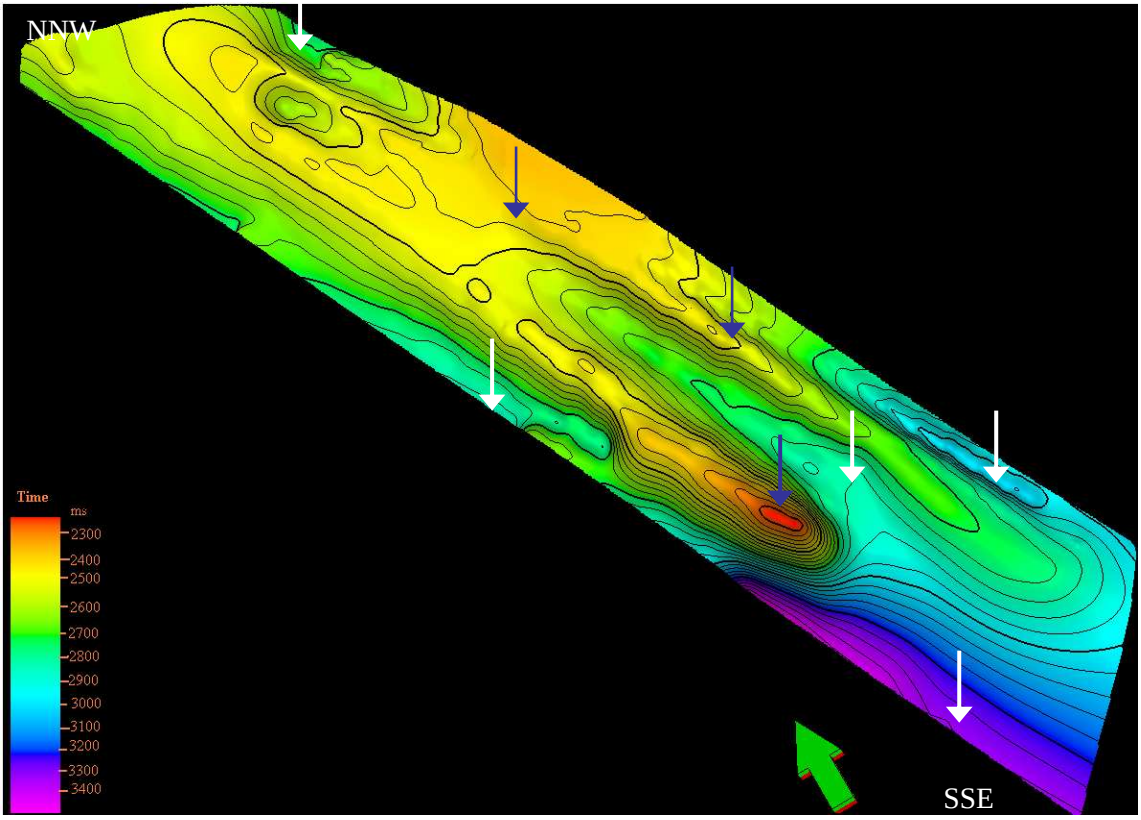

Figure 8.14: Shows an isochrone map for top basement level. Blue arrows mark the position of ridges while the white arrows mark the position of basins. It is obvious from the map that the basement is more faulted in southern and western part of the area.

9. INTERPRETATION DISCUSSION

This chapter describes the structural analysis and the correlation of interpreted results (sedimentary successions interpreted from Devonian to Tertiary age along with the interpretation of top basement and structural features) with some previous studies done in the area. The Carboniferous - Tertiary succession in Spitsbergen overlays unconformably Devonian and Hecla Hoek strata. There are no well log data describing this boundary, but it is only supposed to be represented by a reflector separating strong parallel reflections in Carboniferous-Tertiary from diffuse reflectors in Devonian (Eiken & Austegard, 1994). The structures associated with fold-thrust belt present a complex array and are difficult to observe and interpret accurately in the seismic data. The interpreted details of faulting in duplex zones may be schematic and not the accurate interpretation of duplex zone structures. Figure (9.1) shows the geological and tectonical map of the study area.

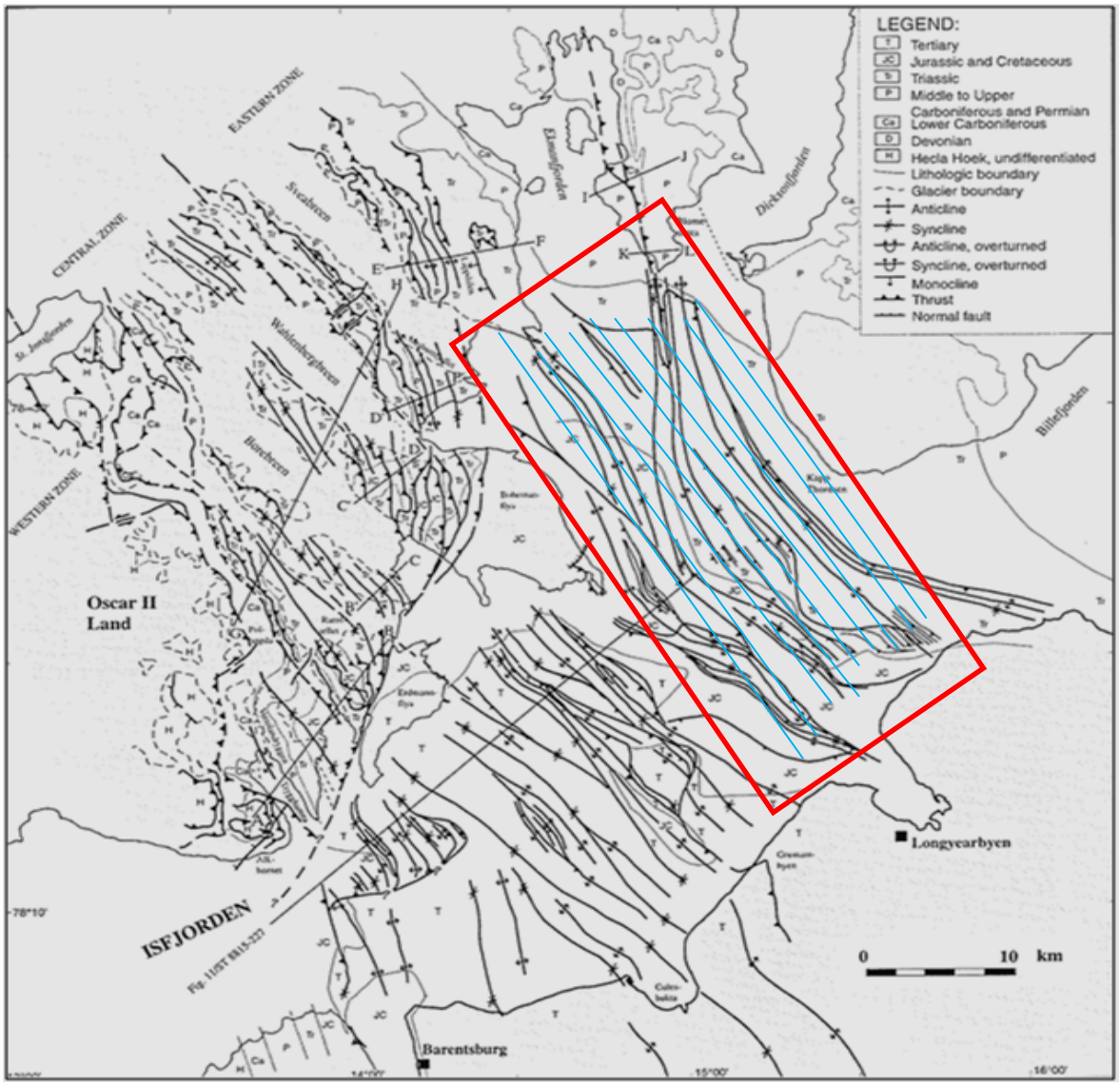

Figure 9.1: Geological and tectonical map of Oscar II land and Isfjorden (outcrop map) divided into western, central and eastern zones (modified from Bergh et al., 1997). Red rectangle marks the study area.

9.1 Devonian and older Basement

The seismic signature of the Devonian unit is characterized by diffuse and weak reflections, which probably represents the Devonian fill basin (figure 8.5a). From the seismic data, these sediments deposited in Devonian are likely preserved in down-faulted blocks. The results from Eiken & Austegard (1994) report the continuation of these Devonian grabens exposed below Isfjorden and these results are based on the interpretation of a seismic line from eastern Isfjorden. Relatively strong reflections observed around 2.5 to 3 sec were observed in some of the profiles, and this was interpreted as top Hecla Hoek. The seismic response from the basement was generally found to be poor, but some strong irregular reflectivity pattern, probably caused by metamorphism was observed within basement in northern half part of some profiles. The results from Blinova et al. (subm) and Eiken & Austegard (1994) also describe the seismic response from basement as few scattered but strong reflections. The top of the basement was interpreted with some normal faults, which outlines a configuration of ridges and basins caused by Devonian extension. This configuration is probably trending N-S, which may be correlated with the results from Blinova et al. (subm) and Bergh et al. (1997). The normal faults may be inferred from abrupt change in seismic continuity. But due to poor resolution of the data it might be difficult to follow and interpret these faults and structures along all profiles. Anyhow, a certain degree of uncertainty is associated with the interpretation of this reflector. The results from Bergh et al. (1997) also describe the seismic signature from basement as scattered, strong and irregular reflections and the overlying unit with diffuse and discontinuous reflections, interpreted as basin fills from Devonian and Carboniferous age.

9.2 Sedimentary successions from Carboniferous to Tertiary

9.2.1 Permian and Carboniferous

The interpretation of top Permian reflector is associated with the strong impedance contrast between the high velocity silicified carbonate of Kapp Starostin Formation and the overlying low velocity shale from Sassendalen group (Triassic). This level also corresponds to the unconformity between Devonian and Paleozoic sedimentary cover. This interpretation is consistent with the results from Bergh et al. (1997) and Blinova et al. (subm). The thickness of the upper Carboniferous - Permian unit varies between 0.3 – 0.4 seconds (TWT) which corresponds to a thickness of 600 - 1200 m and the seismic character in this unit is sub-parallel and continuous. These results are comparable with the results from Eiken & Austegard (1994).

9.2.2 Triassic - Cretaceous

Triassic - Cretaceous deposits (figure 8.5a) represent repeated deltaic - marine coarsening upward sequences. This sequence consists of shale to siltstone and sandstone in Triassic, marine shale in Jurassic and again deltaic siltstone and sandstone in late Jurassic-early Cretaceous. The thickness of this Triassic – Cretaceous sequence is usually between 0.7 – 1.0 second (approximately 1.6 - 2.5 km). This interpretation corresponds to the results from Eiken & Austegard (1994), which describe this thickness between 0.6 – 0.8 second (1.4 – 1.8 km) but it may reach up to 1 second (2.2 – 2.4 km). The Triassic unit is characterized by weak,

discontinuous reflections from shale in Sassendalen group. The high amplitude reflections in upper Triassic are interpreted as sandstone in Kapp-Toscana group. The results from Bergh et al. (1997) describe the same seismic character for strata from Triassic. Unlike over - and underlying successions, the Triassic unit is more or less uniform in thickness.

The Jurassic unit is characterized by shale deposits (weak discontinuous reflections) of Janusfjellet subgroup. The lower boundary is marked by the velocity contrast between Kapp-Toscana group and overlying low velocity shale, while the upper boundary is marked by a sharp contact between the Janusfjellet subgroup and the Helvetiafjellet Formation (sandstone). This interpretation corresponds to the results from Bergh et al. (1997) and Johansen et al. (1994). The Cretaceous unit represents several strong and parallel reflections. The top of this unit is characterized by some weak reflectors and a gradual more chaotic seismic character to the north. The strong reflections in the middle of the unit may be interpreted as intra - Cretaceous (figure 8.9). This is consistent with Blinova et al. (subm.) and Eiken (1985). The results from Blinova et al. (subm) also describe a strong reflectivity contrast between the low velocity shale of Janusfjellet subgroup and the overlying shale of Helvetiafjellet Formation. The interpretation results from Eiken (1985) suggest that above and below this unit, there are thick layers of shale with a slight velocity contrast. The weak reflections in the upper part of the unit can be interpreted as shale in Caroline Mountain formation.

The overall thickness of Jurassic and Cretaceous strata is estimated to approximately 1500 – 1600 m, which is slightly thicker than the measurements of 1350 m for this unit measured in the Grumantbyen borehole in the south of study area (Skola et al., 1980; Eiken, 1985). These values also correspond to values (1500 - 2000 m) described in Eiken (1985). Some very high amplitude reflections were observed in the northern and southern part of the study area from Triassic up to Tertiary succession. Theses high amplitude reflections (figure 8.9) were interpreted as sills (dolerite intrusions). The results from Eiken (1985) and Eiken & Austegard (1994) describe the presence of dolerite intrusions, which can be followed laterally up to 20 to 25 km. Also a 42 m thick dolerite layer in Grumantbyen borehole south of Isfjorden was found within the Triassic sequence (Skola et al., 1980). However, it could be reasonable to assume that it can be traced further out to the Isfjorden area. The thickness of the Cretaceous sequence is uniform in the southern part, but its thickness increases towards the northern part as a result of thrusts and backthrusts figure (8.5a & 8.7).

9.2.3 Tertiary

The tertiary sequence in the study area defines an approximately 18 - 22 km wide asymmetrical basin that correspond with the Central Tertiary Basin (figure 8.5a). Base Tertiary was interpreted and supposed to lie in a thin transparent zone which exits below a strong double reflection and above a series of several strong reflections which can be related to the sandstone of upper Cretaceous. This result corresponds to the study of seismic data interpreted from Isfjorden by Bergh et al. (1997) and can also be correlated with the seismostratigraphic definition by Eiken & Austegard (1994), according to which it is interpreted in the bottom of several strong reflections at approximately 0.6 sec. The thickness of the Tertiary succession is in the deeper part of the study area measured at around 400 ms

(~900 m), which is more or less comparable to the estimation of maximum thickness 1-2 km measured by Bergh et al. (1997) and 1 - 1.2 km by Eiken & Austegard (1994). The seismic reflections on the section show that the Tertiary unit includes interbedded shale (weak reflections) and sandstone (strong reflections) deposits. The Tertiary unit is tectonically disturbed by thrust, backthrusts and imbricates. Duplex structures were interpreted in the Tertiary unit in southern or south-western part of the area. A kinematic model for duplex system with ramp and flat geometry is shown in figure (2.9a); Pluijm & Marshak (2004).

9.3 Structural analysis

The seismic profiles were shot more or less in the strike direction of the main structural features present in the study area, making it difficult to follow and interpret these. Also due to poor quality and resolution of the seismic data, particularly at larger travel time (below 1 sec TWT), it is hard to identify and explain the different structures present in the subsurface. Nevertheless, effort has been made in identifying and interpreting these structures and a few profiles with comparatively better resolution were selected for the presentation of interpreted structures.

Faults present in the study area were identified from fault cutoffs, reflection termination and fold limb termination. It is difficult to follow these faults from profile to profile, and thereby identify the strike of these faults. Some of the structures were interpreted with low level of confidence and marked with dashed lines. For the reference in text, some thrust faults interpreted in Tertiary are named “T” and backthrusts named “J”; in Cretaceous thrusts are named “B” and backthrusts “b” in Jurassic sequence thrusts are named “G” and the major folds are named “F”. The capital letters represent thrusts and small letters represent backthrusts.

9.3.1 Western Spitsbergen fold-and-thrust belt (WSFTB)

Several studies from western Spitsbergen such as Braathen & Bergh (1995); Bergh et al. (1997) divide WSFTB in different zones. The western part of the fold belt is characterized by basement involved folds and thrusts and the eastern part is characterized by thin skin foreland folds and thrusts. The study area is assumed to be covering the eastern foreland part of WSFTB.

Thrusts: thrusts and backthrusts can be seen branching up or through the Jurassic, Cretaceous and Tertiary successions (figures 9.2 - 9.5). Several decollement surfaces (D1, D2, D3 and D4) were identified in the Tertiary succession but it is hard to follow these surfaces as a result of poor resolution of the data. Thrusts T1 and T2 (figure 9.2) were identified and inferred by diffuse reflection termination (reflections look thrusting up). These thrusts seem to merge in decollement surfaces D2 and D4. The inclined seismic reflections observed in the Tertiary package (figures 9.2 - 9.5) may be interpreted as thrusts and backthrusts. Backthrust horses J1 - J8 (figure 9.2) which may represent imbricates, bounded by thrust surfaces, make duplex type systems. These duplex systems show very complex geometries but this aspect was interpreted with lower level of confidence. The complex pattern of thrusts, backthrusts and oblique geometries makes it difficult to determine the transport direction. This interpretation

corresponds with the interpretation results by Bergh et al. (1997) from Isfjorden, which describe that the Tertiary unit is tectonically disturbed by folds and imbricates. According to this interpretation, these folds may also be described as the folding of hanging walls of the thrust ramps. But the results from Bergh et al. (1997) also describes that imbricates in the Tertiary unit seem to emerge from a high-level decollement in Triassic shale.

The Cretaceous sequence also seems deformed by thrusts and backthrusts. A thrust B1 present in the Cretaceous sequence (figure 9.2) may be inferred from fold limb termination. In the north-west part, several backthrusts b1 - b3 (figure 9.2) seem to overstep or overlap against the thrust B1. Several thrusts (figures 9.2 & 9.5) seem to merge in a decollement surface in the upper Jurassic shale probably (called Janusfjellet decollement), which may indicate extensive fracturing at this level (Eiken & Austegard, 1994). Jurassic and lower successions display a diffuse and chaotic pattern. Thrusts G1 - G4 were identified and inferred from reflections termination and seemed to emerge from a decollement surface, which may be supposed to present in Agaradhfjellet FM of lower Jurassic shale. These thrusts can be seen to continue up to the Cretaceous sequence causing deformation there. A thrust G5 was interpreted and inferred by fault cutoff and it appears to continue from Triassic up to the lower Jurassic succession. Triassic - Cretaceous successions were found to be folded by anticlines and synclines (figures 9.3 - 9.5). A few imbricate fans can also be seen in Jurassic strata in the study area (figure 9.2). This part of the interpretation corresponds with the studies from Bergh et al. (1997); Eiken & Austegard (1994) and Blinova et al. (subm). The study of Bergh el al., (1997) describes that the Permian to Jurassic strata are deformed by imbricates and syncline and anticline combination folding. The study also correspond to the results from Eiken & Austegard (1994), which describes that this Mesozoic unit is deformed internally and served as main decollement unit for the eastward translation from the exposed fold- and-thrust belt into and cross the Central Spitsbergen Basin. This study (Eiken & Austegard, 1994) also confirms the existence of the Janusfjellet decollement.

Both regional (Bergh et al., 1988) and seismic studies (Bergh et al., 1997; Eiken & Austegard, 1994) suggested that a major decollement is supposed to exist in Gipshuken evaporites. The Gipshuken decollement is, however, unconfirmed in the study area of Isfjorden. The reason for not identifying the Gipshuken decollement surface in seismic sections may be poor resolutions at these depths.

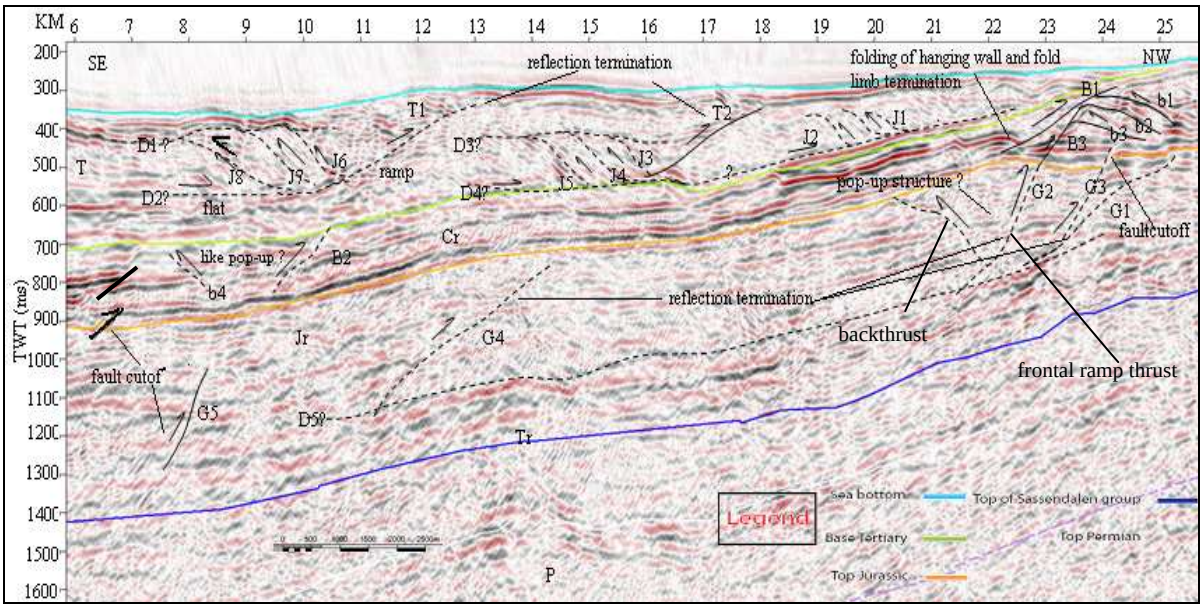

Figure 9.2: Interpretation of thrust faults, backthrusts, and decollements. All the faults and decollements are shown in black. Faults and decollements interpreted with lower level of confidence are marked with dotted lines. Pop-up structures observed were interpreted in the Jurassic succession. (D1, D2, D3, D4, D5 = decollement, T = Tertiary, Cr = Cretaceous, Jr = Jurassic, Tr = Triassic, P = Permian (? = uncertain). This interpretation is from line-16. Geographical location of profile is shown in figure (1.3).

9.4 Results from other profiles

In line-22, several thrusts and backthrusts have been observed and interpreted. In the Tertiary succession, thrusts from T14 - T22 (figure. 9.3) inferred from diffuse fault cutoff and reflection terminations seem to make a duplex system bounded by decollement surfaces D1 and D2. These thrusts (imbricate horses) in the Tertiary succession define ramp and flat geometries. D1 is the roof thrust and D2 is the floor thrust. The D1 surface seems to be more corrugated and folded than D2. The Cretaceous succession seems less deformed compared to the Tertiary. Thrust B8 and backthrust b6 are inferred from fault cutoff. In Jurassic, thrusts G9 and G10 were inferred from reflection termination and thrusting up of the reflections. A backthrust branches up in the upper Triassic, causing synclinal fault-bend folding of the hanging wall (figure. 9.3), it also appears to thrust up into the Jurassic succession. The upper Triassic succession in the middle of the line seems to be folded synclinally (figure. 9.3), that may be related to Tertiary deformation.

Quite a few structures were observed and interpreted in line-20 (figure 9.4). Duplex structures were interpreted in the Tertiary succession as a result of backthrusts J9-J14 bounded by decollement surfaces D1 and D2, which appear hard to follow. Thrust T26 was interpreted as a result of reflection termination in SE. the Cretaceous succession in NW part of the line was found to be deformed and folded (figure 9.4), probably caused by thrusting and backthrusting. A thrust fault named G11 (figure 9.4) with a relatively steep dip in the Jurassic succession was inferred from reflection terminations and thrusting up of the reflections. It appears to thrust up and continue into the Cretaceous succession causing deformation there.

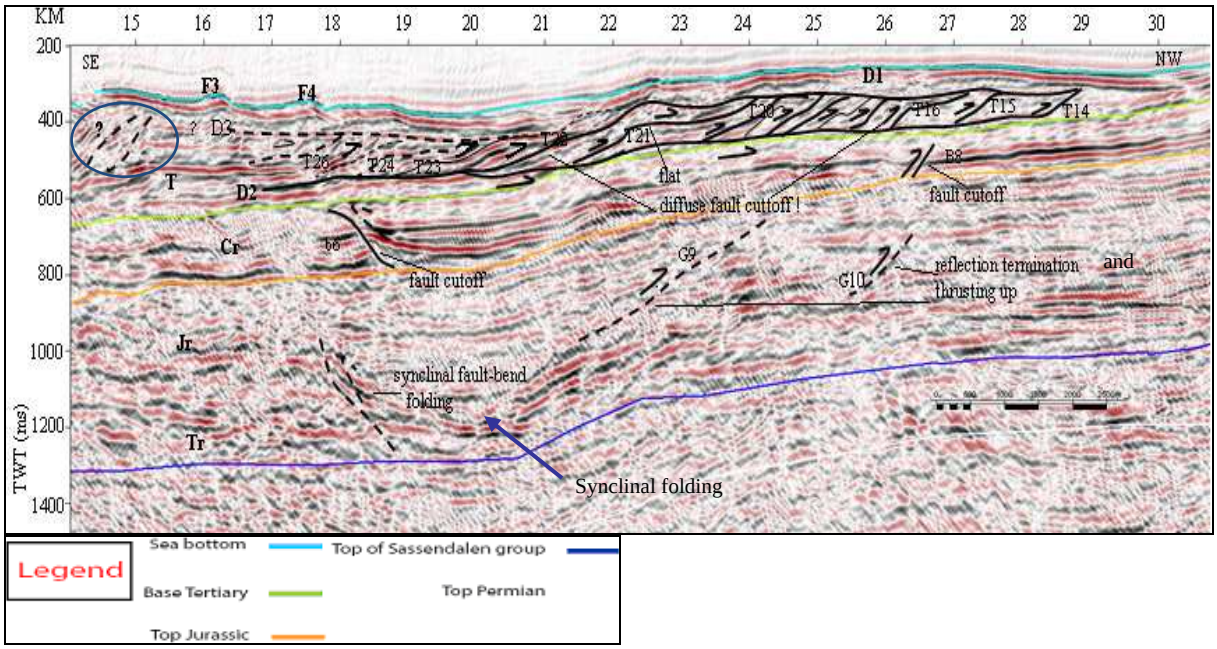

Figure 9.3: Interpretation of thrust faults, backthrusts, folds and decollements. Faults and decollements are shown in black. Faults and decollements interpreted with lower level of confidence are marked with dotted lines. (D1, D2, D3, = decollements, T = Tertiary, Cr = Cretaceous, Jr = Jurassic, Tr = Triassic and ? = uncertain). The blue circle marks unknown. This interpretation is from line-22. Geographical location of profile is shown in figure (1.3).

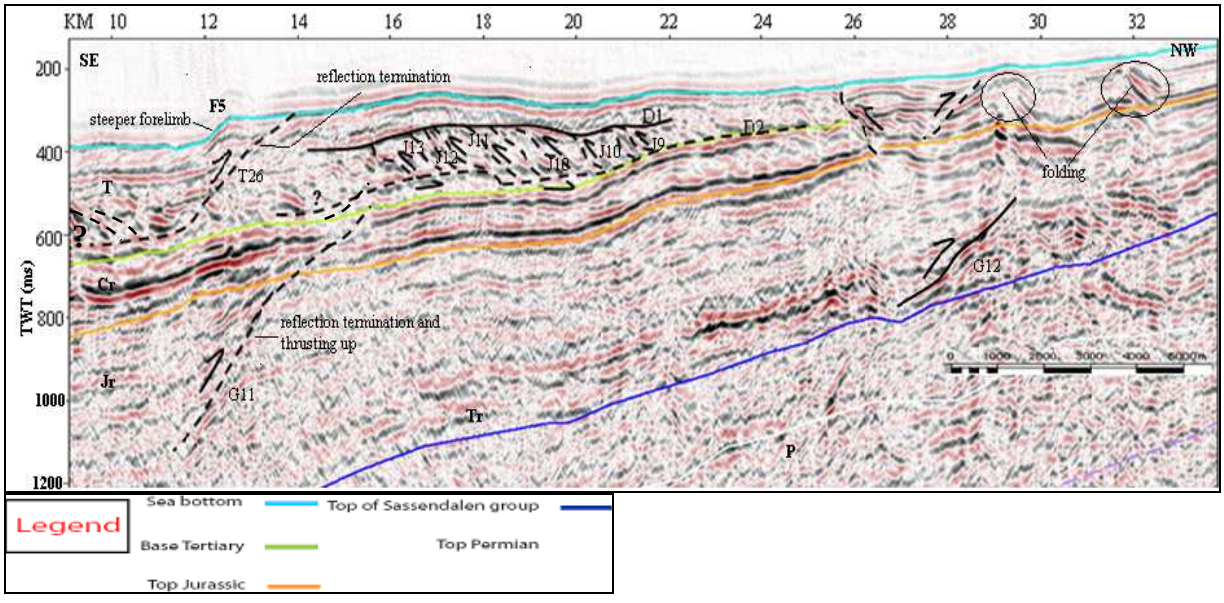

Figure 9.4: Interpretation of thrust faults, backthrusts, duplex structures and decollements. Faults and decollements are shown in black. Faults and decollements interpreted with lower level of confidence are marked with dotted lines. (D1, D2, = decollements, T = Tertiary, Cr = Cretaceous, Jr = Jurassic, Tr = Triassic, P = Permian and ? = uncertain). This interpretation is from line-20.

9.5 Other structures

Duplex structures: Thrusts ramps T3 - T10 (figure 9.5) were interpreted to branch up from the same surface called decollement D2, but thrust ramps T11 - T13 may branch up from another surface called D3. These ramps may be inferred from diffuse faults cutoff and

termination of fold limbs in the hanging walls. All these faults have same orientation and merge with higher level decollement surface D1 to form imbricate duplex systems (I) and (II) (figure 9.5). D1 is the roof thrust for duplex systems (I) and (II). But for duplex system (I), the floor thrusts is D2 surface and for system (II) floor thrust may be D3 surface. Thrusting direction is indicated by arrows toward NNW, but it is difficult to determine the exact transport direction, as all the geometries found are oblique. Both the floor and roof thrusts appear to be corrugated and folded, but the roof thrust D1 is more folded than the floor thrust. Thrust B4-B7 (figure 9.5) branch up into the Cretaceous succession and seem to form imbricate fans. These thrusts might possibly have emerged from the decollement surface D4 (figure 9.5) present in the lower Cretaceous. Thrusts G6 - G8 (figure 9.5) in the Jurassic succession were inferred by reflection terminations and thrusting up of seismic reflections.

Most of the thrust ramps interpreted show sigmoidal shape that link the floor thrust to the roof thrust of the duplex, but some could be interpreted as break-forward sequences (figure 2.9a; Pluijm & Marshak, 2004). This suggests that the thrust ramps to the south or south west originated first, and then perhaps the deformation was gradually transferred towards north or north-east probably by piggy-back propagation.

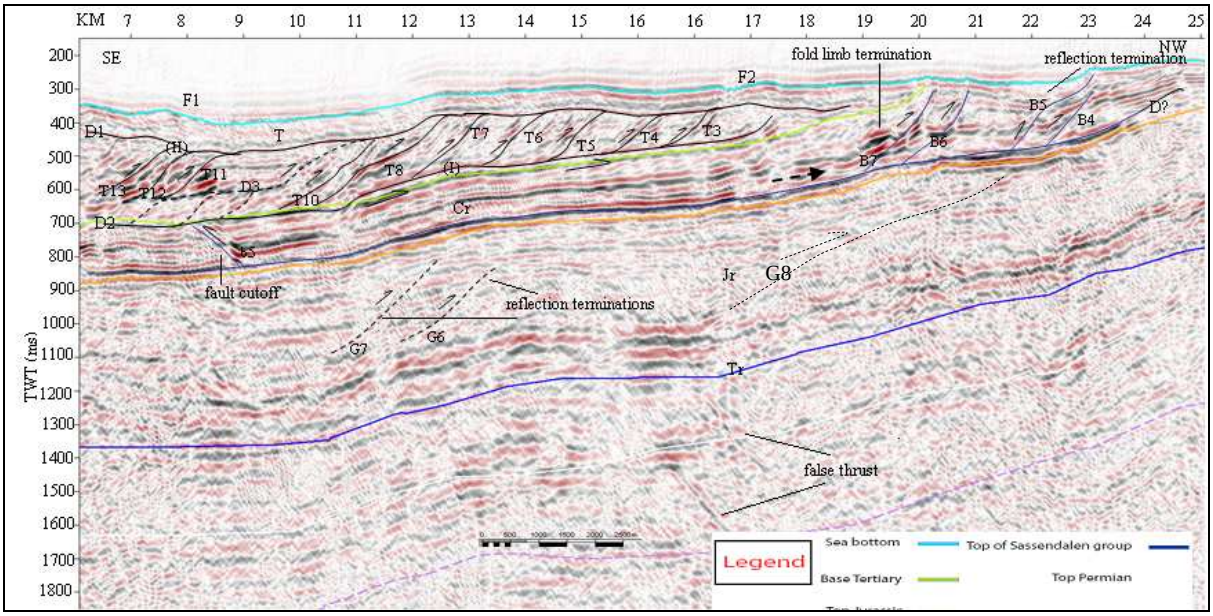

Figure 9.5: Interpretation of thrust faults, backthrusts, folds and decollements. Faults and decollements are shown in black. Faults and decollements interpreted with lower level of confidence are marked with dotted lines. Duplex structures interpreted, are shown in Tertiary sequence. (D1, D2, D3, D4 = decollements, T=Tertiary, Cr= Cretaceous, Jr= Jurassic, Tr = Triassic, &? = uncertain). Geographical location of the profile is shown in figure (1.3). This interpretation is from line-18.

Piggy-back propagation model: Thrust sequence T3-T13 (figure 9.5) suggests that the thrusting seems to die out after the thrust T3 towards NNW or N. Thrust T3 might have formed in the footwall of thrust T4, which means that thrusting propagated from T4 to T3. This probably defines a type of thrust sequence, which supports a piggy-back propagation model (figure 2.9b; Butler, 1982) and gives information about the propagation direction (foreland zone) Also in Cretaceous it defines a thrust sequence, as thrusts B4, B5 and B6 might have formed in the footwall of thrust B7 formed earlier and suggests the same model,

or it can be interpreted other way around. This interpretation is uncertain as a result of the structural complexity.

Pop-up structures: Pop-up structures have been observed and interpreted in the Cretaceous and Jurassic successions (figure 9.2). These structures are formed as result a frontal ramp and a backthrust as described in Butler (1982); McClay (1992). However, this interpretation was done with a little uncertainty.

Folding: The sea bottom in the Tertiary and Cretaceous successions was found folded, but it is hard to determine if the folding is most likely caused by compression. Folding of sea-bottom in the Tertiary succession can be examples of such folds, F1 & F2 in line-18 (figure 9.6) F3 & F4 in line-22 (figure. 9.3) and F5 in line-20 (figure 9.4). Folding in the Cretaceous succession and deeper successions was also identified such as in line-18, 20 & 22 (figures 9.3-9.6) which is consistent with Bergh et al. (1997), who describes folding in Permian to Jurassic successions.

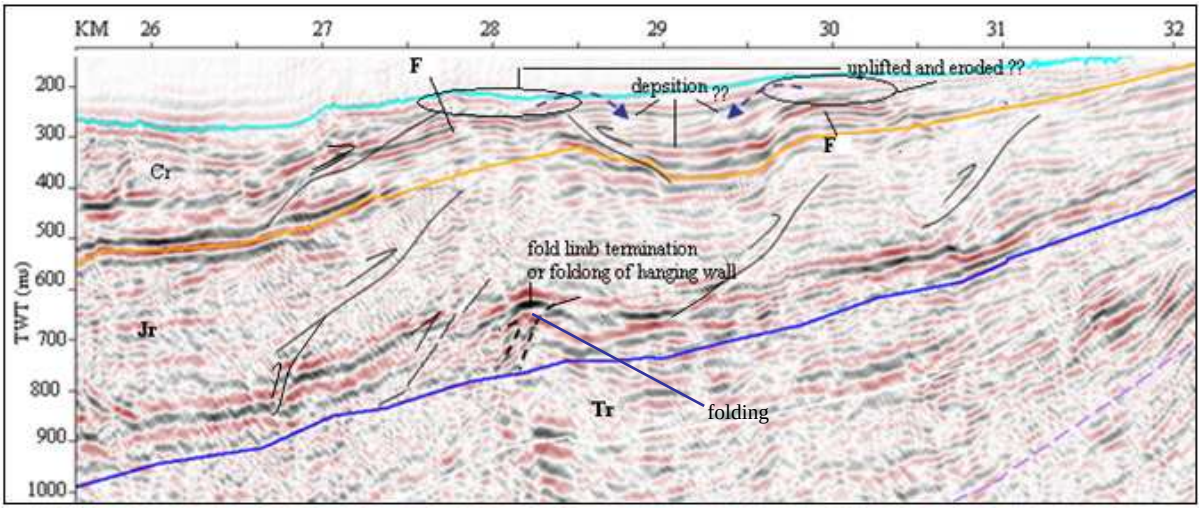

Figure 9.6: Shows interpretation of faults and folds in north-west part of line-18. The figure also shows the folding and erosion of uplifted parts in the Cretaceous succession probably caused by thrusting or back thrusting (difficult to determine). Faults are shown in black (marked with low level of confidence). Cr = Cretaceous, Jr = Jurassic, Tr = Triassic, & ? = uncertain.

The contractional structures in the Triassic – Tertiary successions present in the study area indicate that deformation has been caused by the tectonics of Tertiary age. Most of the structures interpreted in Triassic – Tertiary successions show dip towards SSE to S (verging towards NNW to N). This describes SSE to NNW compressional tectonics with deformation being transferred to N or probably towards NE. But a certain level of uncertainty remains there, because of the complex structural geometries. Studies from Bergh & Andresen, 1990 and Bergh et al. (1988) describe that the deformation was being transferred eastward with a combination of fault-bend folding and thin-skinned decollement thrusting. It suggests that the transport direction may correspond to the northwest or north of Isfjorden in the Tertiary fold-Thrust Belt of Spitsbergen (Dallmann et al., 1993). The presence of different structures e.g. complex imbricate thrust; fault-bend folding and the age of deformation in the study area may suggest the continuation of the Tertiary fold- Thrust Belt in Oscar II land beneath the central

part of Isfjorden (Bergh et al., 1997; Faleide et al., 1988a). The deformation is assumed to be the result of transpressional stress related to dextral transform movement in Paleocene – Eocene during the opening of Norwegian – Greenland Sea (Birkenmajer, 1972a; Steel et al., 1985).

Bergh et al. (1997) have proposed a five stage kinematic evolution model for Tertiary fold-thrust belt of Spitsbergen:

1 - A pre-uplift event with NNE-SSW shorting in the western basement-involved fold and thrust belt started in Late Cretaceous to Early Paleocene (figure 2.8).

2 - Development of main phase of fold- thrust belt (ENE-verging) initiated in Late Paleocene - Eocene, showing in-sequence thrusting and duplex formation develops in Central Zone of fold-thrust belt (figure 2.8).

3 - Continuation of main phase of shortening and rotation of earlier structures in the western basement-involved fold-thrust complex. Further development of ENE-verging fold-thrust complex in the Central Zone and the deformation transferred as layer of parallel shortening in decollement surfaces in the eastern foreland (figure 2.8).

4 - The end of main deformation phase with the formation of NNE-SSW strike-slip faults in the western basement-involved fold-thrust complex and SE-NW thrusting in the Central Zone (figure 2.8).

5 - Extension and truncation (E-W to ENE-WSW) of earlier structures in western basement-involved fold-thrust complex in Late - Eocene to Oligocene. Truncation continued to the fold-thrust complex in the Central Zone and monoclines in the Eastern Foreland Zone.

Since the geometries of structures in the study area represent a complex pattern, it is hard to identify the exact strike and dip of the features. But if we assume that the general dip is towards south to south-west (verging towards north to north-east), the interpretation from this area might correspond to the stages 2 and 3 of the kinematic evolution model.

10. CONCLUSIONS

A total of nine 2D multi-channel seismic profiles from Isfjorden were processed. The main focus of the processing has been the removal of multiples, caused by the hard sea-bed and shallow depth.

- The standard processing was done with the application of some key processing steps such as velocity filtering, velocity analysis, pre-stack migration and finally stacking the data.
- The multiples were strongly attenuated by predictive multi-channel deconvolution. The remaining multiples were removed by stacking.
- The processing of the seismic data thus removed most of the multiple energy and depicted the geological structures in the subsurface down to approximately 2.5 or 3 sec (TWT).

The seismic profiles were interpreted with the main focus on correlating the sedimentary package from Carboniferous to Tertiary with the pre-existing seismo-stratigraphic framework. The main aim was to provide an overview of the large-scale structures and tectonics style present in the study area. These structures were formed by transpressional deformation, related to the Tertiary opening of the Norwegian - Greenland Sea.

- A Carboniferous - Tertiary sedimentary package was identified and interpreted in the uppermost 2 sec (TWT) as layers dipping gently towards south or south-west, lying unconformably on Devonian/metamorphic basement.
- The key interpreted horizons include: base Tertiary, base Helvetiafjellet FM, top Triassic, top Permian, base Carbonate and top Hecla Hoek, along with isochrone maps generated at sea-bed surface, base Helvetiafjellet FM, top Triassic, top Permian and top Hecla Hoek levels.
- A very strong reflection at approximately 0.9 sec in the SSE part of the study area was interpreted as a sill, which is supposed to originate from Arctic volcanic activity in Cretaceous.
- Based on the interpreted structures, each sedimentary unit may be characterized by different structural style.
- Structural geometries (faults and folds) in the area may indicate fault-bend folding, piggy-back sequence and decollement thrusting.
- The complex pattern of thrusts and backthrusts represents geometries which are oblique to the actual tectonics transport.
- The Tertiary succession appears to be more deformed and shortened compared to deeper successions.
- The presence of thrusts, backthrusts, duplex and pop-up systems indicate that the Tertiary fold-thrust belt extends beneath the central basin in Isfjorden.
- The interpreted structures in the study area indicate compressional setting with possible transfer of deformation towards north or probably north-east.

- Several possible structures and decollements present in the Triassic and Permian remain uninterpreted.

REFEENRCES

Badley, M. E. (1985): Practical seismic interpretation. IHRDC, Boston, Reidel, vi, 266 s. P.

Bacon, M., Simm, R and Redshaw, T. (2003): 3-D Seismic Interpretation; Cambridge University press.

Bergh, S. G., A. Andresen., A. Bergvik., & A. I. Hansen. (1988): Tertiary thin-skinned compressional deformation in Oscar II land, Central West-Spitsbergen: Norsk Polarinstitutt Rapport, v. 24.

Bergh, G & Andresen, A. (1990): Structural development of the Tertiary fold-and-thrust Belt in east Oscar II Land, Spitsbergen. Polar Research, 8(2), 217-236.

Bergh, S. G., Braathen, A. & Andresen, A. (1997): Interaction of Basement-Involved and Thin-Skinned Tectonism in the Tertiary Fold-Thrust Belt of Central Spitsbergen, Svalbard. AAPG Bulletin, 81(4), 637-661.

Birkenmajer, K. (1972a): Alpine Fold Belt of Spitsbergen: Report of the Session of the International Geological Congress, v. 24, 282 – 292.

Blinova, M., Faleide, J., Gabrielsen, R. H., & Mjelde, R. (subm): Analysis of structural trends of sub-bottom strata in the area of West Spitsbergen Fold-and-thrust Belt (Isfjorden) based on multichannel seismic data.

Blinova, M., Faleide, J. I., Gabrielsen, R. H. & Mjelde, R. (subm.): Seafloor expression and shallow structure of a surfacing fold-and-thrust system. An example from Isfjorden, West Spitsbergen. Submitted to Polar Research.

Braathen, A., Bergh, S. G. & Maher Jr, H. D. (1995): Structural outline of a Tertiary basement-cored uplift/inversion structure in western Spitsbergen, Svalbard: Kinematics and controlling factors. Tectonics, 14, 95-119.

Braathen, A., Bergh, G & Maher, H. (1999): Application of critical wedge taper model to the Tertiary transpressional fold-thrust belt on Spitsbergen, Svalbard: Kinematics and controlling factors. GSA Bulletin, 111 (10).

Brown, A. R. (1999): Interpretation of Three-Dimensional Seismic Data. American Association of Petroleum Geologists (AAPG).

Butler, R. (1982): The terminology of structures in thrust belts. Journal of Structural Geology, Vol. 4, printed in Great Britain.

Capron, A. (2005): Seismic Interpretation: General Principles.

CGGVeritas (2008): Geocluster Release Notes.

Dallmann, W., A, Andresen., Bergh, G., Maher, D and Ohta, Y. (1993): Tertiary fold-and-thrust belt of Spitsbergen Svalbard: Norsk Polarinstitutt Meddelelser 5, v. 128.

Dallmann, W. (Ed.). (1999): Lithostratigraphic Lexicon of Svalbard: Review and recommendations for Nomenclature Use: Upper Paleozoic to Quaternary Bedrock. Norsk Polarinstitutt.

Dallmann, W. (2009): Svalbard geological development. Norwegian polar institute, cruise handbook for Svalbard.

Dix, C. H. (1955): Seismic velocities from surface measurements: Geophysics, 20, 68–86.

Dobrin, B., & Savit, H. (1988): Introduction to geophysical prospecting, 4th ed. New York.
Eiken, O. (1981): An examination of the sedimentary strata in Agardhdalen, Svalbard.
Eiken, O. (1985): Seismic mapping of the post-Caledonian strata in Svalbard. Polar Research, 3, 167-176.
Eiken, O., Austegard, A. (1994): Seismic Atlas of western Svalbard: Norsk Polarinstitutt.
Evans, J. B (1997): A hand book for seismic data acquisition in exploration: Geophysical monograph series, Society of exploration geophysicist (SEG).
Faleide, J. I., Gudlaugsson, S., Eiken, O and Hanken, N.-M. (1988a): Seismic structure of Spitsbergen: Implications for Tertiary deformation: Norsk Polarinstitutt Rapport, v. 46.
Faleide, J., Vågnes, E., & Gudlaugsson, S.T. (1993): Late Mesozoic Cenozoic evolution of the south-western Barents Sea in a regional rift-shear tectonic setting. Marine and Petroleum Geology 10, 186-214.
Faleide, J., Solheim, A., Fiedler, A., Hjelstuen, B. O., Andersen, E. S., & Vanneste, K. (1996): Late Cenozoic evolution of the western Barents Sea-Svalbard continental margin. Global and Planetary change 12, 53-74.
Faleide, J., Filippos, T., Breivik, A. J., Mjelde, R., Ritzmann, O., Engen, Ø., Wilson, J., & Eldholm, O. (2008): Structure and evolution of the continental margin of Norway and the Barents Sea. Episodes, 31, 82-91.
Faleide, J., Bjorlykke, K and Gabrielsen, R .H. (2010): Petroleum Geoscience - Geology of Norwegian Continental Shelf, 10.1007/978-3-642-02332-3_22@ Springer Berlin Heidelberg, 467-499.
Hamming, R. (1983): Digital Filters, Prentice-Hall, 1983.
Harland, W., & Dowdeswell, E. K. (1988): Geological Evolution of the Barents Shelf Region: Graham and Trotman.
Helland-Hansen, W. (1990): Sedimentation in a Paleocene foreland basin, Spitsbergen; AAPG Bull, Vo.76.
Hjelle, A. (1993): The Geology of Svalbard; Norsk Polarinstitutt.
IAGC (International Association of Geophysical Contractors). (2002): An overview on marine seismic operations.
Ingólfsson, O**,** (2004): Outline of the geography and geology of Svalbard; UNIS Course Packet, UNIS.
Johanson, S, E., Kibsgaard, S., Andresen, A., Henningsen, T and Granli john, R. (1994): Seismic modeling of a strongly emergent thrust front, West Spitsbergen fold belt, Svalbard: AAPG Bulletin, V. 78.
Johanson, S, E., Granberg, D., Melere, B., Andresen, A and Olsen, T. (2007): Decoupling of seismic reflectors and stratigraphic timelines: A modeling study of Tertiary strata from Svalbard; Geophysics, v. 72.
Kearey, P., Brooks, M., & Hill, I. (2002): An Introduction to Geophysical Exploration: Blackwell Publishing.
Manum, S. B., & Throndsen, T. (1986): Age of Tertiary formations on Spitsbergen. Polar Research 4, 103-131.
McClay, K. R. (1992): Glossary of thrust tectonics terms. Thrust Tectonics, 419-433.

Mjelde, R. (2003): “Seismic Equipment”, e-learning module from www.lg.eage.net.
Mjelde, R. (2008): Svalex survey reports (UiB) for Mijenfjorden and Isfjorden.
Mjelde, R. (2009): Svalex survey reports (UiB) for Mijenfjorden and Isfjorden.
Mitchum, R. M., Vail, P. R., & Thompson, I. (1977): Seismic Stratigraphy and Global changes of Sea Level, Part 2: The Depositional Sequence as a basic Unit for Stratigraphic Analysis; Seismic Stratigraphy-application to hydrocarbon exploration, AAPG, 26.
Myhre, A., Eldholm, O., Faleide, J., Skogseid, J., Gudlaugsson, S.T., Planke, S., Stuevold, L.M., & Vågnes, E. (1992): Norway-Svalbard continental margin: structural and stratigraphical styles. In Poag, C. W. & Graciansky, P. C. (eds): Geologic Evolution of Atlantic Continental Rises, 157-185. Van Nostrand Reinhold, New York.
Nøttvedt, A., Livbjerg, F., & Midbøe, P. S. (1993 a): Hydrocarbon potential of the Central Spitsbergen Basin. Norsk Petroleumsforening (NPF) Special Publications, 2, 333-361.
Oakey, N., & Stephenson, R. (2008): Crustal structure of the Innuitian region of Arctic Canada and Greenland from gravity modeling: implications for the Paleocene Eurekan orogen. Geophysical Journal International 173, 1039–1063.
Ohta, Y., Hjelle, A., Dallmann, W. K and Salvigsen, O. (1992): Geological map of Svalbard, 1: 100.000 Sheet B9G Isfjorden (1:100,000): Norsk Polarinstitutt.
Personal communications: Mjelde, R and Rudd, O. B.
Pluijm, B. V. D., & Marshak, S. (2004): Earth Structure. Norton & Company Press, 2.
Rafaelsen, B., Andreassen, K., Kuilman, L. W., Lebesbye, E., Hogstad, K., & Midtbø. M. (2002): Geomorphology of buried glacigenic horizons in the Barents Sea from 3-dimensional seismic data. Glacier-Influenced Sedimentation on High-Latitude Continental Margins (203): 259-276.
Ritzmann, O., Jokat, W., Mjelde, R., & Shimamura, H. (2002): Crustal structure between the Knipovich Ridge and the Van Mijenfjorden (Svalbard). Marine Geophysical Researches 23, 379-401.
Robinson, E., & Coruh, C. (1988): Basic exploration geophysics. New York.
Sheriff, R. E., & Geldart, L. P. (1995): Exploration Seismology, Cambridge University Press.
Siggerud, E & Thor. (2008): Petroleum Geological Excursion, Svalbard. 3rd edition, UBBRB Box 559.81 P 42-50.
Skola, I. V., Pcelina, T. M., Mazur, V. B. and Alter, S. M. (1980): New data on the composition and structure of the sedimentary platform cover (jacket) on the basis of materials from the drilling of a parametric hole at Grumantbyen. Pp.13-24 in geology of the sedimentary platforms cover (jacket) of the Archipelago of Svalbard. Collection of scientific papers. NIIGA, Leningrad.
Steel, R. J., & Worsley, D. (1984): Svalbard’s post-Caledonian strata-An atlas of sedimentation patterns and palaeogeographic evolution. Petroleum Geology of the North European Margin, 109-135.
Steel, R. J., Gjelberg, J., Helland-Hansen, W., Kleinspehn, K., Nøttvedt, A., & Larsen, M. R (1985): The Tertiary strike-slip basins and orogenic belt of Spitsbergen. SEPM, Special publication, 37, 339-359.

Srivastava, S. P. (1978): Evolution of the Labrador Sea and its bearing on the early evolution

of the North Atlantic. Geophysics. J. Roy. Astr. Soc. 52, 313-357.
Srivastava, S. P. (1985): Evolution of the Eurasian Basin and its implications to the motion of Greenland along Nares strait. Tectonophysics 114.
Srivastava, S. P., & Tapscott, C. R. (1986): Plate Kinematics of the North Atlantic. In Vogt, P. R. & Tucholke, B. E. (eds.): The Geology of North America, Volume M, The Western North Atlantic Region, 379-402. The Geological Society of America.
Talwani, M., & Eldholm, O. (1977): Evolution of the Norwegian-Greenland Sea. GSA Bulletin, 88 (7), 969-999.
Tessensohn, F., & Piepjohn, K. (2000): Eocene Compressive Deformation in Arctic Canada, North Greenland and Svalbard and Its Plate Tectonic Causes, Polarforschung, 68, 121-124.
Worsley, D. (2006): The post Caledonian geological development of Svalbard and the Barents Sea. NGF Abstract and proceedings, 3, 5-21.
Worsley, D. (2008): The post-Caledonian development of Svalbard and the western Barents Sea. Polar Research, 27, 298-317.
Yilmaz. (2001): Seismic data Analysis, processing, Inversion and Interpretation of seismic data. Society of exploration Geophysics, Tulsa, Oklahoma.

APPENDICES

Profiles ISF 16, 20, 24, 28, 29 were shot from SSE to NNW orientation, while the profiles 18, 22, 26, 27 were shot from NNW to SSE orientation.

Appendix I

Display of the final pre-stack migrated sections.

Appendix II

Display of the sections with interpreted horizons and sedimentary successions.

Appendix I

Pre-stack migrated sections.

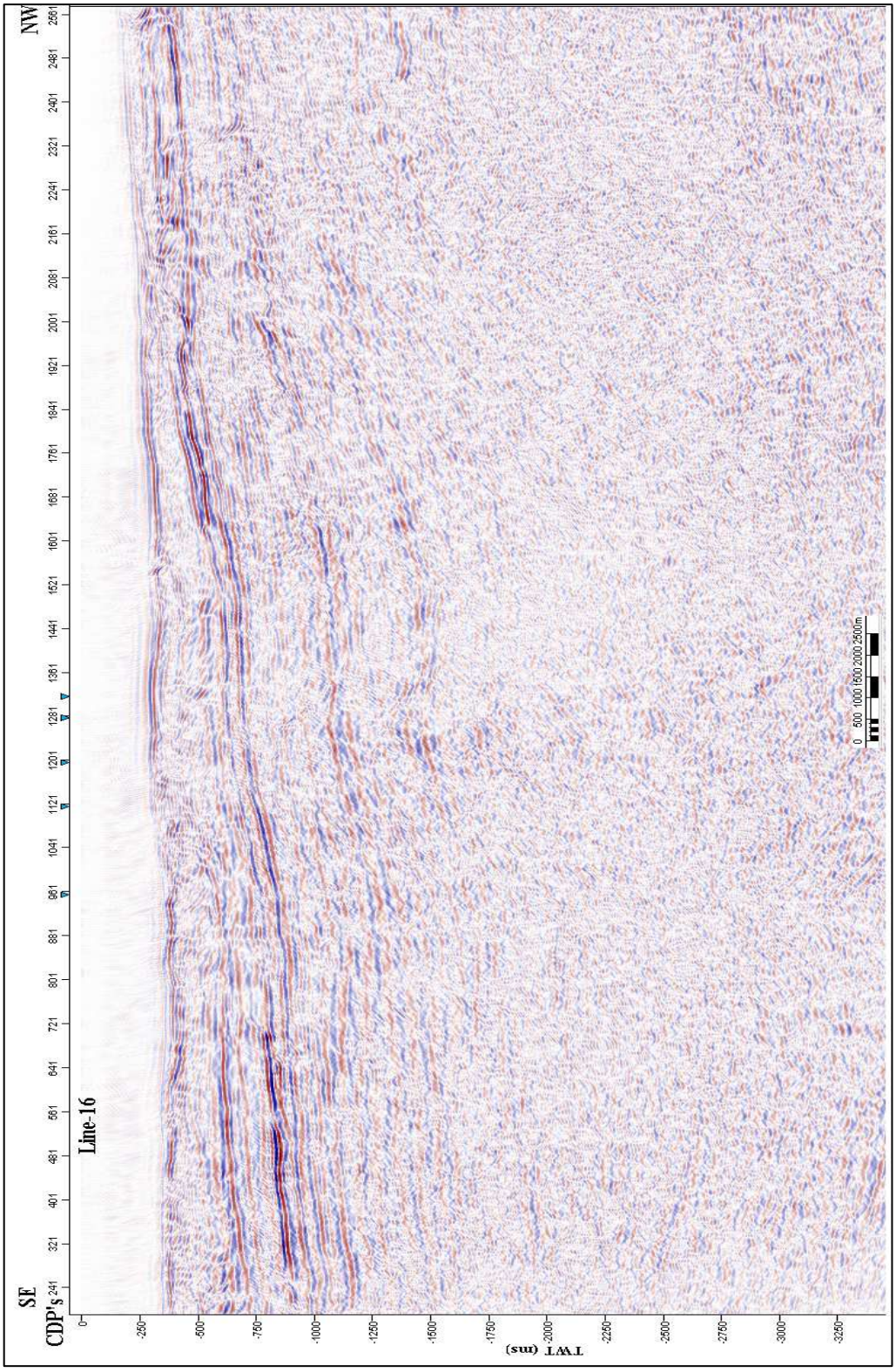

Line-16

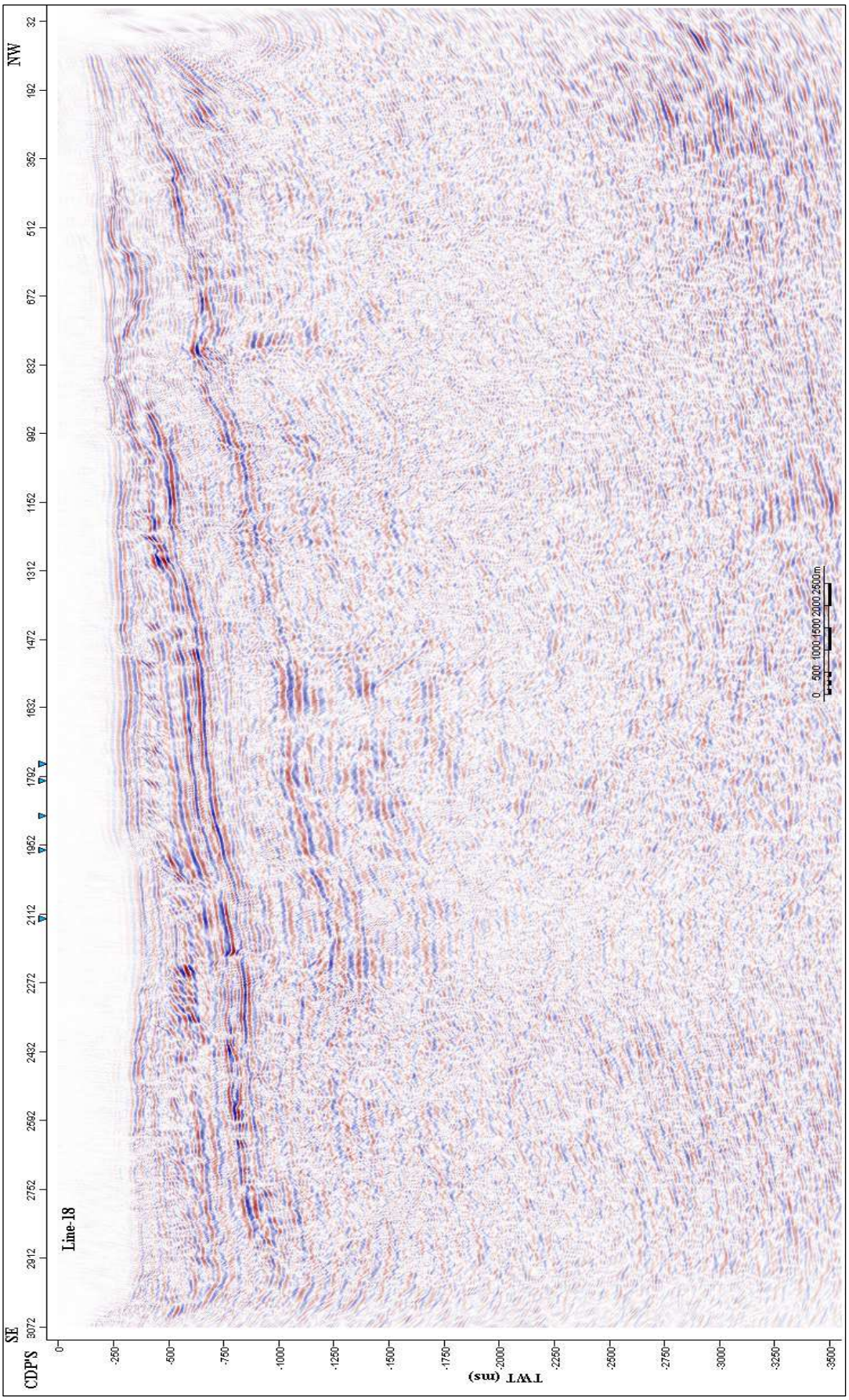
NW
SE
CDP'S
32
192
352
512
672
832
992
1152
1312
1472
1632
1792
1952
2112
2272
2432
2592
2752
2912
3072
Line-18
0
250
500
750
1000
1250
1500
1750
2000
2250
2500
2750
3000
3250
3500
TWT (ms)
0 500 1000 1500 2000 2500m

Line-18

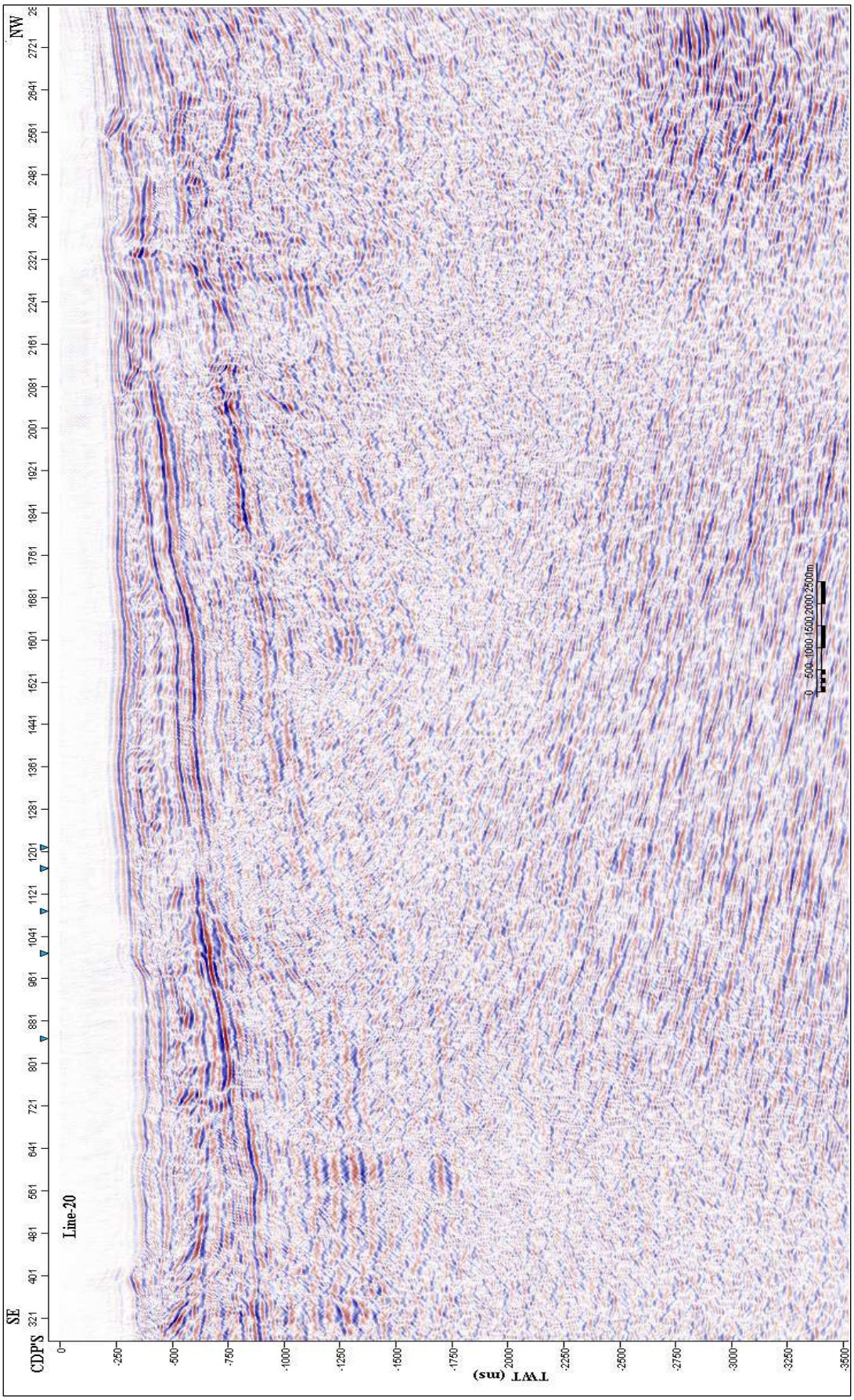

Line-20

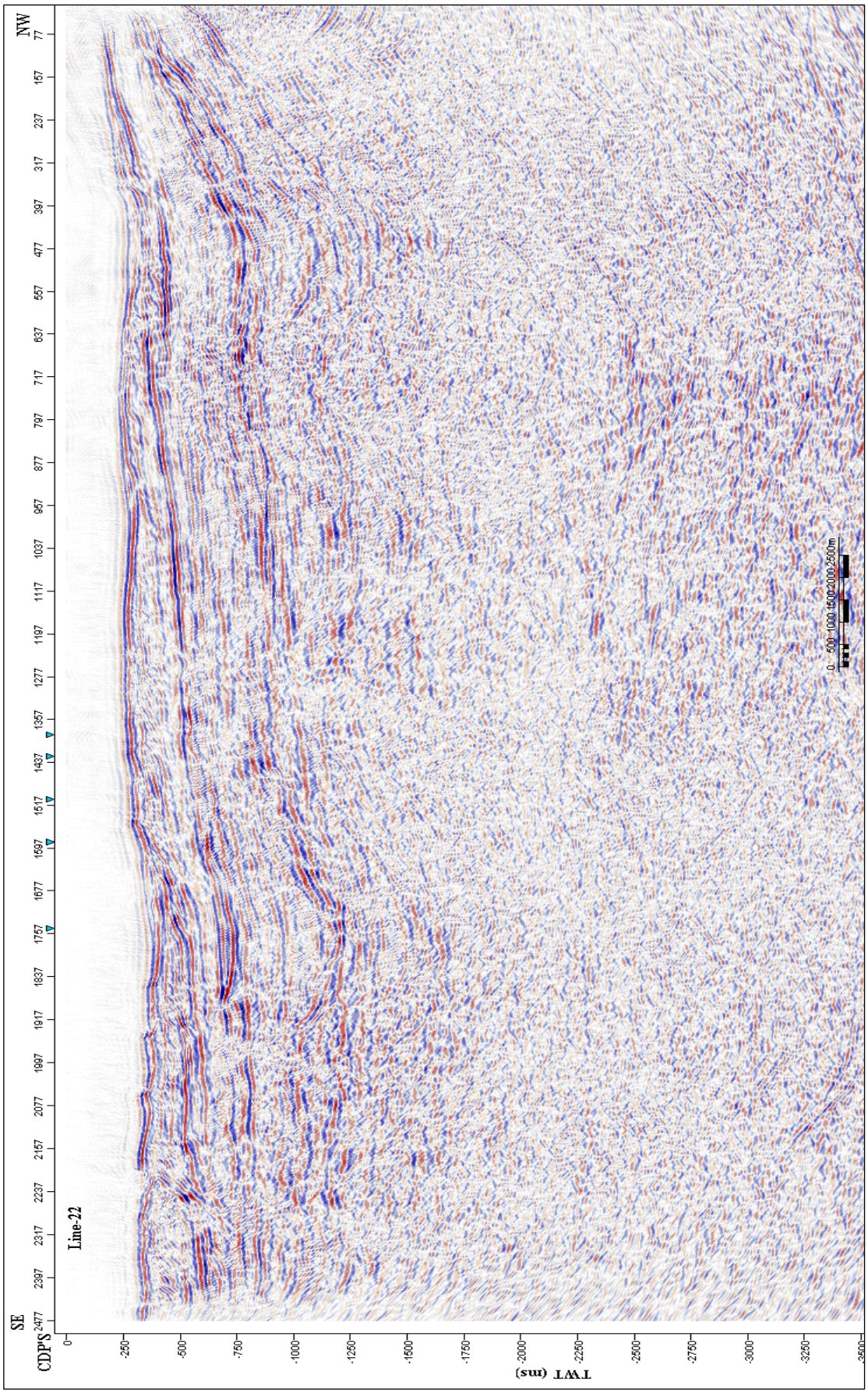

Line-22

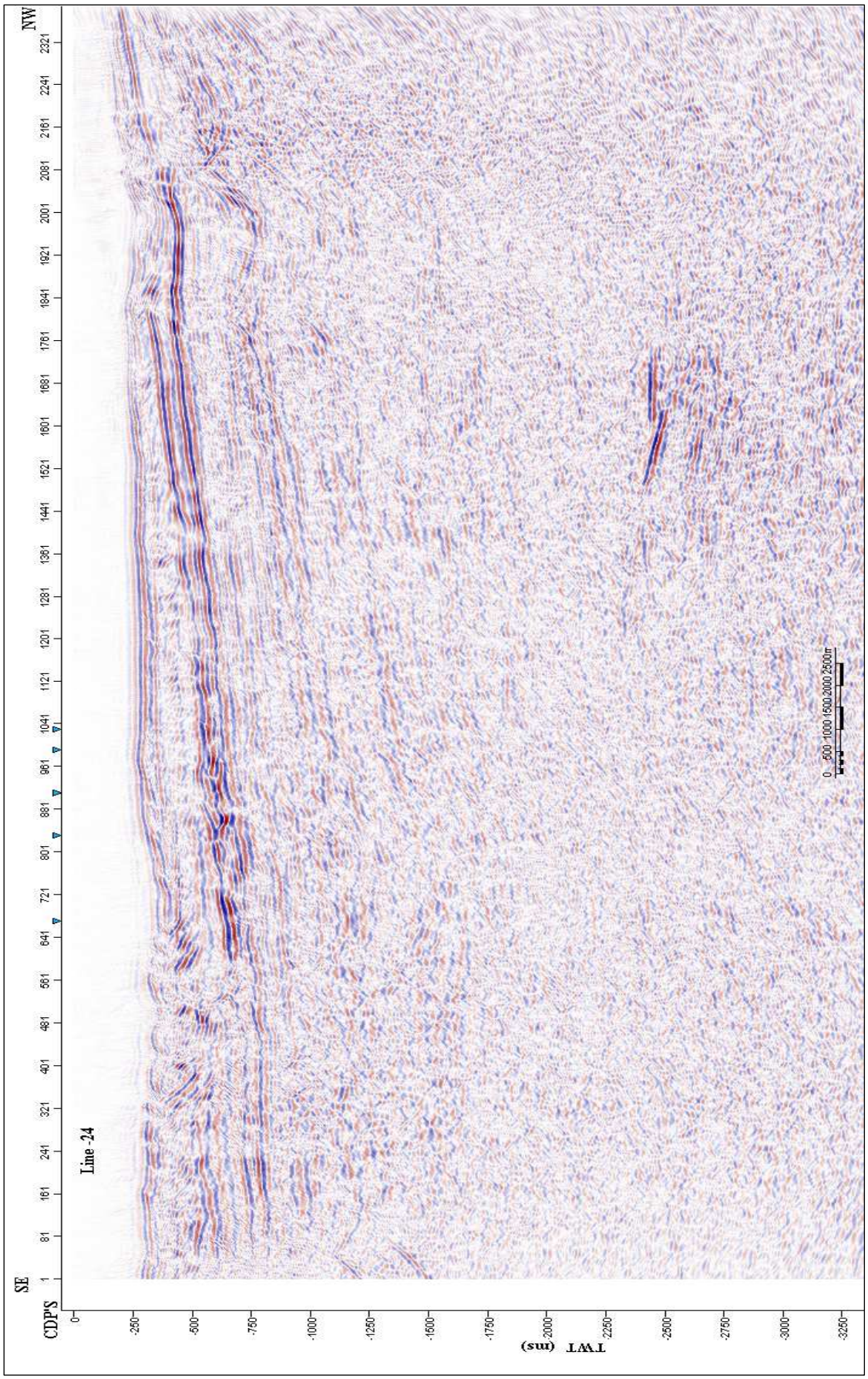

Line-24

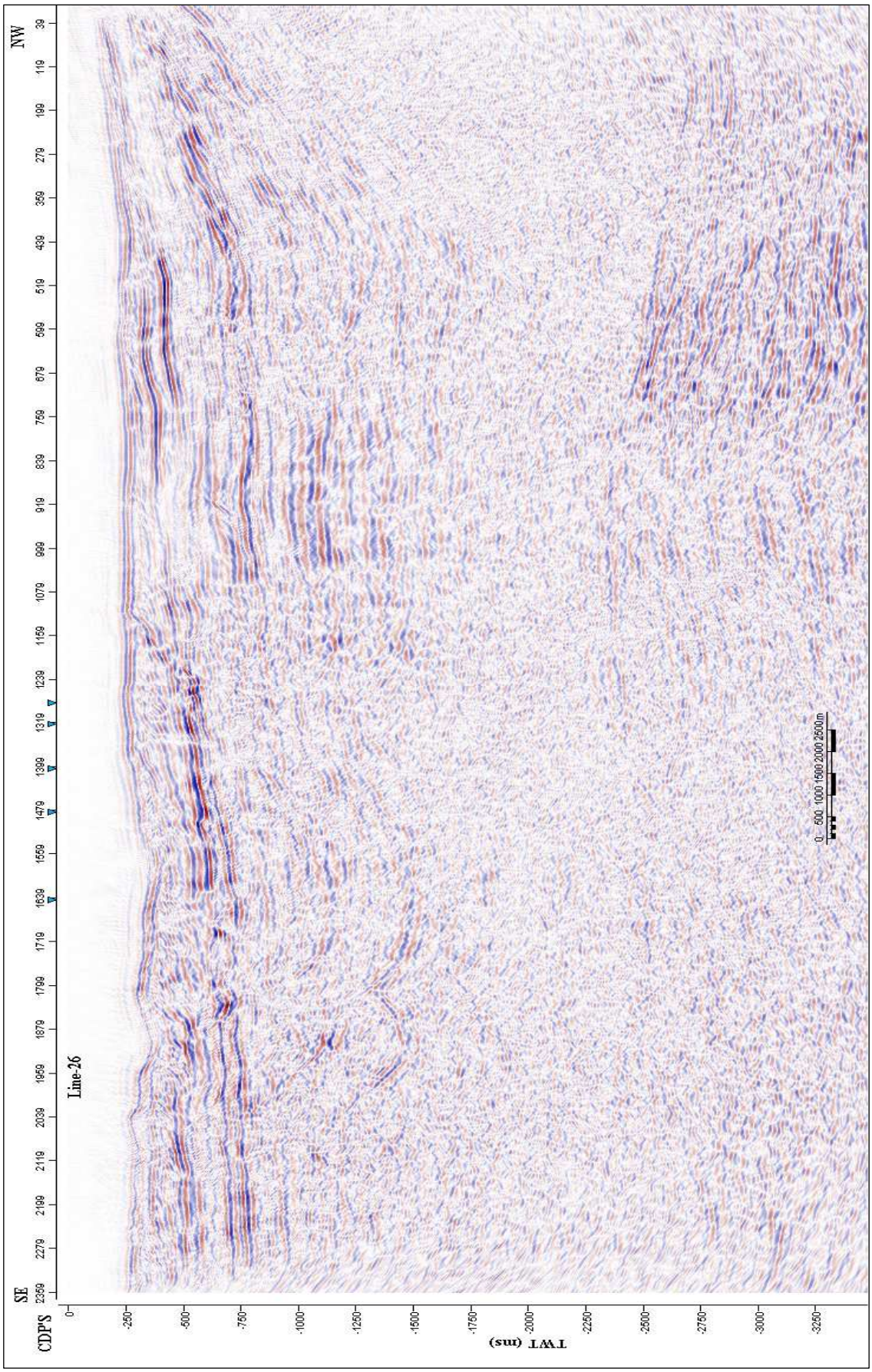

Line-26

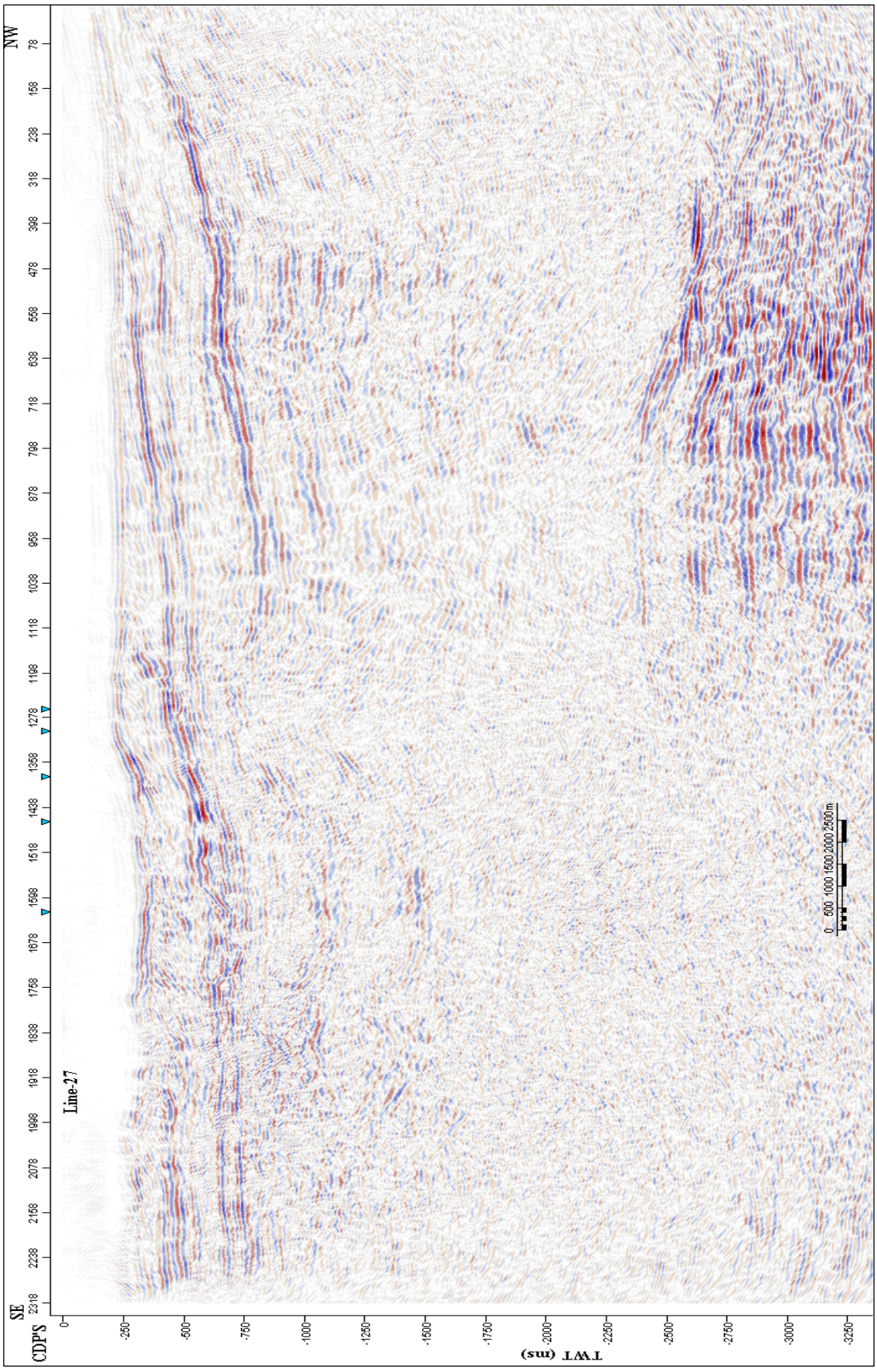

Line-27

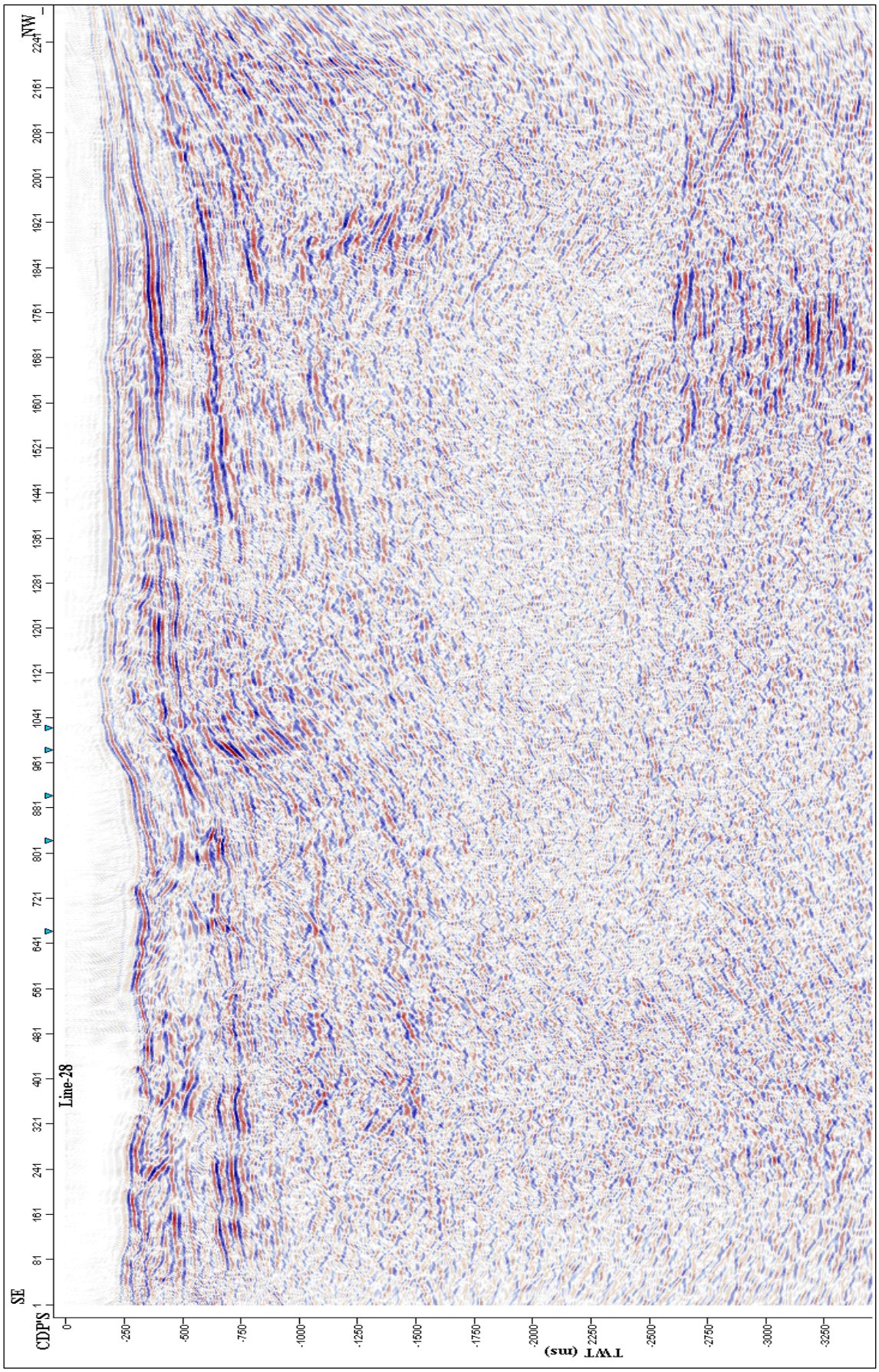

Line-28

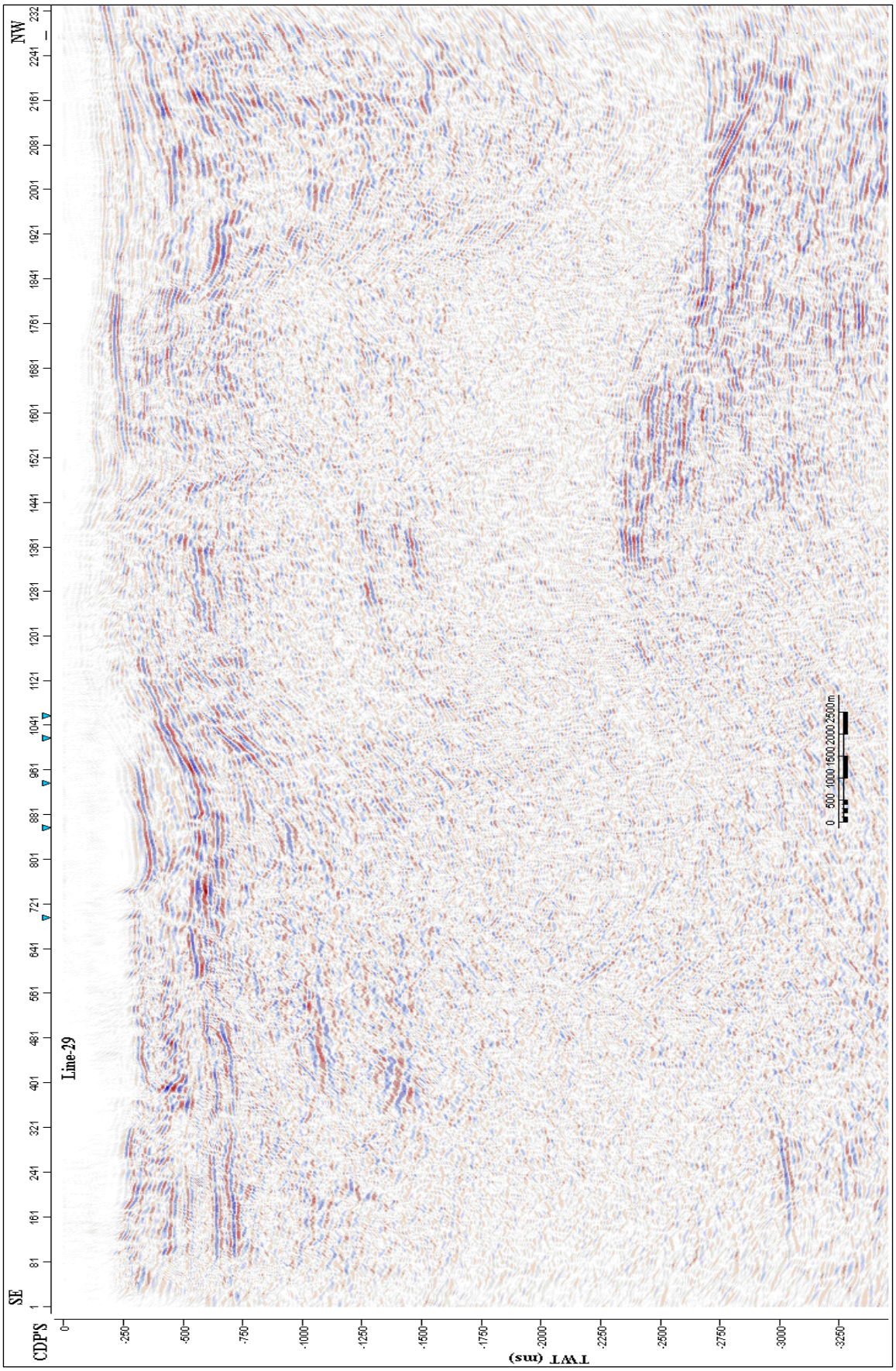

Line-29

Appendix II

Interpretation of horizons and sedimentary successions. The dashed lines mark the interpretation done with some uncertainty, (Gr = Group).

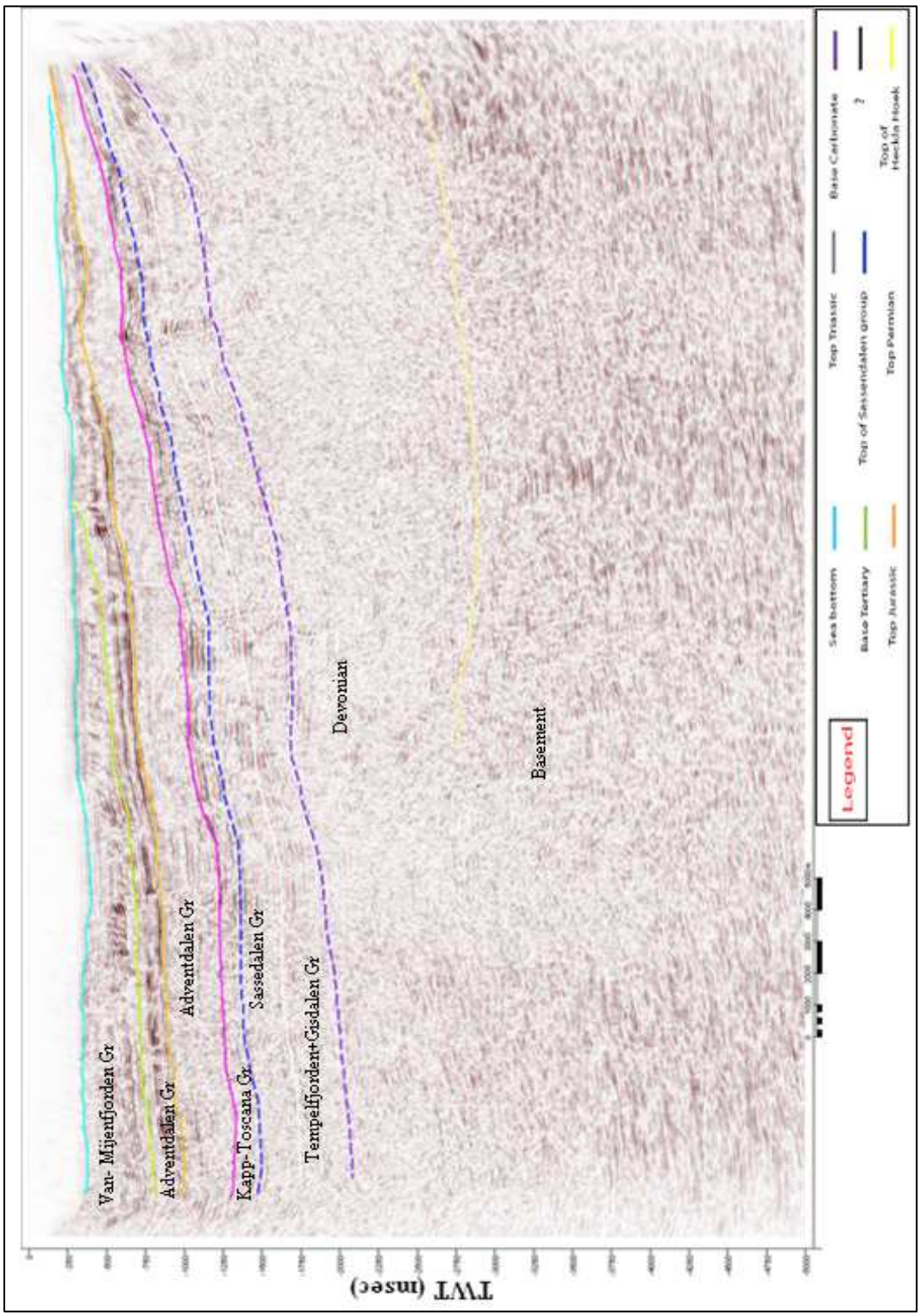

Profile-18

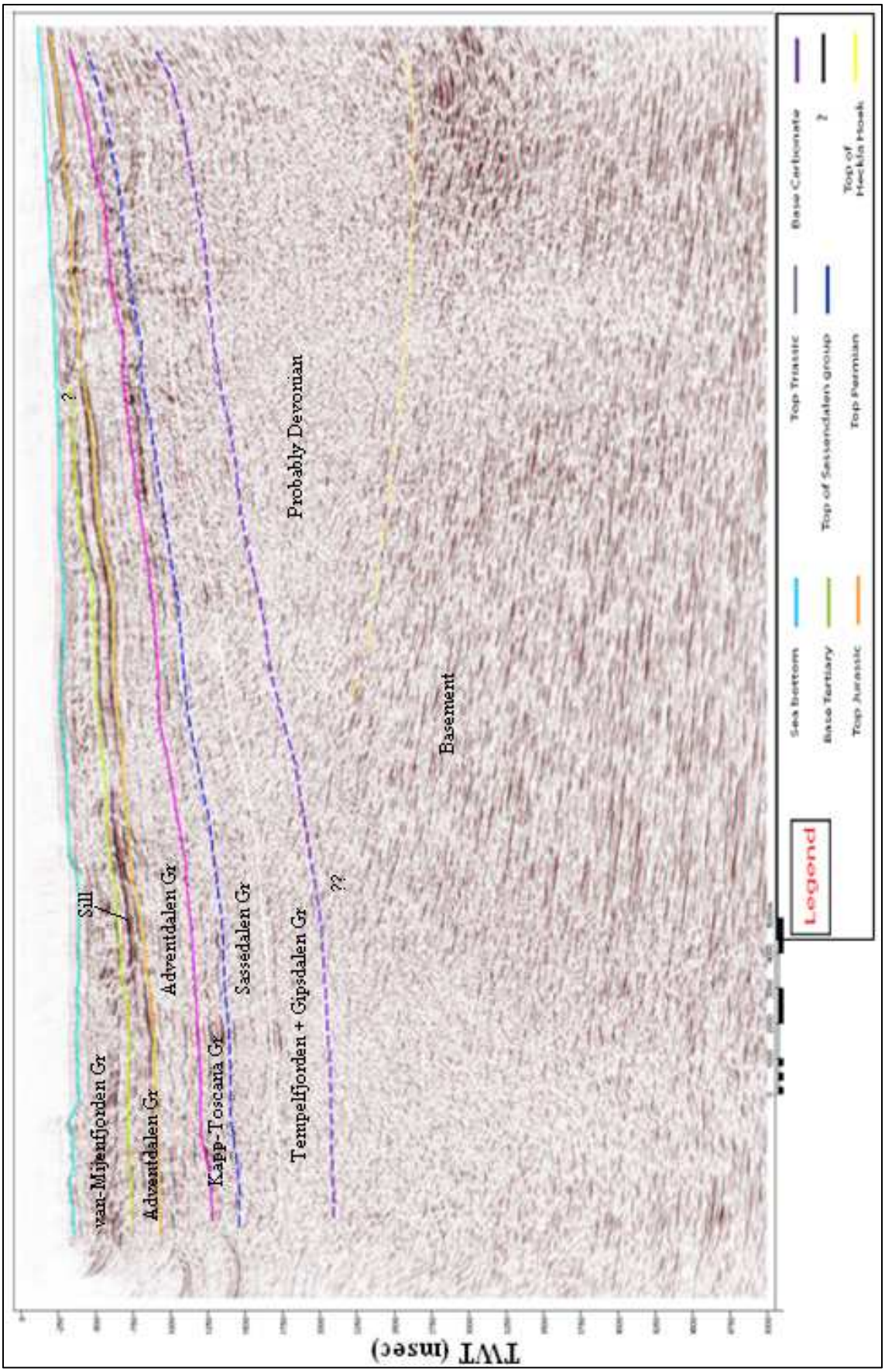
TWT (msec)
Sea bottom
Base Tertiary
Top Jurassic
Top Triassic
Top of Sassendalen group
Top Permian
Base Carbonate
?
Top of Heckla Hoek
Legend
?
Sill
van-Mijenfjorden Gr
Advantdalen Gr
Adventdalen Gr
Kapp-Toscana Gr
Sassedalen Gr
Tempelfjorden + Gipsdalen Gr
??
Probably Devonian
Basement

Profile-20

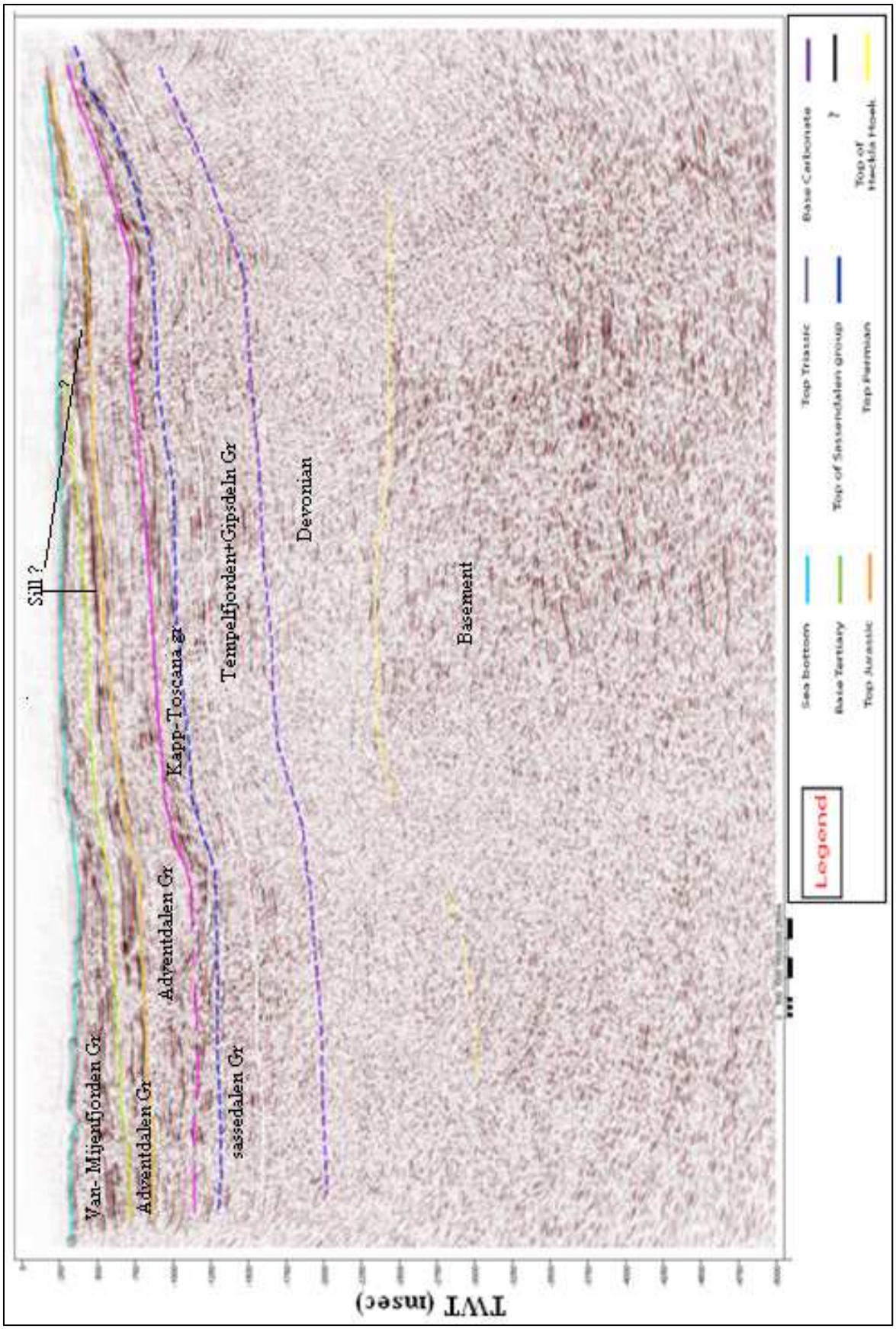
Sill ?
?
Van- Mijenfjorden Gr
Adventdalen Gr
Adventdalen Gr
Kapp-Toscana gr
sassedalen Gr
Tempelfjorden+Gipsdeln Gr
Devonian
Basement
Legend
Sea bottom
Base Tertiary
Top Jurassic
Top Triassic
Top of Sassendalen group
Top Permian
Base Carbonate
?
Top of Hecla Hoek
TWT (msec)

Profile-22

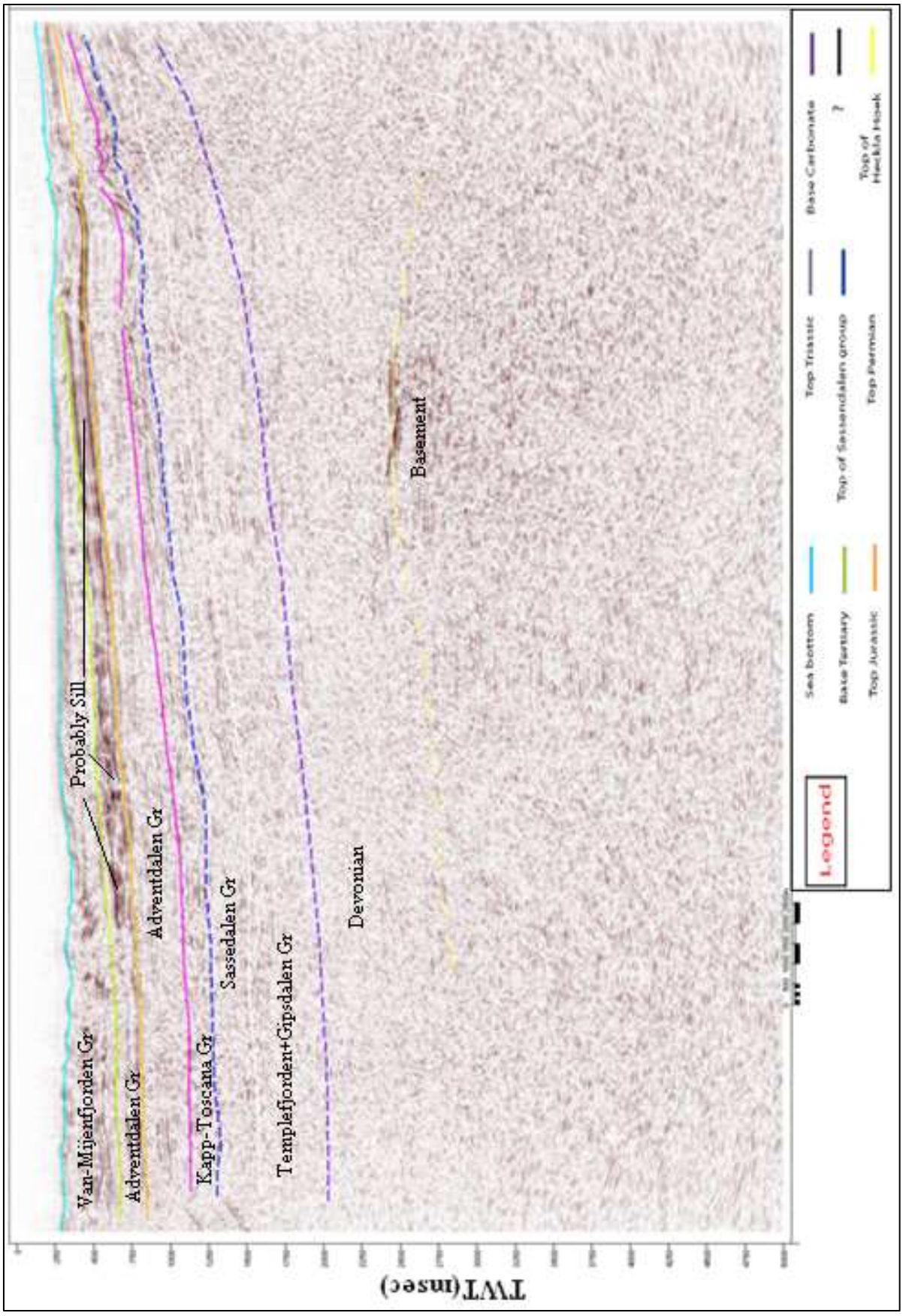
Probably Sill
Van-Mijenfjorden Gr
Adventdalen Gr
Adventdalen Gr
Kapp-Toscana Gr
Sassedalen Gr
Templefjorden+Gipsdalen Gr
Devonian
Basement
Legend
Sea bottom
Base Tertiary
Top Jurassic
Top Triassic
Top of Sassendalen group
Top Permian
Base Carbonate
?
Top of Hecklahook
TWT(msec)

Profile-24

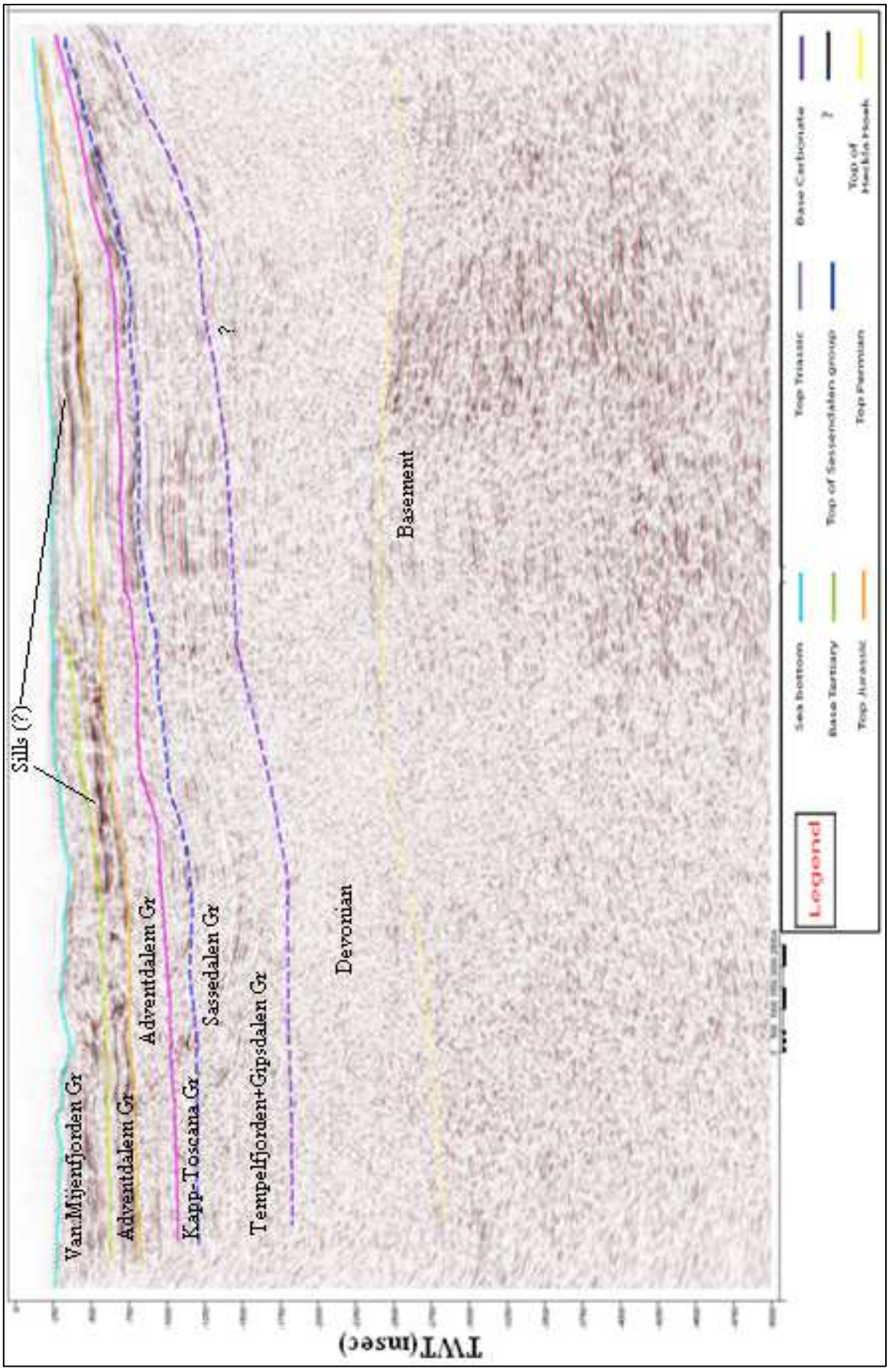
Sills (?)
Van Mijenfjorden Gr
Adventdalem Gr
Adventdalem Gr
Kapp-Toscana Gr
Sassedalen Gr
Tempelfjorden+Gipsdalen Gr
Devonian
Basement
?
TWT (msec)
Legend
Sea bottom
Base Tertiary
Top Jurassic
Top Triassic
Top of Sassendalen group
Top Permian
Base Carbonate
?
Top of Hecla Hoek

Profile-26

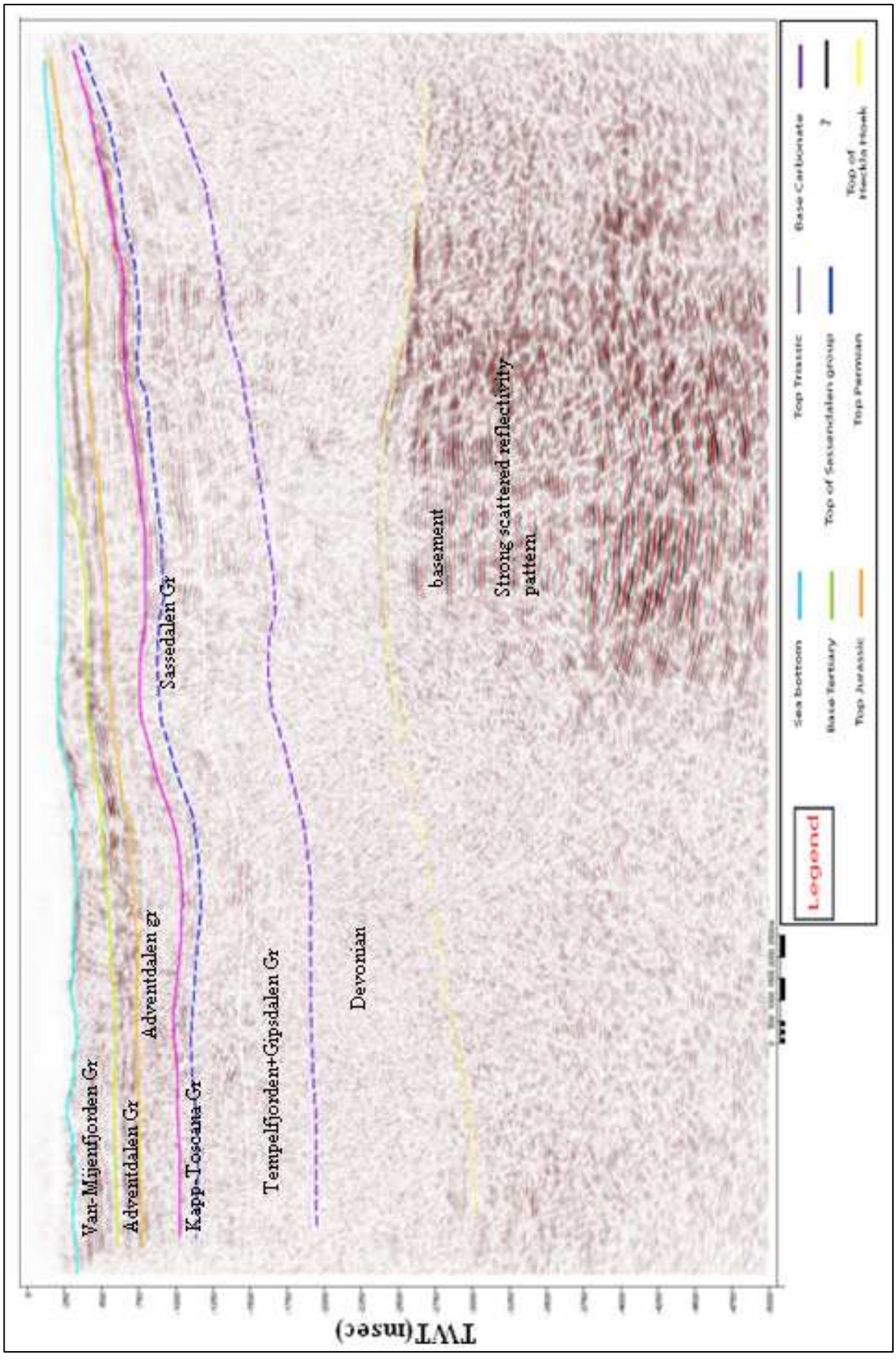
TWT(msec)
Van-Mijenfjorden Gr
Adventdalen Gr
Adventdalen gr
Kapp-Toscana Gr
Sassedalen Gr
Tempelfjorden+Gipsdalen Gr
Devonian
basement
Strong scattered reflectivity pattern
Legend
Sea bottom
Base Tertiary
Top Jurassic
Top Triassic
Top of Sassendalen group
Top Permian
Base Carbonate
?
Top of Hecla Hoek

Profile-27

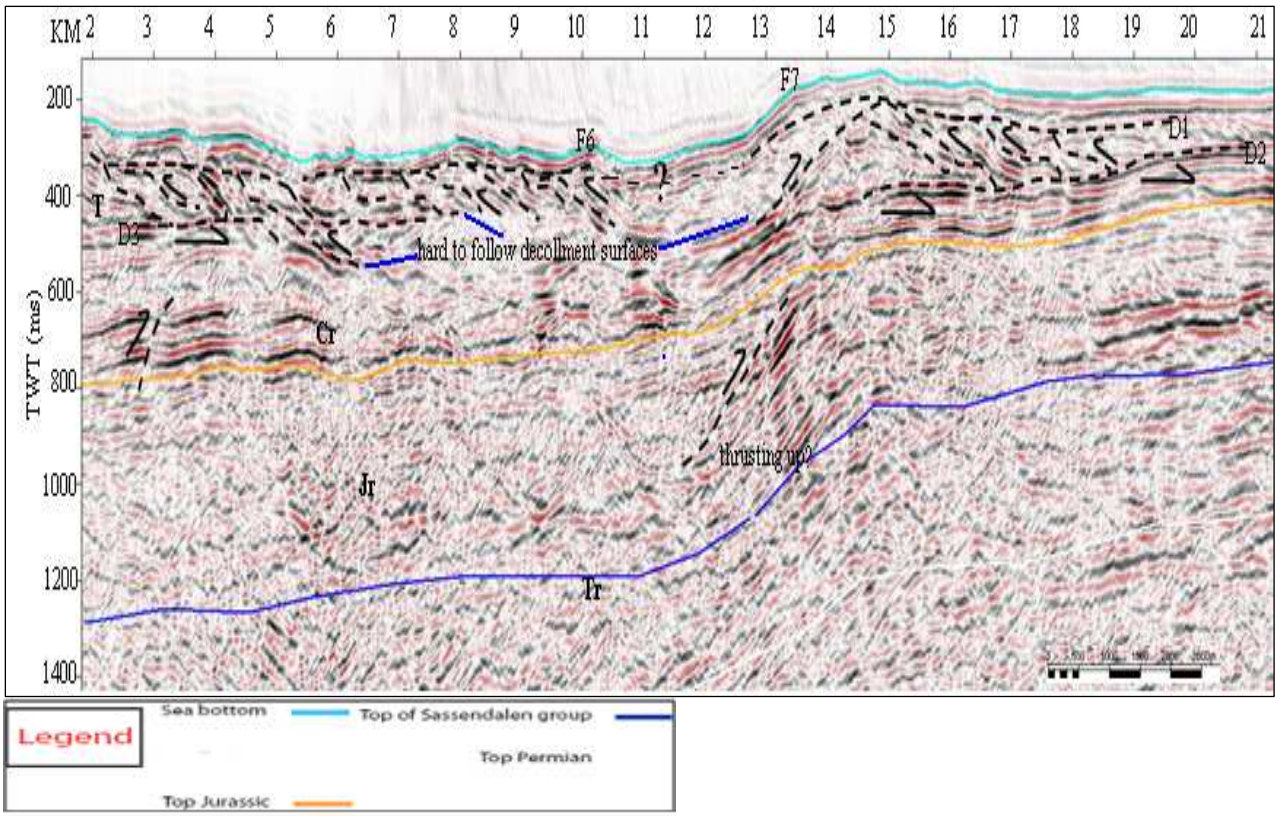

Profile-28: Interpretation of horizons and faults. The dashed lines mark some uncertainty.